Novel Optical Transmitters for High Speed Optical Networks

John O'Carroll

B.Eng., M.Eng.

A thesis submitted in part fulfilment of the
requirements for the Degree of
Doctor of Philosophy (Ph.D)

to the

Dublin City University
Faculty of Engineering & Computing
School of Electronic Engineering

Supervisor: Prof. Liam P. Barry

January 2013

Declaration

I hereby certify that this material, which I now submit for assessment on the programme of study leading to the award of Doctor of Philosophy (Ph.D) is entirely my own work, that I have exercised reasonable care to ensure that the work is original, and does not to the best of my knowledge breach any law of copyright, and has not been taken from the work of others save and to the extent that such work has been cited and acknowledged within the text of my work.

Signed: _____

ID No.: 58104321

Date: _____

Abstract

The objective of this thesis is to investigate the performance of novel optical transmitter lasers for use in high speed optical networks. The laser technology considered is the discrete mode laser diode (DMLD) which is designed to achieve single wavelength operation by etching features on the surface of the ridge waveguide. This leads to a simplified manufacturing process by eliminating the regrowth step used in conventional approaches, presenting an economic approach to high volume manufacture of semiconductor lasers. Two application areas are investigated in this work.

The bit rate in next generation access networks is moving to 10 Gbit/s. This work characterises the performance of DMLDs designed for high speed operation with the objective of identifying the limitations and improving performance to meet the specifications for uncooled operation at 10 Gbit/s.

With the deployment of advanced modulation formats the phase noise of the laser source has become an important parameter, particularly for higher order formats. DMLDs were developed for narrow linewidth operation. The linewidth of these devices was characterised and a value as low as 70 kHz was demonstrated. Transmission experiments were also carried out using a coherent transmission test bed and the performance achieve is compared with that of an external cavity laser.

Acknowledgement

First and foremost, I would like to thank my supervisor Prof. Liam Barry for his excellent supervision and for providing me with the opportunity to work on this project. I would particularly like to thank Liam for his assistance in helping me balance my commitments to DCU and Eblana, without which the completion of this work would not have been possible.

Thanks also to Dr. Prince Anandarajah for his help over the years with setups and organising equipment.

I would also like to thank past and present members of the group for help with various setups over the years, particularly Prince, Tam, Barry, Frank and Sylwester.

I am also grateful to Eblana Photonics for the support the company has given me over the course of this project, and I would like to thank the following:

Dr. James O'Gorman, for first proposing that I pursue this project with DCU.

Dr. Richard Phelan, for his insight into laser design; the many discussions over the years have been invaluable.

Dr. Brian Kelly, for the many useful discussions, particularly relating to device processing.

Dr. Diarmuid Byrne, for his advice on laser modelling.

Jim Somers, for making time available to carry out work relating to this project and also for granting me a leave of absence to complete this thesis.

Also, Rob, Diarmuid, Richard and Brian for reading through this thesis and providing useful feedback.

I would like to thank Radan Slavík at the ORC in the University of Southampton for performing a power spectral density measurement on a laser, which is presented in this thesis.

Finally, I would like thank my parents for their constant love and support. To my brothers Eamon and Mike, thanks for all the encouragement.

Contents

List of Figures

List of Tables

Acronyms

AR	Anti-reflection
ASE	Amplified spontaneous emission
ASK	Amplitude shift keying
ATM	Asynchronous transfer mode
AWG	Arbitrary waveform generator
BER	Bit error ratio
CATV	Community access television
CW	Continuous wave
DBPSK	Binary differential phase shift keying
DBR	Distributed Bragg reflector
DCF	Dispersion compensating fibre
DFB	Distributed feedback
DMLD	Discrete mode laser diode
DP-QPSK	Dual-polarisation quadrature phase shift keying
D-SH	Delayed self-heterodyne
DSL	Digital subscriber line
DSP	Digital signal processing
DWDM	Dense wavelength division multiplexing
EAM	Electroabsorption modulator
ECL	External Cavity laser
EDFA	Erbium doped fibre amplifier
EML	Externally modulated laser
EVM	Error vector magnitude
FEC	Forward error correction
FFT	Fast Fourier transform
FIBE	Focused ion beam etching
FP	Fabry Pérot

FTIR	Fourier transform infrared
FTTC	Fibre-to-the-curb
FTTH	Fibre-to-the-home
HR	High reflectivity
ICP	Inductive coupled plasma
IEEE	Institute of electrical and electronics engineers
IQ	In-phase quadrature
ISI	Inter-symbol interference
ITU	International telecommunications union
L-I	Light-current
$LiNbO_3$	Lithium niobate
LO	Local oscillator
LPE	Liquid phase epitaxy
LR	Low reflectivity
MAN	Metropolitan area network
MBE	Molecular beam epitaxy
MEMs	Micro-electro-mechanical system
MOCVD	Metal-organic chemical vapour deposition
MPLS	Multiprotocol label switching
MQW	Multi-quantum well
MZI	Mach-Zehnder interferometer
MZM	Mach-Zehnder modulator
NRZ-OOK	Non-return-to-zero on/off keying
OADM	Optical add-drop multiplexer
OECD	Organisation for Economic Co-operation and Development
OEO	Optical-electrical-optical
OMVPE	Organometallic vapour-phase epitaxy
OOK	On/off keying
OPLL	optical phase locked loop
OSA	Optical spectrum analyser
OSNR	Optical signal to noise ratio
PIC	Photonic integrated circuit
PLC	Planer lightwave circuit

PM	Polarization maintaining
PON	Passive optical network
p-p	Peak-to-peak
PRBS	Pseudo random binary sequence
PSK	Phase shift keying
QAM	Quadrature amplitude modulation
QPSK	Quadrature phase shift keying
RF	Radio frequency
RIN	Relative intensity noise
rms	Root-mean-square
ROADM	Reconfigurable optical add-drop multiplexer
RZ-OOK	Return-to-zero on/off keying
SCH	Separate confinement heterostructure
SDH	Synchronous digital hierarchy
SEM	Scanning electron microscope
SGDBR	Sampled grating distributed Bragg reflector
SMSR	Side mode suppression ratio
SNR	Signal to noise ratio
SNR_b	Signal to noise ratio per bit
SOA	Semiconductor optical amplifier
SONET	Synchronous optical networking
SQW	Single quantum well
SSMF	Standard single mode fibre
T	Temperature
TEC	Thermoelectric cooler
TX	Transmitter
VCSEL	Vertical cavity surface emitting laser
VDSL2	Very high data rate digital subscriber line 2
VNA	Vector network analyser
WDM	Wavelength division multiplexing

Chapter 1

Introduction

Delivering high speed broadband connections to a country's population is recognised as an important driver for economic growth in knowledge based economies as well as being of benefit to society as a whole. Targets set by the European Union state that by 2020 all Europeans should have access to connection speeds of at least 30 Mbit/s and 50 %, or more, of European households should have subscriptions above 100 Mbit/s [1]. Also, all member states are required to put in place a broadband strategy to meet these goals. The Irish government recently announced its strategy, with objectives to deliver by 2015, 70 to 100 Mbit/s to more than half the population, at least 40 Mbit/s to a further 20 to 35 %, centred around smaller towns and villages, and a minimum of 30 Mbit/s throughout the country, even in remote locations [2]. The United States has also set out a broadband strategy, with a goal of having 100 million households with access to connection speeds of 100 Mbit/s by 2020 [3]. In order to meet these targets existing network infrastructure will have to be upgraded. Operators will have to ensure that the connection to the customer has sufficient bandwidth to deliver these higher speeds, and that the network as a whole has sufficient capacity to handle the cumulative increase in data traffic.

Increasing the capacity of fibre optic networks will require continued development of these systems, and their constituent components. This thesis primarily looks at one component, the semiconductor laser diode, and considers a novel approach for producing single mode lasers called a discrete mode laser diode (DMLD). This approach offers the potential for high-volume, low-cost fabrication of single-mode lasers as no regrowth is required. Two application areas are considered, directly modulated transmitters and a continuous wave (CW) source for use with advanced modulation formats where external modulation is used. Throughout this thesis, unless otherwise stated, single mode refers to single longitudinal mode.

Key results from the work carried out towards this thesis are:

- Demonstration of 10 Gbit/s operation using DMLDs at both 1310 nm and 1550 nm.
- Demonstration of a linewidth as low as 70 kHz from a DMLD designed for low linewidth operation.
- Demonstration of a low linewidth DMLD exhibiting a wide operating temperature range. At a constant power of 4 mW a maximum linewidth of 235 kHz was measured at 85 ˚C, and a minimum value of 212 kHz was measured at 25 ˚C, corresponding to a variation in the linewidth of only 23 kHz over the range 0 to 85 ˚C.
- Low linewidth DMLDs were characterised in a coherent transmission setup employing quadrature phase shift keying (QPSK) and 16-ary quadrature amplitude modulation (16-QAM). The performance achieved in the setup using DMLDs was compared with that achieved using an external cavity laser (ECL) and similar performance was achieved at baud rates as low as 2.5 Gbaud and 5 Gbaud for QPSK and 16-QAM, respectively. These were the

first experimental demonstrations where DMLDs were used as the transmitter (TX) or local oscillator (LO) in a coherent transmission setup where either of these modulation formats were employed.

This thesis is structured as follows:

Chapter 2 gives an overview of optical communication networks. The growth in capacity and issues related to maintaining growth levels to meet future bandwidth demands are discussed. The final section in the chapter looks at optical modulation formats and the technologies used to modulate the optical carrier.

Chapter 3 gives an overview of semiconductor laser diodes, and looks at the materials and structures used in their fabrication. Approaches used to achieve single mode operation are discussed, along with important characteristics for devices targeted at optical communication applications.

Chapter 4 gives an overview of DMLDs and describes how single mode operation is achieved in this type of laser. A simplified model is presented which describes how the single mode characteristics of the device can be controlled by modifying design parameters in this device. Static characterisation results are presented for two types of device, the first targeted at direct modulation applications and the second at optical coherent communications.

Chapter 5 looks at the performance of DMLDs under direct modulation at a bit rate of 10 Gbit/s. Results are presented for lasers operating in both the 1310 nm and 1550 nm wavelength windows, and includes the transmission performance over single mode fibre.

Chapter 6 looks at the performance of DMLDs designed for narrow linewidth emission in a test bed employing advanced modulation formats. Two modulation

formats are considered; QPSK and 16-QAM, and the performance achieved using low linewidth DMLDs and an ECL is compared.

Chapter 7 presents a brief conclusion to the thesis and discusses the potential for future work in this area.

Finally, Appendix A presents a list of the author's publications arising from this work.

References

[1] European Commission, "European Broadband: investing in digitally driven growth," 2010. [Online]. Available: http://ec.europa.eu/information_society/activities/broadband/docs/bb_communication.pdf.

[2] Department of Communications, Energy and Natural Resources, "Delivering a Connected Society - A National Broadband Plan for Ireland," 30 August 2012. [Online]. Available: http://www.dcenr.gov.ie/NR/rdonlyres/1EA7B477-741B-4B74-A08E-6350135C32D2/0/NBP.pdf.

[3] US, Federal Communications commission, "National broadband plan, Chapter 2 Goals for a high performance America," 16 March 2010. [Online]. Available: http://download.broadband.gov/plan/national-broadband-plan-chapter-2-goals-for-high-performance-america.pdf.

Chapter 2

High speed optical communication networks

This chapter gives an overview of optical communication networks. It looks at the growth in capacity of these networks and how growth levels can be maintained to meet future capacity needs. Optical modulation formats and the technologies used to modulate the optical carrier are discussed.

2.1 The growth in capacity

Since fibre optics were first introduced to telecommunication networks the growth in capacity has been remarkable. Fibre has led to cheaper voice calls, lower maintenance costs [1] and provided a high capacity and low cost data network that has been a key ingredient in the development of the internet [2]. Over the last 20 years, the internet has evolved from a primarily text based medium to a multimedia platform used in the office, home and on mobile devices. Applications such as video on demand, video conferencing, online gaming and cloud computing are a reality, and will undoubtedly see continued development in the coming years. Internet video

traffic alone now accounts for almost 50 % of consumer internet traffic and this is forecast to grow to 62 % by 2015 [3]. Getting to this point has been made possible by continuous technical innovation. One example is the erbium doped fibre amplifier (EDFA), which enabled transmission over long distances without optical-electrical-optical (OEO) conversion. Significantly, the wide optical bandwidth of the EDFA meant that multiple wavelength channels could be amplified simultaneously, making possible the cost effective deployment of wavelength division multiplexing (WDM) technology. The timing of its commercial deployment in the mid 90's was also significant as it coincided with the commercial deployment of the internet. Fig. 2.1 shows the internet traffic per month for North America from 1990 to 2015 [3, 4]; between 1994 and 1996 the internet traffic increased by over 90 fold coinciding with the introduction of WDM. Since then, growth in internet traffic has been relentless, facilitated by WDM and other technological advances in fibre optics.

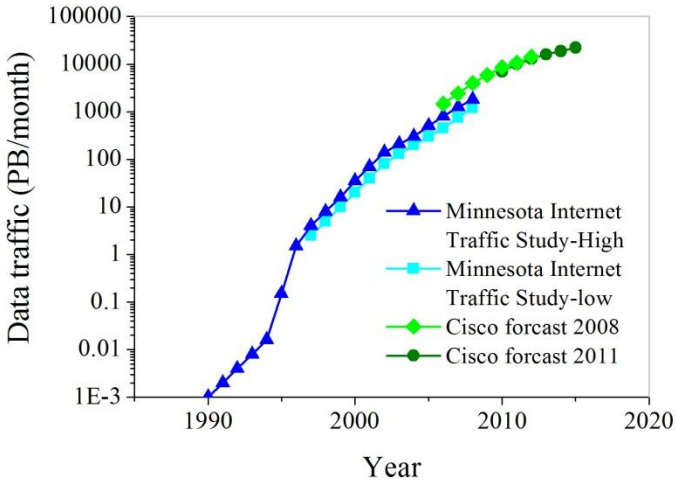

Fig. 2.1 North American internet traffic by year.

With the increased popularity of mobile devices, such as smart phones, tablet computers and portable gaming consoles, worldwide mobile data traffic grew by 133 % in 2011 and growth rates of 110 % and 78 % are forecast for 2012 and 2014, respectively, resembling the growth patterns seen in fixed line traffic in the late

nineties and early two thousands [5]. It is forecast that global IP traffic will grow to almost 1 Zettabyte per year by 2015, a fourfold increase from 2010 levels [3], providing an impetus for continued innovation in communication systems.

2.2 Optical networks

An optical network consists of a number of interconnected sub-networks, each with their own architecture designed to perform specific functions within the network. The technological challenges that need to be overcome to grow capacity vary according to network type.

2.2.1 Long haul network

Long haul networks are used to connect countries and continents and can be made up of terrestrial links, covering distances of a few thousands km, and ultra-long haul submarine links, covering distances from 6,000 to 12,000 km [6]. Modern submarine cables are designed to transmit bit rates in excess of 1 Tbit/s per fibre [7], and because of the distances involved the technical obstacles can be quite challenging. However, they are essentially point-to-point links allowing a certain degree of flexibility in their design, and design parameters such as amplifier position and dispersion compensation can be optimised to maximise performance. With the development of forward error correction (FEC) an increased number of channels can be transmitted per fibre using tighter WDM grid spacing and because of their point-to-point architecture submarine cables don’t necessarily have to comply with the ITU grid [8].

2.2.2 Core network

The core is the backbone of a national fibre optic network, connecting several regional networks together. The connection point in the regional networks is called a node. The core also connects with long haul networks to extend global interconnectivity between national domains [6]. Data from many users is amalgamated and transported through different nodes in the network. The links between individual nodes are point-to-point WDM links, and each node can be connected to several nodes in the network, producing an interconnected network with a mesh structure. When transmitting an optical signal through the network it can be routed through several nodes through switching operations which direct the optical signal to the correct destination in the network. In legacy networks the signals were routed by OEO cross connects, where the optical signals entering the node are converted to the electrical domain and routing performed electronically before retransmitting the optical signals to the appropriate destination. The preferred option, where possible, is to route the signals in the optical domain. A significant step towards all optical routing was the development of the optical add-drop multiplexer (OADM), which allowed signals not destined for a node to by-pass it and remain in the optical domain, therefore significantly reducing the cost and size of the OEO cross-connects required in each node [9]. The development of tuneable transponders, wavelength selective switches, and reconfigurable OADMs (ROADMs) have increased the flexibility of all-optical networks and have contributed to all-optical solutions permeating today's core networks [10].

2.2.3 Metropolitan area network

The metropolitan area network (MAN) is the fibre transport network and covers a geographical area which can range from several blocks of buildings to entire cities [11]; it typically has a ring topology spanning distances up to 250 km. The MAN provides interconnectivity between the core and the access network, and must support a large range of technologies such as synchronous digital hierarchy/synchronous optical networking (SDH)/(SONET), dense wavelength division multiplexing (DWDM), asynchronous transfer mode (ATM), multiprotocol label switching (MPLS) and Ethernet, all of which may be operating at different data rates. A further requirement is that it needs to be reconfigurable, and this is achieved using ROADMs, allowing dynamic and flexible node-to-node connections [6].

2.2.4 Access network

The access network connects the customer to the rest of the network; it is often referred to as the last mile although typical distances can be up to 20 km. Traditionally, the access network was a copper network infrastructure. However, since the beginning of this century fibre has seen growing commercial importance [12]. The level of penetration of fibre in access varies between countries and this is shown in Fig. 2.2 which plots data gathered by the Organisation for Economic Co-operation and Development (OECD) for the number of fibre connections as a percentage of total broadband connections among OECD countries reporting fibre subscribers as of June 2011 [13]. The OECD data did not give a figure for the USA; however, a survey carried out on behalf of the fibre-to-the-home (FTTH) council found that 6 % of homes were connected with 18 % of homes passed for FTTH as of March 2011 [14]. In Japan, the county with highest percentage of fibre broadband

connections, FTTH became the leading access technology in September 2008 [15]. For a considerable period of time, barriers to FTTH deployment were the high cost of fibre optic components and the lack of applications to take advantage of the high bandwidth offered by FTTH [12]. Therefore, when upgrading existing copper infrastructure most operators opted against providing FTTH, instead opting for an incremental upgrade by retrofitting existing infrastructure, which in general meant extending the reach of fibre in the field. In fibre-to-the-curb (FTTC) the fibre connection is provided to the curb of a community and is converted to an electrical signal which is then transported to the customer via the existing copper infrastructure. The copper wiring is either twisted pair, in the case of a telecoms operator, or coaxial cable, for community access television (CATV) operators. For the twisted pair case, digital subscriber line (DSL) modems have been developed which can achieve relatively high connection speeds, and by decreasing the transmission distance over copper these can be increased further. In very high data rate DSL2 (VDSL2) using vectoring, which is a technique to cancel far end cross talk between adjacent copper wires in the bundle, it is possible to achieve downstream bit rates in excess of 100 Mbit/s over short distances of 600 m or less [16, 17]. Table 2.1 summarises the maximum transmission speeds achievable and the corresponding maximum transmission distances for various DSL technologies [12, 16]. CATV systems can achieve even higher bit rates as coaxial cable is a better high frequency transmission medium than twisted pair and with the latest DOCSIS 3.0 modems downstream data rates of 160 Mbps are possible [12]. In recent years the cost of optical components has come down significantly, and this, coupled with the projected capacity demand, make FTTH an attractive solution for operators.

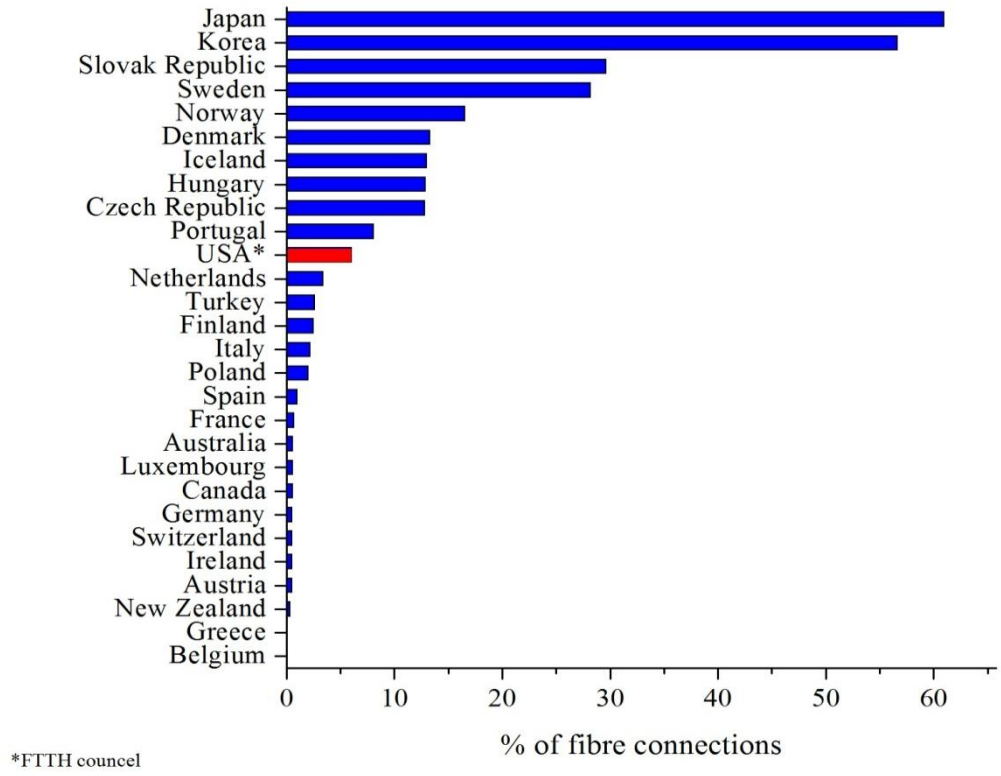

Fig. 2.2. Number of fibre connections as a percentage of broadband connections among OECD countries reporting fibre subscribers, as of June 2011.

DSL type	Max Speed		Max. transmission distance (m)
	Upstream	Downstream	
IDSL (ISDN)	144 kbps	144 kbps	10700
ADSL (asymmetric DSL)	800 kbps	8 mbps	5500
MSDSL (multirate symetric DSL)	2 Mbps	2 Mbps	8800
VDSL (very high data rate DSL)	16 Mbps	52 Mbps	1200
VDSL2 with vectoring	50 Mbps	100 Mbps	600

Table 2.1. Transmission speeds for DSL modem technologies.

Access equipment is usually deployed in large volumes and is therefore very cost sensitive [12]. The fibre infrastructure uses passive components, such as splitters and combiners, and for that reason is called a passive optical network (PON). The passive infrastructure has an advantage of reduced maintenance costs. The shorter transmission distances ease component specifications, and uncooled direct

modulation transmitter lasers can be used allowing devices with lower cost packages, such as TO-cans, to be used.

2.2.5 Meeting future capacity needs

The level of service provided to the customer can be compromised if the network as a whole has insufficient capacity or if a bottleneck is created in any part of the network. Existing networks will need to be upgraded to meet forecast capacity needs. In the core, the approach adopted is to replace conventional on/off keying (OOK) with advanced modulation formats to increase spectral efficiency in WDM systems. This approach is now a commercial reality with the deployment of 40G and 100G systems. For 100G, and certain implementations of 40G, dual-polarisation quadrature phase shift keying (DP-QPSK) is being employed. In the next evolution of these systems higher order modulation formats have the potential to significantly increase capacity; a further advantage of these new formats is that increased capacity can be achieved while maintaining the baud rate at levels which allow the use of readily available lower cost electro-optics and high speed electronics [18, 19]. An advantage of DP-QPSK 100G systems is compatibility with 50 GHz DWDM channel spacing [20]. By moving to dual-polarisation 16-QAM the bit rate could be doubled to 224 Gbit/s, while maintaining the same baud rate and wavelength channel spacing as current 100G systems [21, 22]. To move to 400G, and beyond, channel spacing will be an issue and the adaption of a flexible wavelength grid may be necessary [23, 24], although this will have significant cost implications as the optics in current systems are designed for a 50 GHz grid. Coherent technology could also be applied to metropolitan [25] and access networks [26] to meet future bandwidth demands in those applications.

Limitations in the capacity of the access network can create a bottleneck. The primary limitation is the proximity of the fibre network to the end customer, the solution is to bring fibre closer to the customer, ideally to the home or failing that as close as possible so as to maximise the data rate using DSL technology. As capacity demands increase, standardisation bodies such as the international telecommunications union (ITU) and the institute of electrical and electronics engineers (IEEE) have put in place standards to increase the bit rate from 1 Gbit/s (IEEE) and 2.5 Gbit/s (ITU) to 10 Gbit/s [27, 28]. Another solution being investigated is WDM PON; utilising WDM technology would lead to a significant increase in capacity, but also a substantial increase in cost as splitters and combiners would have to be replaced with arrayed waveguide grating multiplexers and de-multiplexers. The monetary benefits of the various approaches will determine which approach is taken; a possible situation may develop where 10 Gbit/s PON is initially used for residential applications while WDM-PON is investigated for business or bandwidth intensive backhaul [29].

2.3 Modulation formats

2.3.1 Non-return-to-zero on/off keying

Non-return-to-zero OOK (NRZ-OOK) is the most widely used modulation format in today's fibre optic networks. The primary reason for this is that its simplicity makes it cost effective. While advanced modulation formats are being adopted for long haul applications NRZ-OOK will still be used in MAN and access networks for the foreseeable future. In NRZ-OOK the information is encoded in the intensity of the optical signal and recovered through direct detection at the receiver. In the simplest

case logic ‘1’ is transmitted by light with intensity P_1 and logic ‘0’ is transmitted by the absence of light. In practical implementations when transmitting logic ‘0’, a low level of light with intensity P_0 is still transmitted. The extinction ratio describes the modulation efficiency and is defined by the ratio of P_1 & P_0, measured in decibels:

$$\text{Extinction ratio} = 10 \times \log(P_1 / P_0)\ (\text{dB}) \tag{2.1}$$

The format can be generated through direct modulation of the laser’s current or by modulating a continuous wave laser source using an external modulator. The method used is determined by the specification of the end application.

2.3.1.1 Direct modulation

The intensity of light emitted from a laser diode is linearly proportional to the bias current when operated above threshold. By modulating the current the electrical modulation signal can be transferred to the light output from the laser. Fig. 2.3 shows the light current characteristic for a laser and the ideal behaviour where a current pulse train with bias levels I_{off} and I_{on} are converted to an optical pulse train with levels P_0 and P_1, respectively [30]. Direct modulation lasers provide a cost effective optical transmitter for optical communications. By comparison external modulation solutions utilising continuous wave lasers followed by electro-optic modulators, or integrated electro-absorption modulators are relatively complex devices. However, the intensity modulation from a directly modulated laser is always accompanied by a frequency modulation which broadens the spectral linewidth. This broadening is known as chirp and it limits the bit rate length product [30]. In cost sensitive applications such as access, which cover short to medium range distances, directly modulated lasers are the optical transmitter of choice, and at current speeds chirp doesn’t limit performance significantly. However, as the bit rates of these systems

increase from 2.5 Gbit/s to 10 Gbit/s their application is likely to be limited to transmitters in the 1310 nm window, while more advanced transmitter structures with lower chirp are likely to be the preferred option for 1550 nm, where dispersion in standard single mode fibre (SSMF) is higher.

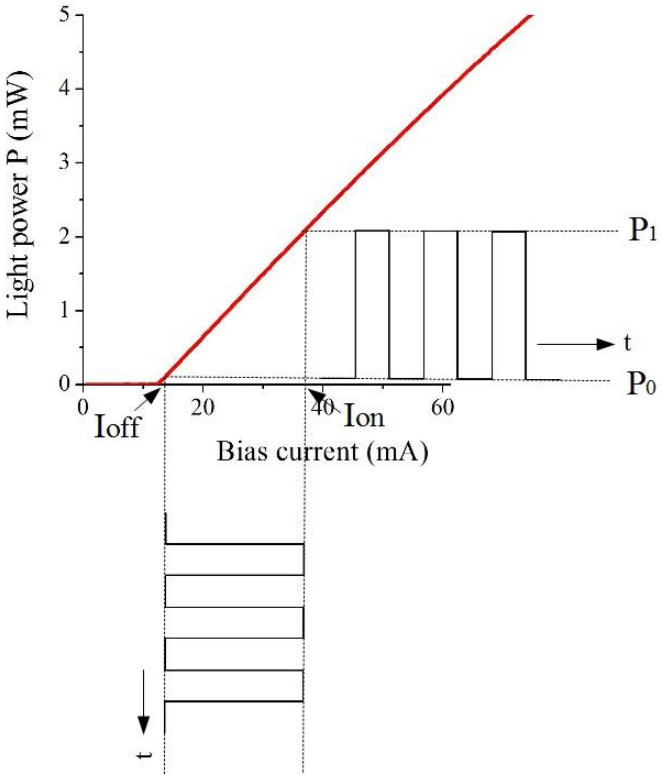

Fig. 2.3. Light current characteristic of a laser, showing the idealised conversion of a current pulse train to an optical pulse train under direct modulation.

2.3.1.2 External modulation

In structure an electroabsorption modulator (EAM) is quite similar to a laser. The device has a waveguide structure and is fabricated from PIN semiconductor materials. It is designed to be transparent to laser light at a particular wavelength, with the level of transparency controlled by the application of an electric field. When no voltage is applied the bandgap is designed to be wide enough so as to be transparent to the laser light. Applying a reverse bias voltage decreases the bandgap

causing the laser light to be absorbed. The reverse bias is typically in the region of 2 V and extinction ratios of ≈ 10 dB can be achieved. Discrete devices are not normally used, instead EAMs are monolithically integrated with a single mode laser to form a device called an externally modulated laser (EML). In order to achieve high extinction ratios the peak wavelength of the laser needs to be detuned from the modulator material in order to design the optimum bandgap separation. This can be achieved through separate growth stages for both devices [31]. In comparison to directly modulated lasers EMLs can achieve much longer transmission distances due to lower chirp, at the expense of a more complex device structure. At 1550 nm EMLs operating at 10 Gbit/s are available for operation at distances of up to 80 km. Devices operating at 40 Gbit/s are available for short reach applications up to 2 km, with research devices operating up to 80 Gbit/s demonstrated [8].

Fig. 2.4(a) shows a Mach-Zehnder modulator (MZM) structure that can be used for amplitude modulation. It consists of a Mach-Zehnder interferometer (MZI) where the input signal is split in two and one, or both, of the paths is equipped with a phase modulator. Changing the electric field applied to the phase modulators controls whether the two beams interfere constructively or destructively at the output. Fig. 2.4(b) shows the sinusoidal power transmission characteristic for an MZM. To go from minimum to maximum extinction requires a phase shift of π between the arms of the MZM, the differential drive voltage required to generate this phase shift is called the switching voltage V_π. MZMs are used in long haul NRZ-OOK applications as they can be operated to give chirp free operation [8]. Devices are manufactured from lithium niobate ($LiNbO_3$) or from InP based semiconductors. InP based devices can be used as a building block in more complex photonic integrated circuits (PICs) [32].

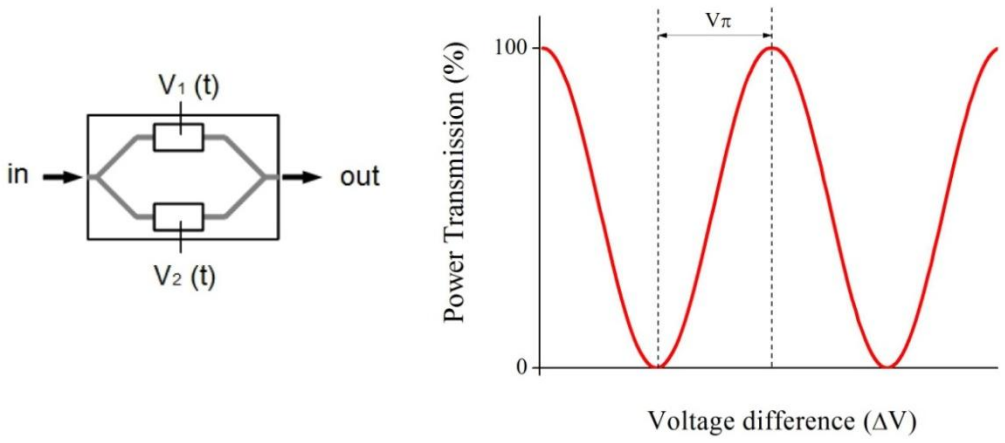

(a) (b)

Fig. 2.4. MZM (a) modulator structure and (b) transmission characteristic.

2.3.2 Return-to-zero on/off keying

In NRZ-OOK when transmitting logic '1' light with power P_1 is transmitted for the duration of the symbol period. In return-to-zero OOK (RZ-OOK) modulation P_1 is transmitted for a fraction (such as ⅓ or ½) of the symbol period and the optical power goes to P_0 within each symbol period. RZ pulses can be generated either electrically or in the optical domain through the use of an additional modulator called a pulse carver. The former is feasible up to 10 Gbit/s whereas the latter has to be employed at bit higher bit rates up to 40 Gbit/s and beyond. The shorter pulse duration reduces the impact of inter-symbol interference (ISI), leading to a reduction of 1 to 3dB in the optical signal to noise ratio (OSNR) required to achieve a given bit error rate (BER) when compared to NRZ. This made RZ formats attractive for long haul 10 Gbit/s submarine links. However, the introduction of forward error correction FEC revitalised interest in NRZ as a lower BER could be tolerated. The narrower spectral width of NRZ also enables the denser packing of channels and therefore an increased capacity [8].

2.3.3 Advanced modulation formats

New network roll outs can be designed for optimum performance using spectrally efficient modulation formats and optimally designed fibre links. Because of the capital expense involved in deploying fibre optic links the main focus is developing technologies that can be deployed in the upgrade of existing infrastructure. Existing systems are mainly based on WDM intensity-modulation direct-detection (IM-DD) and operate at 10 Gbit/s per channel; it is not feasible to simply increase the bit rate of these systems as transmission impairments, such as dispersion and nonlinear effects, have more of an impact at higher bit rates. Instead the solution that has been adopted by the industry is to migrate to advanced modulation formats which have a higher tolerance to transmission impairments. Conventional IM-DD systems use only the amplitude to transmit information, whereas, advanced modulation formats primarily use phase to modulate the optical carrier enabling multiple bits to be transmitted per symbol [33]. In conjunction with phase, the amplitude and, or, polarisation can be exploited for modulation enabling even higher spectral efficiencies. While it is possible to transmit multiple bits per symbol using multi-level amplitude shift keying (ASK), the OSNR requirements make this impractical except for short link applications [33]. Increasing the number of bits transmitted per symbol increases the spectral efficiency for a given bit rate, it also reduces the baud rate to levels which allow the use of readily available lower cost electro-optics and high speed electronics [18, 19]. In higher order modulation formats the number of bits transmitted per symbol, *m*, is related to the number of symbols *M* by:

$$m = \log_2 M \tag{2.2}$$

In the reception of optical signals the BER is used as a figure of merit for the quality of a received signal. In characterising a received optical signal the BER is measured versus a system parameter which describes the received signal. The signal can be characterised by measuring the optical power, or by measuring the ratio of signal power to noise power. Two parameters commonly used are the signal to noise ratio (SNR) and the OSNR. The SNR is an electrical parameter and is the ratio of the received signal power versus electrical noise power and the OSNR is the ratio of optical signal power to optical noise power. The SNR is related to OSNR by [33]:

$$SNR = \frac{E_{s,avg}}{N_0} = 2\,.\,OSNR\,.\frac{\Delta f}{r_s} \tag{2.3}$$

Where $E_{s,avg}$ is the energy per symbol, N_0 is the noise power spectral density, Δf is an optical reference bandwidth and r_s is the symbol rate. Practically, a value of 12.5 GHz is normally used for Δf unless a specific value is specified [34]. The SNR can also be quoted as SNR per bit (SNR_b) and is defined as [35]:

$$SNR_b = SNR/m \tag{2.4}$$

2.3.3.1 Binary differential phase shift keying

Binary differential phase shift keying (DBPSK) is a binary modulation format where the phase of adjacent bits is used to encode the information; logic '1' is represented by π phase change in the optical carrier and logic '0' is represented by the absence of a phase change [36]. The phase of the optical carrier is modulated using either an electro-optic phase modulator or, preferably in terms of performance, an MZM. Advantages of the format include a higher tolerance to nonlinear effects in fibre transmission and up to 3 dB improved receiver sensitivity, when compared to OOK. Apart from performance advantages, a contributing factor to its deployment in

commercial systems was that it could be implemented with a relatively small increase in system complexity, when compared to existing OOK systems [33]. By placing an optical interferometer, with a one bit delay in one of its arms, in front of the photodiode, variations in phase are converted to variations in amplitude that can be directly detected. The modulation format is a strong candidate for 40 Gbit/s systems, particularly long haul links [7]. A distance of 9420 km over legacy submarine fibre has been reported using dual polarisation BPSK and coherent detection [37].

2.3.3.2 Quadrature phase shift keying

Multi-level modulation formats can achieve higher spectral efficiency than binary formats. QPSK is a multilevel format that has been extensively studied and chosen for use in state of the art commercial 100 G systems [18, 19]. Four phase states, each separated by 90°, are used to encode the data onto the optical carrier. Two bits per symbol are transmitted achieving double the spectral efficiency of binary formats. QPSK is normally generated using an in-phase quadrature (IQ) modulator. The IQ modulator is a nested MZM structure with a second phase modulator on one, or both, of the arms to introduce a phase shift of $\pi/2$ as shown in Fig. 2.5 (a). QPSK can also be generated using two phase modulators in series, where the first introduces a phase shift of 0 or π and the second 0 or $\pi/2$ [33]. Fig. 2.5 (b) shows the constellation for a QPSK signal. The spectral efficiency can be increased further through the use of more phase levels with 8PSK and 16PSK being the next logical steps. Increasing the number of phase states decreases the separation between the constellation points, and therefore increasing the SNR requirement for these formats.

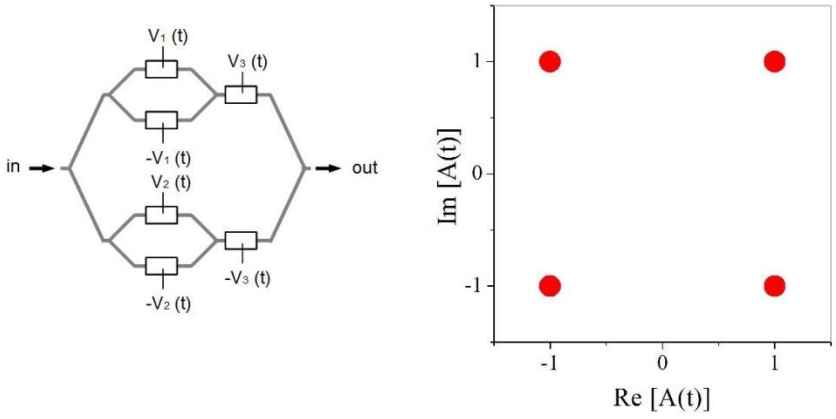

(a) (b)

Fig. 2.5 (a) IQ modulator structure and (b) QPSK constellation diagram.

2.3.3.3 16-ary quadrature amplitude modulation

Quadrature amplitude modulation (QAM) employs both the amplitude and phase to modulate the optical carrier. In higher order formats, employing phase modulation with constant amplitude, increasing the number of symbols decreases the separation between constellation points. The separation between constellation points can be increased using amplitude in combination with phase to map each point. Increasing the distance between adjoining constellation points makes it easier to identify the correct symbol at the receiver and thereby reduces the SNR requirement. The BER versus OSNR can be estimated for M-ary PSK and M-ary QAM from (2.5) and (2.6), respectively [33, 38].

$$BER_{(M)PSK} \approx \frac{2}{m} erfc\left(\sqrt{SNR}\,.\sin\left(\frac{\pi}{M}\right)\right) \tag{2.5}$$

$$BER_{Square(M)QAM} \approx \frac{2}{m}\left(1-\frac{1}{\sqrt{M}}\right) erfc\left(\sqrt{\frac{3SNR}{2(M-1)}}\right) \tag{2.6}$$

Fig. 2.6 plots BER versus OSNR obtained using (2.5) and (2.6) at a bit rate of 40 Gbit/s. To achieve a BER of 1×10^{-3} an OSNR of 17 dB is required for 16-PSK

compared to 12.6 dB for 16-QAM. Also shown is the OSNR requirement for higher order QAM formats. The higher OSNR requirements of 16-QAM, compared to QPSK, will make achieving ultra-long transmission distances challenging. Transmission distances of 1000 km are possible in systems using 16-QAM operating at a bit rate of 200 Gbit/s, this compares to distances of 2500 km in 100 Gbit/s systems where QPSK is used [39]. For 32-QAM, 64-QAM and above, the increase in the required OSNR will limit the achievable transmission distance using these formats even further. Therefore, the design of future systems may involve comprise between capacity and distance, with higher order modulation formats being preferred for shorter distances. Improving the overall noise performance of optical links can extend the transmission distance. One potential option is to decrease the spacing between optical amplifiers in the optical link in order to reduce the overall system noise [19].

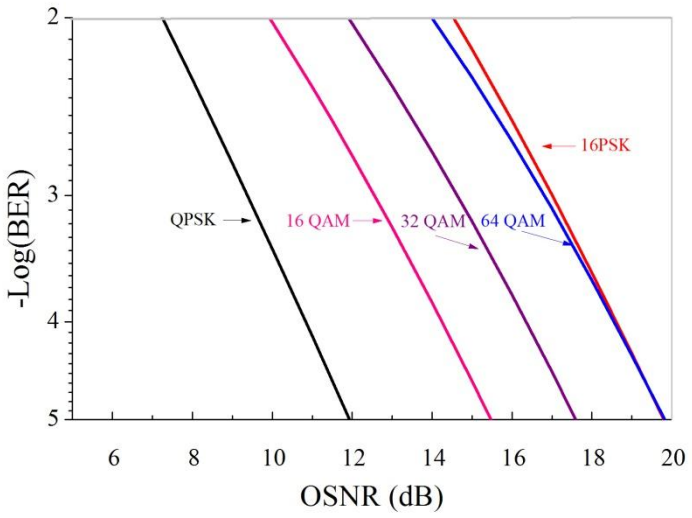

Fig. 2.6 Theoretical BER versus OSNR for phase modulation formats.

16-QAM can be generated using an IQ modulator where multi-level signals (quaternary) are applied to the I and Q inputs. The electrical requirements for the drive signals can be simplified to binary levels at the expense of increasing the complexity of the optical modulator [33].

2.3.3.4 Detection of phase modulation formats

When a phase modulated optical signal is applied to a conventional square law detector the phase information is lost. In order to detect the signal the optical phase information needs to be converted to an optical intensity which can then be detected using conventional detectors. When two optical signals are combined in a 3 dB coupler, depending on the phase difference, they either interfere constructively or destructively at the output. To demodulate the received signal a phase reference is required at the receiver. This can be generated using a delayed version of the received signal or using a second optical source to act as a phase reference; these configurations are termed self-coherent and coherent, respectively. In DBPSK an MZI with a one bit delay on one arm is placed before the photodetector. When the paths are recombined at the interferometer's output coupler, two adjacent bits either interfere constructively or destructively depending on the phase difference between them, which is 0 or π. To achieve the 3 dB improvement in sensitivity possible using DBPSK the constructive and destructive ports of the interferometer are applied to a balanced detector. This configuration can be extended for use with higher order modulation formats. However, as the order increases the complexity of the optics required also increases. For M-ary PSK as the value of M increases the SNR penalty also increases, differential detection also incurs an additional penalty with increasing M, termed the differential-detection penalty. From values of approximately 0.4 dB and 2 dB for DBPSK and DQPSK, respectively, the differential-detection penalty approaches 3 dB as M increases further; for $M \geq 8$ this limits its application to systems with sufficiently high SNR [8].

Coherent detection can be used to extract all the information relating to an optical signal (amplitude, frequency, phase and polarisation) by taking the product of the

electric fields of the modulated optical carrier and the CW LO. To detect the in-phase and quadrature components an optical quadrature front end is employed as shown in Fig. 2.7 [33]. The front end consists of a 90˚ hybrid and a pair of balanced detectors. The 90˚ hybrid consists of two optical splitters, one splits the received optical signal and the other splits the LO. A 90˚ phase shifter is inserted into one of the branches of the LO splitter. The structure of the 90˚ hybrid allows the incoming signal to be mixed with the four quadratural states associated with the reference signal in the complex-field space. The four outputs are then applied to two pairs of balanced detectors [40]. The balanced detectors give in-phase, I_I *(t)*, and quadrature, I_Q *(t)*, current outputs which can then be used to recover the full constellation. Before the transmitted signal can be recovered further processing of the signals obtained from the detector outputs is necessary. The signals are digitised using high speed analogue to digital converters and digital signal processing (DSP) of these signals is carried out. In the reception of phase modulated signals the DSP is responsible for some major tasks such as symbol timing, correction of the frequency offset between the received signal and LO, and the resolving, correcting and tracking of the phase error between the received signal and the LO [8].

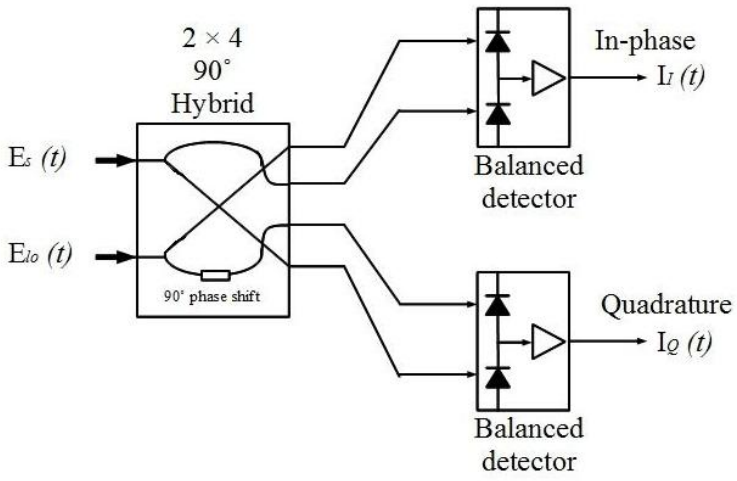

Fig. 2.7 Optical quadrature front end.

Similar to OOK, FEC can be performed in DSP but because coherent receivers recover the full information relating to the optical field it enables other functions to be carried out using DSP including compensation of chromatic dispersion and polarisation mode dispersion. Compensating for dispersion in DSP as opposed to using dispersion compensating fibre (DCF) reduces the latency of the network which would be beneficial for delay sensitive applications [41]. It also improves the received OSNR as DCF introduces loss to the link. There is also the potential to compensate for fibre nonlinear effects in DSP, however, the algorithms are quite complex and require a lot of processing power which has implications for power consumption.

2.3.3.5 Linewidth requirements for advanced modulation formats

In coherent detection the optimum performance would be achieved in an ideal case where the TX laser and LO laser are aligned in frequency and synchronised in phase. The phase noise of a laser can be characterised as a random walk process. In an observation time interval, τ, the phase, $\varphi(t)$, exhibits a random phase change of $\Delta\varphi(t) = \varphi(t) - \varphi(t-\tau)$. The phase difference between t and $t-\tau$ is Gaussian distributed with zero mean and the phase variance, $\langle\Delta\varphi^2(t)\rangle$, is proportional to the product of the observation time interval and the combined linewidth of the TX laser, $\Delta\nu_{TX}$, and the LO laser, $\Delta\nu_{LO}$,: $\langle\Delta\varphi^2(t)\rangle = 2\pi(\Delta\nu_{TX} + \Delta\nu_{LO})\tau$. The observation time interval can be related to the symbol interval in a coherent system. An increase in the linewidth or symbol interval leads to an increase in the phase variance [18, 42], which is why lower baud rate systems have more stringent linewidth requirements. In phase modulated formats increased phase variance causes broadening of the constellation points. As the separation between the constellation

points decreases for higher order modulation formats any broadening of the constellation points leads to an increased possibility of an error occurring. The sensitivity of the receiver to this phase variance is dependent on how phase synchronisation is achieved. Prior to the development of DSP, the linewidth was a critical parameter as the baud rates were lower and phase synchronisation was carried out using hardware based optical phase locked loops (OPLLs). Implementing an OPLL in hardware is not trivial and the performance achievable is very sensitive to the loop delay. In a QPSK experimental setup operating at 40 Gbit/s an OPLL with a loop delay of 12 ns had a linewidth requirement of 24 kHz [33]. Integrated solutions could enable optimisation of the OPLL design by minimising delays in the circuit. Modern coherent receivers implement algorithms to estimate the phase in DSP and this has eased the linewidth requirements. Two widely used algorithms include a decision feedback loop where a phase estimate is extracted from a number of symbols and feedforward schemes where the phase modulation is removed by raising it to the M^{th} power. Table 2.2 summarises calculated combined linewidth, $\Delta\nu$, requirements at a bit rate of 10 Gbit/s and bit period T_b for an OPLL [43], a feedback algorithm utilising a digital phase locked loop (DPLL) [35] and four implementations of feedforward based digital carrier phase estimation algorithms [35, 42, 44, 45]. Feedforward algorithms can tolerate higher linewidths than feedback algorithms based on DPLLs. The feedforward algorithm proposed in [44] reduces the linewidth requirements for 16-QAM to levels that can be achieved by standard single mode lasers such as a DFB. However, for higher order QAM formats, M > 16 and depending on the baud rate, lasers with linewidths of 100 kHz and below will still be necessary even when feedforward are used. In [45] the optimum phase noise estimate is obtained by applying a finite Wiener filter to reduce the effect of

shot-noise/amplifier noise, allowing a combined linewidth of 8 MHz to be tolerated at 10 Gbit/s for QPSK. While feedforward circuits can be designed to implement filter circuits in memory and can tolerate large linewidths, this comes at the expense of significantly more gates in the ASIC circuit and therefore increased footprint size and increased power consumption [18]. Feedback algorithms, while less tolerant to linewidth have the advantage of being simpler to implement allowing simplified ASIC circuits to be used, thereby reducing the footprint of the ASIC and importantly reducing power consumption. The availability of low linewidth laser sources allows simplified algorithms to be used in the receivers of systems.

In the reception of a coherent signal a cycle slip occurs when the phase estimate is incorrect by 90˚ in formats with square constellations. Contributing sources of cycle slips include laser phase noise, non-linear effects and amplified spontaneous emission (ASE) noise [46]. Differential encoding can be employed to prevent catastrophic failures due to cycle slips. In comparison to uncoded QPSK, differential encoded QPSK has an equivalent OSNR penalty of 1.1 dB at a BER of 1×10^{-2} [47]. Avoiding the use of differential encoding is advantageous in that it allows high coding gain soft decision FEC to be used, which can extend the reach of coherent systems. In order to dispense with differential encoding the probability of a cycle slip needs to be very low, below 10^{-17} [48]. Reducing the linewidth decreases the probability of a cycle slip; in [45] using the finite delay Wiener filter phase estimation algorithm the probability of a cycle slip drops to 10^{-18} for $\Delta\nu.T_b = 1.1 \times 10^{-5}$. For QPSK operating at a bit rate of 10 Gbit/s this corresponds to a combined linewidth of 110 kHz as opposed to a value of 8 MHz when cycle slips are not taken into account. Coherent QPSK systems operating at high bit rates would

require low linewidth devices, with combined linewidths below 1 MHz required for a bit rate of 126 Gbit/s [48].

Phase synchronisation method	QPSK		16-QAM		64-QAM		Target BER	Reference
	$\Delta\nu \cdot T_b$	Max. $\Delta\nu$, T_b = 1÷10 Gbit/s	$\Delta\nu \cdot T_b$	Max. $\Delta\nu$, T_b = 1÷10 Gbit/s	$\Delta\nu \cdot T_b$	Max. $\Delta\nu$, T_b = 1÷10 Gbit/s		
OPLL	3.5×10^{-5}	350 kHz	1.3×10^{-6}	13 kHz			1×10^{-9}	43
Feedback (DPLL) Algorithm	6.9×10^{-5}	690 kHz	7.9×10^{-6}	79 kHz			1×10^{-3}	35
Feedforward Algorithm	1.3×10^{-4}	1.3 MHz	1.5×10^{-5}	150 kHz			1×10^{-3}	35
Feedforward Algorithm	4.8×10^{-4}	4.8 MHz	6×10^{-6}	60 kHz	6×10^{-8}	600 Hz	1×10^{-4}	42
Feedforward Algorithm	2.05×10^{-4}	2.05 MHz	3.5×10^{-5}	350 kHz	6.67×10^{-6}	67 kHz	3×10^{-3}	44
Feedforward with Wiener filter	8×10^{-4}	8 MHz						45

Table 2.2. Linewidth bit rate products and maximum combined linewidth requirements for phase estimation methods.

2.4 Conclusion

The continuous growth in capacity of optical networks since they were first deployed is set to continue. This has provided the impetus for the development of innovative solutions designed to increase capacity, with the most recent example being the commercial deployment of coherent systems in the core network. To continue to meet this challenge will require on-going development of systems across the entire network and the individual components which make up those systems. The next chapter reviews the laser sources used in optical networks and discusses the development of devices for next generation optical systems.

References

[1] R. K. Snelling, “Telecommunications industry rationale for fibre-optics-a business perspective,” in LEOS Summer Topical on Broadband Analog Optoelectronics: Devices and Systems,, Monterey, Jul. 1990.

[2] A. Gladisch and F. J. Westphal, “Directions of Next Generation Transport Network Development,” in Optical Fiber Communication Conference (OFC), Los Angeles, Mar. 2012.

[3] Cisco systems Inc., White paper, “Cisco Visual Networking Index: Forecast and Methodology, 2010–2015,” 1 June 2011. [Online]. Available: http://www.cisco.com/en/US/solutions/collateral/ns341/ns525/ns537/ns705/ns827/white_paper_c11-481360.pdf.

[4] R. W. Tkach, “Scaling Optical Communications for the Next Decade and Beyond,” Bell Labs Technical Journal, vol. 14, no. 4, pp. 3-9, 2010.

[5] Cisco Systems Inc., White Paper, “Cisco Visual Networking Index: Global Mobile Data Traffic Forecast Update, 2011–2016,” 14 February 2012. [Online]. Available: http://www.cisco.com/en/US/solutions/collateral/ns341/ns525/ns537/ns705/ns827/white_paper_c11-520862.pdf.

[6] J. M. Senior, Optical Fiber Communications: Principles and Practice, 3rd ed., New York: Prentice Hall, 2009.

[7] I. Takonori, “Large-capacity Optical Transmission Technologies Supporting the Optical Submarine Cable System,” NEC Technical Journal, vol. 5, no. 1, pp. 8-12, 2010.

[8] I. P. Kaminow, Optical fiber telecommunications V: B: systems and networks, Boston: Academic Press, 2008.

[9] M. J. O'Mahony, C. Politi, D. Klonidis, R. Nejabati and D. Simeonidou, “Future Optical Networks,” Journal of Lightwave Technology, vol. 24, no. 12, pp. 4684-4696, Dec. 2006.

[10] A. A. Saleh and J. M. Simmons, “All-Optical Networking—Evolution, Benefits, Challenges, and Future Vision,” Proceedings of the IEEE, vol. 100, no. 5, pp. 1105-1117, May 2012.

[11] IEEE, “IEEE802: IEEE Standard for Local and Metropolitan Area Networks: Overview and Architecture,” 7 February 2002. [Online]. Available: http://standards.ieee.org/getieee802/download/802-2001.pdf.

[12] C. Lam, Passive Optical Networks: Principles and Practice, Boston: Academic Press, 2007.

[13] OECD, “OECD Broadband Portal, Percentage of fibre connections in total broadband (June 2011),” Jun. 2011. [Online]. Available: http://www.oecd.org/document/54/0,3746,en_2649_34225_38690102_1_1_1_1,00.html.

[14] FTTH council, “The Growth of Fiber to the Home,” Mar. 2011. [Online]. Available: http://www.ftthcouncil.org/en/content/the-growth-of-fiber-to-the-home.

[15] K. Tanaka, A. Agata and Y. Horiuchi, “IEEE 802.3av 10G-EPON Standardization and Its Research and Development Status,” Journal of Lightwave Technology, vol. 28, no. 4, pp. 651-661, Feb. 2010.

[16] V. Oksman, H. Schenk, A. Clausen, J. M. Cioffi, M. Mohseni, G. Ginis, C. Nuzman, J. Maes, M. Peeters, K. Fisher and P. E. Eriksson, “The ITU-T's new g.vector standard proliferates 100 mb/s dsl,” IEEE Communications Magazine, vol. 48, no. 10, pp. 140-148, Oct. 2010.

[17] A. Leshem and L. Youming, “A Low Complexity Linear Precoding Technique for Next Generation VDSL Downstream Transmission Over Copper,” IEEE Transactions on Signal Processing, vol. 55, no. 11, pp. 5527-5534 , Nov. 2007.

[18] K. Roberts, M. O'Sullivan, K. T. Wu, H. Sun, A. Awadalla, D. Krause and C. Laperle, “Performance of Dual-Polarization QPSK for Optical Transport Systems,” Journal of Lightwave Technology, vol. 27, no. 16, pp. 3546-3559, Aug. 2009.

[19] K. Roberts, D. Beckett, D. Boertjes, J. Berthold and C. Laperle, “100G and beyond with digital coherent signal processing,” IEEE Communications Magazine, vol. 48, no. 7, pp. 62-69, Jul. 2010.

[20] B. Zhang and S. Khatana, “From lab demo to field trial: Real-time coherent 127 Gb/s PM-QPSK transmission,” in Photonics Global Conference (PGC), Singapore, Dec. 2010.

[21] A. H. Gnauck, P. J. Winzer, S. Chandrasekhar, X. Liu, B. Zhu and D. W. Peckham, “10 × 224-Gb/s WDM transmission of 28-Gbaud PDM 16-QAM on a 50-GHz grid over 1,200 km of fiber,” in Optical Fiber Communication conference (OFC), Los Angeles, Mar. 2011.

[22] M. S. Alfiad, M. Kuschnerov, S. L. Jansen, T. Wuth, D. van den Borne and H. de Waardt, “11 x 224-Gb/s POLMUX-RZ-16QAM Transmission Over 670 km of SSMF With 50-GHz Channel Spacing,” IEEE Photonics Technology Letters, vol. 22, no. 15, pp. 1150-1152, Aug. 2010.

[23] D. van den Borne, V. Sleiffer, M. S. Alfiad and S. L. Jansen, “Towards 400G and beyond: How to design the next generation of ultra-high capacity transmission systems,” in 16th OptoeElectronics and Communications Conference (OECC), Kaohsiung, Jul. 2011.

[24] V. A. J. M. Sleiffer, D. van den Borne, V. Veljanovski, M. Kuschnerov, M. Hirano, Y. Yamamoto, T. Sasaki, S. L. Jansen and H. de Waardt, “Transmission of 448-Gb/s

dual-carrier POLMUX-16QAM over 1230 km with 5 flexi-grid ROADM passes," in Optical Fiber Communication Conference (OFC), Los Angeles, Mar. 2012.

[25] A. Al-Bermani, C. Wordehoff, S. Hoffmann, K. Puntsri, T. Pfau, U. Rückert and R. Noé, "Realtime 16-QAM transmission with coherent digital receiver," in 15th OptoeElectronics and Communications Conference (OECC), Sapporo, Jul. 2010.

[26] D. Lavery, E. Torrengo and S. Savory, "A long-reach ultra-dense 10 Gbit/s WDM-PON using a digital coherent receiver," in Optical Fiber Communication Conference (OFC), OTuB4, Los Angeles, Mar. 2010.

[27] IEEE, "IEEE 802.3™: ETHERNET," [Online]. Available: http://standards.ieee.org/about/get/802/802.3.html.

[28] ITU-T, "10-Gigabit-capable passive optical networks (XG-PON): General requirements," Jan. 2010. [Online]. Available: http://www.itu.int/rec/dologin_pub.asp?lang=e&id=T-REC-G.987.1-201001-I!!PDF-E&type=items.

[29] C. Ling, S. Dahlfort and D. Hood, "Evolution of PON: 10G-PON and WDM-PON," in Communications and Photonics Conference and Exhibition (ACP), Beijing, Dec. 2010.

[30] K. Petermann, Laser Diode Modulation and Noise, London: Kluwer Academic, 1991.

[31] W. Kobayashi, M. Arai, T. Yamanaka, N. Fujiwara, T. Fujisawa, M. Ishikawa, K. Tsuzuki, Y. Shibata, Y. Kondo and F. Kano, "Wide Temperature Range (-25C–100C) Operation of a 10-Gb/s 1.55 um Electroabsorption Modulator Integrated DFB Laser for 80-km SMF Transmission," IEEE Photonics Technology Letters, vol. 21, no. 15, pp. 1054-1056, Aug. 2009.

[32] L. A. Coldren, Diode Lasers and Photonic Integrated Circuits, Hoboken: Wiley, 2012.

[33] M. Seimetz, High-Order Modulation for Optical Fiber Transmission, Berlin: Springer, 2009.

[34] R. Hui and M. O'Sullivan, Fiber Optic Measurement Techniques, Burlington: Elsevier Academic Press, 2009.

[35] E. Ip, A. Pak Tao Lau, D. J. F. Barros and J. M. Kahn, "Coherent detection in optical fiber systems," Optics Express, vol. 16, no. 2, pp. 753-791, Jan. 2008.

[36] P. J. Winzer and R. J. Essiambre, "Advanced Modulation Formats for High-Capacity Optical Transport Networks," Journal of Lightwave Technology, vol. 24, no. 12, pp. 4711-4728, Dec. 2006.

[37] V. A. J. M. Sleiffer, V. Veljanovski, D. van den Borne, J. Capasso, H. Kuluslu, J. Seixas, V. Schramm, A. Tschersich, R. Nogueira, N. B. Pavlovic, K. Ivarson, S. Spaelter and H. de Waardt, "45.8 and 125 Gb/s CP-QPSK/CP-BPSK Field Trial Over Installed Submarine Cable," Journal of Lightwave Technology, vol. 30, no. 4, pp. 624-633, Feb. 2012.

[38] J. G. Proakis, Digital communications, Boston: McGraw-Hill, 2001.

[39] M. W. Chbat and S. Spalter, "From 100G to 1000G: Is there a straight road ahead?," in European Conference and Exhibition on Optical Communication (ECOC), Torino, Sept. 2010.

[40] Optoplex Inc., "White paper: Optical Hybrid Enables Next-Generation Optical Communication," 2006. [Online]. Available: http://www.optoplex.com/download/coherent_detection_and_optical_hybrid.pdf.

[41] T. Schmidt, C. Malouin, B. Zhang, R. Saunders, J. Hong and R. Marcoccia, "100G coherent DWDM transponder module enabling seamless upgrade of long haul optical transmission systems," in Optical Fiber Communication conference (OFC), Los Angeles, Mar. 2010.

[42] M. Seimetz, "Laser Linewidth Limitations for Optical Systems with High-Order Modulation Employing Feed Forward Digital Carrier Phase Estimation," in Optical Fiber communication conference, Los Angeles, Feb. 2008.

[43] E. Ip and J. M. Kahn, "Feedforward Carrier Recovery for Coherent Optical Communications," Journal of Lightwave Technology, vol. 25, no. 9, pp. 2675-2692, Sept. 2007.

[44] T. Pfau, S. Hoffmann and R. Noe, "Hardware-Efficient Coherent Digital Receiver Concept With Feedforward Carrier Recovery for M-QAM Constellations," Journal of Lightwave Technology, vol. 27, no. 8, pp. 989-999, April 2009.

[45] M. G. Taylor, "Phase Estimation Methods for Optical Coherent Detection Using Digital Signal Processing," Journal of Lightwave Technology, vol. 27, no. 7, pp. 901-914, Aprl. 2009.

[46] Y. K. Lize, C. Malouin, E. Ibragimov, B. Zhang and T. Schmidt, "Implementation challenges of 100G coherent transponders," in IEEE Photonics Society Summer Topical Meeting Series, Playa del Carmen, Jul. 2010.

[47] T. Mizuochi, Y. Miyata, K. Kubo, T. Sugihara, K. Onohara and H. Yoshida, "Progress in soft-decision FEC," in Optical Fiber Communication Conference (OFC), Los Angeles, Mar. 2011.

[48] E. Ibragimov, B. Zhang, T. J. Schmidt, C. Malouin, N. Fediakine and H. Jiang, “Cycle slip probability in 100G PM-QPSK systems,” in Optical Fiber Communication conference (OFC), Los Angeles, Mar. 2010.

Chapter 3

Single mode lasers

This chapter gives an overview of semiconductor laser diodes and looks at the materials and structures used in their fabrication. Approaches used to achieve single mode operation are considered, and characteristics important in optical communication applications are discussed.

3.1 Semiconductor materials

Semiconductor laser diodes are manufactured from the III/V group of semiconductor materials. These are direct bandgap materials in that the minimum of the conduction band and the maximum of the valence band have the same wave vector. A number of ternary and quaternary compounds have been developed to produce lasers, and LEDs, emitting light from the visible to the mid-infrared region of the spectrum. The semiconductor wafers are eptaxially grown by depositing different layers of material on a substrate. A prerequisite to successfully grow defect-free layers is that the lattice constants of the deposited layer and the material it is deposited on match. However, as the lattice constants of different semiconductor materials do not naturally match, matching has to be created artificially using ternary and quaternary compounds [1].

The ternary AlGaAs material system can be used to produce lasers operating from 0.7 μm to 0.9 μm, with the structures grown on GaAs substrates. By replacing Ga atoms with Al atoms the lattice constant of any $Al_xGa_{1-x}As$ alloy will match that of the substrate. The subscript x denotes the relative number of Ga atoms that are replaced with Al atoms. Changing the material composition by adjusting x changes the band gap energy (E_g) of the material, which can be approximated by the simple linear relation [1]:

$$E_g(x) = 1.424 + 1.247x \qquad (0 < x < 0.45) \tag{3.1}$$

Lasers designed for fibre optic communications are primarily based on two quaternary material systems, $In_{1-x}Ga_xAs_yP_{1-y}$ and $In_{1-x-y}Ga_xAl_yAs$, both of which are grown on InP substrates. The composition of these quaternary compounds is determined by the values of x and y. InGaAlAs laser diodes are attractive for uncooled applications as they show improved static and dynamic performance at high ambient temperatures, compared with lasers made in the InGaAsP material system. This is primarily attributed to their larger conduction band offset of $\Delta E_c = 0.7E_g$, compared to a value of $\Delta E_c = 0.4E_g$ for the InGaAsP material system [2]. Increasing the conduction band offset reduces electron heterobarrier leakage from the active region at high temperatures, and the material's increased electron effective mass produces a higher differential gain. An advantage of InGaAsP is that it is easier than InGaAlAs to process, where great care is required to prevent unintended oxidation of the Al bearing layers, which would compromise material integrity and performance.

The three most common epitaxial growth techniques used are liquid phase epitaxy (LPE), molecular beam epitaxy (MBE) and organometallic vapour-phase epitaxy

(OMVPE). OMVPE is also referred to as metal-organic chemical vapour deposition (MOCVD) [2]. Using a semiconductor substrate as a base material, layers with different thickness and material composition are grown, one on top of the other, to form the laser structure. Accurate control of the material composition and layer thickness is required to ensure that the laser performs as designed.

3.1.1 Multi-quantum well structures

The first semiconductor lasers used a bulk active region, consisting of a layer of intrinsic semiconductor material with a thickness in the region of 100 nm to 300 nm. In such a structure the carriers are confined within a three dimensional potential well. When the thickness of the heterostructure is reduced to the extent that it is comparable to the de Broglie wavelength of the carrier, referring to the coordinates shown in Fig. 3.1, the kinetic energy corresponding to the carrier motion along the y direction is quantised. Since the electrons are still free to move in the x and z directions this leads to a two dimensional quantisation of the density of states [3]. A device with one thin active region such as this is called a single quantum well (SQW) laser. Improved device performance can be achieved from a multi-quantum well (MQW) structure [4], where multiple thin active layers are effectively stacked, one on top of the other. The individual quantum wells are separated by thin barrier layers of semiconductor material with a higher band gap than the quantum well layers. The typical thickness of the quantum well and barrier layers is in the region of 5 to 20 nm. The energy band diagram for a MQW laser is illustrated in Fig. 3.2(a). Fig. 3.2(b) illustrates the density of states for a MQW device where it has a step like progression, also shown is the density of states for a bulk device which displays a

parabolic change in the density of states for a corresponding change in the carrier density [3, 5].

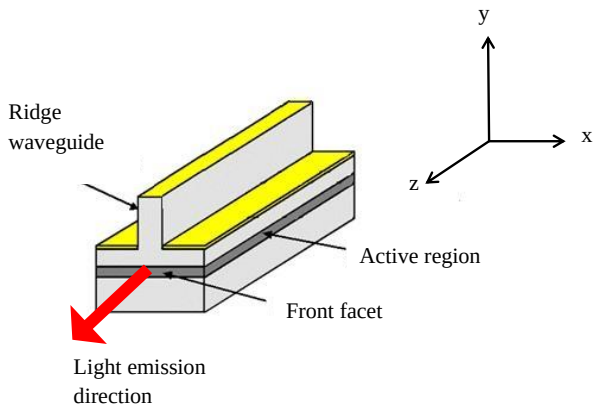

Fig. 3.1. Schematic of an in-plane ridge waveguide laser diode.

The properties of a quantum well laser can be improved by introducing strain to the active region. When depositing very thin layers, with a thickness of 10 nm or less, a small lattice mismatch, of 1.5 % or less, can be tolerated. The crystal lattice of the thin deposited layer (a_0) distorts to match that of the substrate lattice (a_1) in the plane, introducing strain in the structure. Compressive or tensile strain can be generated by making $a_0 > a_1$ or $a_0 < a_1$, respectively [2, 4].

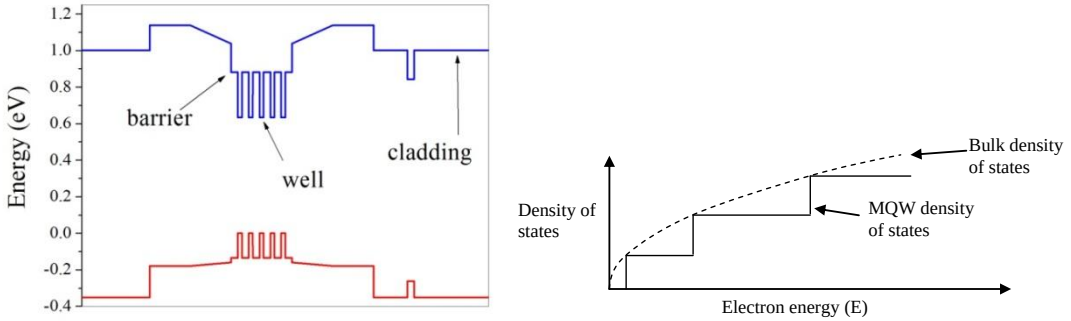

(a) (b)

Fig. 3.2. MQW (a) energy band diagram and (b) density of states (solid line), also shown is the density of states for a bulk structure (dashed line).

3.2 Carrier and photon confinement

The most efficient type of laser is the electrically pumped semiconductor laser diode. Overall power conversion efficiencies of ≈ 50 % are not uncommon, compared to ≈ 1 % for gas and solid state lasers. The higher efficiencies of diode lasers have also been exploited by solid state lasers, where incoherent optical flash lamp sources are replaced with diode laser pump sources [2]. An ideal laser diode generates a photon for each injected carrier, with the photons being emitted in a controlled way so as to maximise the amount of photons collected at the output. The efficiency of a real device is determined by how well injected carriers and generated photons are confined to the active region, and a number of structures have been developed which achieve confinement in both the transverse and lateral directions.

3.2.1 Transverse confinement

Confinement is achieved in the transverse direction through the design of the material layer structure. Modern semiconductor lasers are based on the double heterostructure, where an intrinsic active region is sandwiched between highly doped p and n cladding layers. The cladding layers have a higher conduction-valence band energy gap ensuring that recombination of carriers can only take place in the active region. The intrinsic active region, with its lower band gap, has a slightly higher refractive index than the cladding layers and forms a dielectric waveguide in the transverse direction [2]. In comparison to homojunctions, the double heterostructure reduces the threshold currents necessary for lasing by a factor of ≈ 100, enabling the development of modern semiconductor lasers [5, 6]. When quantum-well active regions were first developed the thin dimensions of these structures produced weak optical confinement. While MQWs did achieve higher confinement, the most

efficient solution was to add additional layers to act as passive waveguides forming a structure called a separate confinement heterostructure (SCH) [4]. The SCH effectively separates the design of the quantum well active region from the optical confinement structure [6].

3.2.2 Lateral confinement

Confinement in the lateral direction is achieved by modifying the layers which were uniformly deposited during the wafer growth. A structure with no lateral confinement, apart from roughening the sides of the chip, is a broad-area structure. Current is applied to the entire area of the substrate and light is emitted across the width of the device. In modern applications such an inefficient structure is of limited use, apart from quality control. Structures designed to achieve confinement in the lateral direction have two main classifications, gain guided and index guided.

3.2.2.1 Gain guided structures

In a gain guided structure the optical mode is determined by the width of the optical gain region. In contrast to a broad area device, current injection is limited to a defined region of the junction, the dimensions of which determines the width of the gain region. The simplest method used to achieve this is an oxide stripe structure, where SiO_2 oxide layers are formed at either side of the p contact layer. The SiO_2 layers are insulating layers, therefore current only flows through the contact layer to the active region under the p layer. Gain guided structures can also be fabricated using a proton stripe structure where implanted ions (protons) create damage and trap out mobile charge carriers, forming a highly resistive region at either side of the p contact layer [2, 3]. Prior to the development of viable etching and regrowth

techniques, these structures were used [2]. In comparison to index guided structures, discussed in the next section, gain guided structures are inefficient which limits their suitability in most application areas. However, along with broad area devices, they are useful in process control as the material quality can be characterised independently of the processing steps.

3.2.2.2 Index guided structures

In an index guided structure the optical mode is formed by a region of higher refractive index and the light is confined in a manner similar to an optical fibre. Index guided structures can be described as weakly index guided or strongly index guided [3]. The ridge waveguide structure combines current confinement with weak index guiding of the optical mode. The ridge provides loading for index guiding, while also acting as a narrow current confining strip [5, 3]. Optical lithography and standard etching processes, such as inductive coupled plasma (ICP) dry etching, are used to realise the ridge. The efficiency of the structure can be high, but because the etching process used to form the ridge stops just above the active region, a portion of the injected carriers can still diffuse laterally and recombine without contributing to gain [2]. Fig. 3.3 (a) shows a facet view of a fabricated ridge waveguide taken using a scanning electron microscope (SEM). Fig. 3.3 (b) shows a picture of the top surface of a ridge waveguide laser chip. The ridge width is 2 μm in this device.

A buried heterostructure achieves strong confinement of carriers and photons. The active region is completely surrounded by material with a wider bandgap and lower refractive index; electromagnetically the active region forms a rectangular dielectric waveguide. In comparison to the ridge waveguide structure, it is a more complex structure, requiring a multistep growth process. Fig. 3.4 shows a cross section of one

type of structure called a semi-insulating buried heterostructure. In this example, material is etched away from either side of the active region. The wafer is placed back in the growth chamber and semi-insulating semiconductor material is regrown to replace the material that was removed. There are a number of variations in the structures that can be used to produce buried heterostructures but most employ a regrowth step [2, 5].

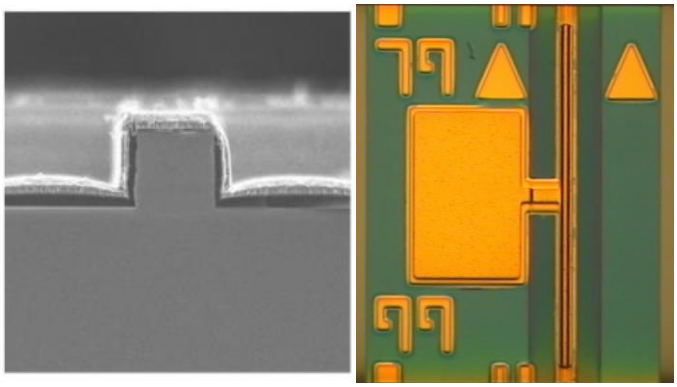

(a) (b)

Fig. 3.3. Ridge waveguide (a) SEM image showing the front facet view and (b) a picture of the top-surface of a fabricated laser diode chip.

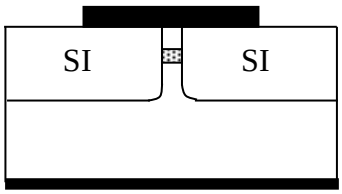

Fig. 3.4. Buried hetrostructure with regrown semi-insulating semiconductor material.

3.3 Lasers for optical communications

Semiconductor laser diodes are the predominant optical source used in fibre optic communications, providing transmitter sources as well as pump sources for optical amplifiers. The devices used in the industry range from Fabry Pérot (FP) lasers to more complex integrated tuneable modules. The first optical links used multimode

FP lasers, however, the achievable bit-rate distance product was limited by dispersion effects in optical fibre and mode partition noise in the laser [7, 8]. Increasing the bit-rate distance product provided the incentive to develop single longitudinal mode lasers. This was particularly important in exploiting the lower loss window at 1550 nm, as single mode operation was essential in minimising the effects of higher dispersion in standard single mode fibre (SSMF) at this wavelength. Optical communication applications employing single mode lasers specify a high degree of spectral purity. The ratio of power in the single mode to the power in the FP modes is a key figure of merit, characterised by the side mode suppression ratio (SMSR), and for most applications a value greater than 30 dB is required. A number of approaches have been developed to achieve single mode operation, but the basic principle is to provide a filter mechanism, either internal in the laser cavity or external, which delivers selective feedback to the laser cavity in order to select a particular operating wavelength [2]. Fig. 3.5 shows typical optical spectra from (a) an FP laser and (b) a single mode laser. A root-mean-square (rms) spectral width of 2 to 4 nm is typical for FP lasers, whereas values << 1 nm are required for single mode lasers.

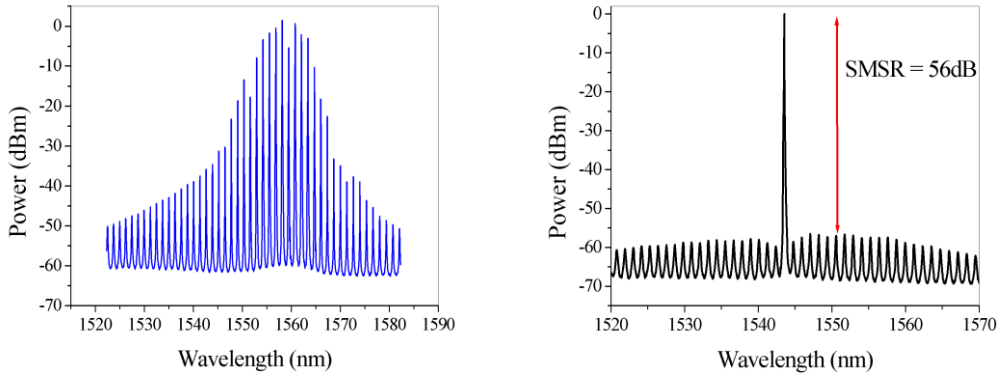

(a) (b)

Fig. 3.5. Optical spectrum from (a) an FP laser and (b) a single mode laser.

3.3.1 Fabry Pérot lasers

The simplest semiconductor laser diode structure is the FP laser, where a resonator is formed by placing a gain medium between two mirrors. The mirrors in this case are formed by the cleaved laser facets, which if left uncoated have a reflectivity of ≈ 30 %. The amount of light emitted from the front facet can be increased by placing a high reflectivity (HR) coating on the back facet (>90 % typical) and a low reflectivity (LR) coating on the front (10 to 30 % typical). In contrast to single mode lasers, which will be discussed in subsequent sections, FP lasers have no frequency selective elements and produce a multimode spectrum. The spectral modes are equally spaced in frequency, ν, by $\Delta\nu = c/2nL$, where c is the speed of light, n is the group index of the waveguide and L is the cavity length [9]. FP lasers are still an important source in optical communications, particularly in short reach applications. As FPs are mainly used in low cost applications, ridge waveguide devices are preferred; also, the relative simplicity of the structure makes it cost effective to produce, with high yields, theoretically 100 %. In the low dispersion window at 1310 nm, directly modulated lasers FP lasers can achieve relatively high bit rates over short distances. In [8] it has been shown that by optimising the centre wavelength, to take account of dispersion in single mode fibre, a transmission distance of 7 km can be achieved in the 1310 nm window at 10 Gbit/s. At 1550 nm the performance is limited by dispersion but they are still an important device for lower speed short reach applications.

3.3.2 Single mode lasers

3.3.2.1 Distributed feedback laser

The distributed feedback (DFB) laser has become the predominant single mode laser used in fibre optic communications. Single mode operation is achieved by etching a corrugated grating along the entire length of the cavity, as shown in Fig 3.6 (a) [2]. Instead of the facet mirrors, the reflections necessary for laser operation are now provided by the grating, but unlike the facet mirrors, the grating is designed to provide a selective reflection at one particular wavelength called the Bragg wavelength. The reflection, or feedback, is achieved through Bragg diffraction, a phenomenon that couples the waves propagating in the forward and backward directions in the cavity. Coupling only occurs when the Bragg condition is satisfied at a wavelength, $\lambda_b = 2n\Lambda/m$, where n is the phase refractive index of the waveguide mode, Λ is the period of the grating, and m is the order of the grating. Most modern DFBs use first order gratings, $m = 1$, as it provides the strongest coupling between the backward and forward direction [1]. In theory a standard DFB with both facets perfectly anti-reflection (AR) coated and without any phase shifts in the grating will have two modes located symmetrically on either side of the Bragg wavelength; both modes experience the same low threshold gain and therefore lase simultaneously [5, 10]. In practice when cleaving the laser chip a random phase shift is introduced at both facets which reduces, but not eliminates, the possibility of this degeneracy occurring. Normally devices are AR coated on the front facet and a HR coating is applied to the back facet. This has been shown to increase the yield by increasing the asymmetry between the two competing modes, while also increasing the output power from the front facet [10]. To improve the performance of the DFB

it is desirable to leave a fraction of a wavelength shift near the centre of the cavity, as shown in Fig. 3.6 (b), where the grating is shifted by $\lambda_b/4$. This produces a phase shift of $\pi/2$ and facilitates lasing at the Bragg wavelength [2, 1]. These are called quarter wave shifted DFBs.

In comparison to an FP wafer, the fabrication of a DFB wafer is more complex requiring additional steps. The grating is formed by transferring the grating pattern to a resist using a high precision lithography technique, such as Ebeam. The patterned resist acts as a mask for a chemical etching process used to form the grating. After formation of the grating, the wafer is placed back in the growth chamber and additional layers are deposited in a second regrowth step [1].

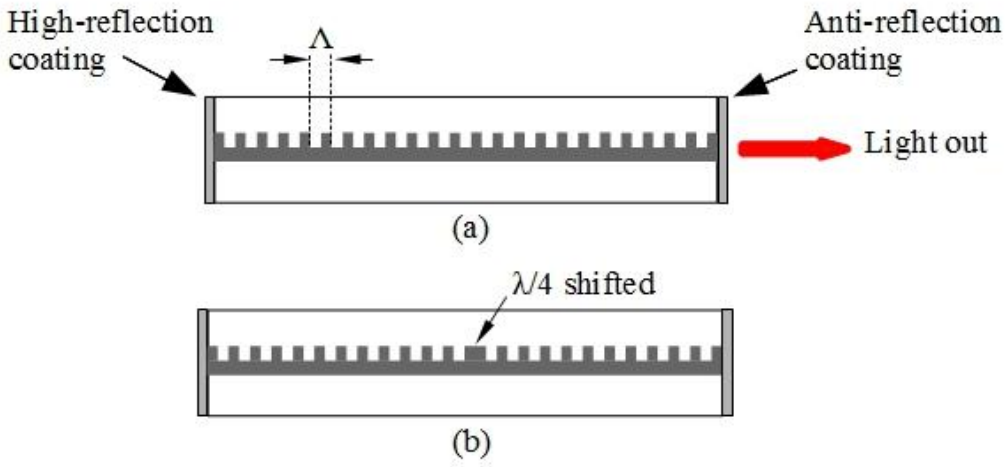

Fig. 3.6. Schematic for (a) standard DFB and (b) quarter wave shifted DFB.

3.3.2.2 Distributed Bragg reflector laser

In a distributed Bragg reflector (DBR) laser one, or both, of the facet mirrors is replaced with a passive grating reflector. In comparison to a DFB, where the grating is embossed on the active material over the entire cavity length, the grating in a DBR is formed in a passive section at one, or both, ends of the laser, as shown in Fig. 3.7 [1]. The processing required to fabricate a DBR is quite complex. Active and

passive sections are grown in a multistep growth process, and very accurate control of the layer thickness is required to ensure coherence along the axial direction. Because the DBR process is more complex than the DFB manufacturing process, DBRs are not normally used as single frequency devices, but instead utilised when their unique properties are required [2]. Multi-section devices have been fabricated where the gain, phase and Bragg frequency can be independently controlled via separate bond pads in order to tune the wavelength. Widely tuneable lasers covering the entire C or L-band have been commercialised based on multi section DBRs called sampled grating DBRs (SGDBR). Instead of periodic gratings, a periodic modulation is introduced enabling tuning over a wide wavelength range.

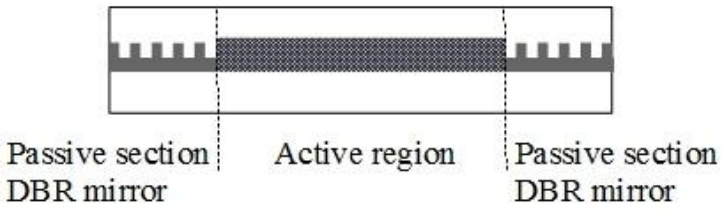

Fig. 3.7. Schematic of a DBR laser.

3.3.2.3 Vertical cavity surface emitting laser

The emission direction in a vertical cavity surface emitting laser (VCSEL) is perpendicular to the wafer surface, making it possible to achieve very short cavities, as the cavity length is dependent on the layer thickness and not the cleaved cavity length. The device is grown in a stack like process and the structure is illustrated in Fig. 3.8, where a cross section shows the active region sandwiched between two high reflectivity DBR mirrors [1]. As the gain region is very short, mirrors with high mean reflectivity, typically > 99 %, are required, in order to produce an efficient device [2]. The DBR mirrors produce a relatively wide mirror loss minimum, compared to that achieved in an in-plane DBR laser. This is offset by the VCSELs

short cavity, which increases the mode spacing so that adjacent modes experience a higher mirror loss. When the gain curve of the laser is taken into consideration, the roll-off in gain experienced by the adjacent modes is more important than the roll-up in the mirror loss in achieving single mode operation [2]. Current confinement can be achieved by ion implantation, where ions are implanted to a selected area making it non-conducting. The top of the device is metallised for contacting but a circular aperture is created for light emission. The device produces an emitted beam with a circular far field, which is beneficial when coupling light to an optical fibre. An advantage of VCSELs, over edge emitters, is that the surface emitting geometry facilitates wafer level testing of the devices. A high level of precision is needed in the growth of a VCSEL wafer, as the single mode wavelength has a high dependence on the thickness of the structure's epitaxial layers. Specifically, a 1% change in thickness of the structure's epitaxial layers will result in a 10 nm shift in the cavity resonance [11] with consequent variation in the lasing wavelength, threshold gain and threshold current. The VCSEL's short cavity length places significant demands on the high mirror reflectivity required to allow lasing. For short wavelengths the AlGaAs material system can provide high reflectivity (>0.999) from two dozen periods. Unfortunately, lattice matched semiconductor materials in the InP material system have low absorption at long wavelengths and provide insufficient index contrast. This makes the realisation of highly reflective mirrors difficult, requiring an impractically large number of mirror pairs. Therefore, in this system usually one, or both, of the mirrors is formed by non-epitaxial growth [2, 12], which is undesirable as it adds an additional high complexity step to the fabrication process.

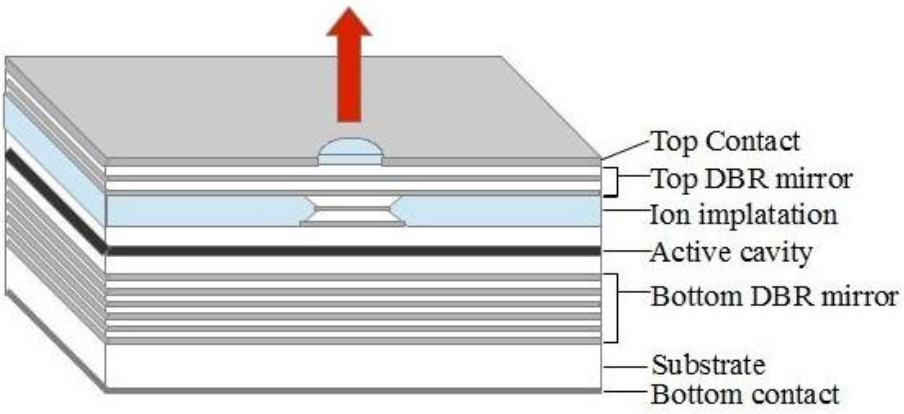

Fig. 3.8. Cross section of a VCSEL.

3.3.2.4 External cavity laser

In the ECL the reflective element, which provides the frequency specific feedback, is external to the laser chip. The optical gain is provided by an FP laser with an AR coated front facet, to suppress the FP modes, and is also referred to as a gain chip. A number of different types of ECL have been developed, ranging from single frequency devices, to more complex widely tuneable devices, and the following are some examples of different types. Using a fibre Bragg grating as the reflective element a device with a relatively simple structure can be produced, where the Bragg grating is written on the fibre used to couple light from the laser chip [13]. A disadvantage of a fibre grating device is a high sensitivity to vibrations [14]. A more advanced approach uses a silicon based planer lightwave circuit (PLC), where the Bragg grating is etched into a silicon waveguide and the laser chip is bonded in place to the PLC, as shown in Fig. 3.9 [14, 15]. The PLC approach produces a more rugged component, which is less sensitive to vibrations. Careful alignment of the chip and waveguide is necessary to achieve good coupling efficiency. The wavelength of operation is set by the grating, but a small amount of wavelength tuning is still possible by adjusting the temperature. In [16] a change in the peak wavelength of

0.014 nm / ˚C was reported for a PLC based device; however, mode hopping was observed in this device over a temperature range 16 to 42 ˚C.

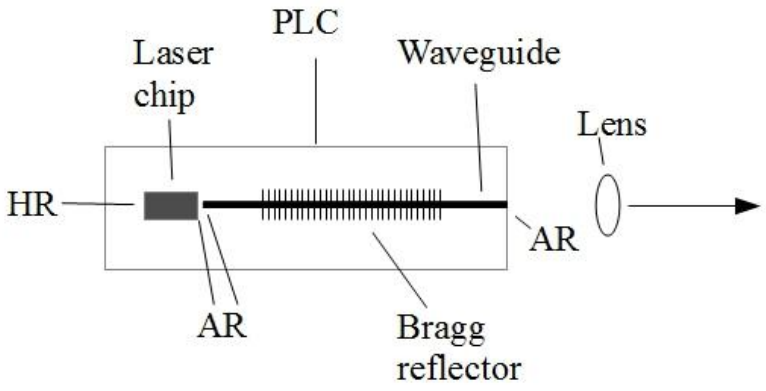

Fig. 3.9. Schematic of an ECL based on a PLC platform [14].

Tuneable ECLs can be realised using diffraction gratings to select different longitudinal mode numbers by controlling the angle of the grating, or the angle at which light hits the grating, to provide selective feedback to the laser. Two commonly used configurations are Littrow and Littman. In the Littrow configuration the operating wavelength is selected by rotating the grating, as shown in Fig. 3.10 (a). In the Littman configuration, shown in Fig. 3.10 (b), the light from the grating hits a reflective element, either a mirror or a prism, and the feedback to the laser is controlled by the angular position of the reflective element. As the grating is fixed, the position of the output beam remains constant. Littrow and Littman ECLs have different characteristics making them suitable for different types of applications. The Littrow ECL is easy to align, cost effective and has a larger output power than Littman ECL. The main drawback is that the position of the beam moves when tuning the wavelength. If wavelength tuning of more than a few GHz is required and the positional stability of the beam is a requirement, as is the case when coupling to an optical fibre, the Littman resonator is preferable [17].

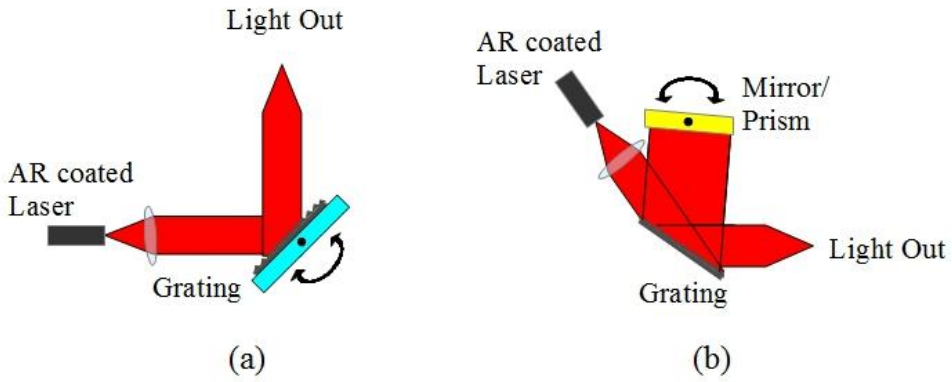

Fig. 3.10. ECL in (a) Littrow configuration and (b) Littman configuration [17].

A second, more compact, ECL structure uses two thermally tuneable silicon etalon filters to select the operating wavelength [18, 19]. A simplified diagram of the structure is shown in Fig. 3.11. The silicon etalon filters form a pair of FP filters with slightly differing periods. Tuneability is achieved using the Vernier effect, and full C or L-band coverage can be achieved. To select a particular wavelength the temperature of the first etalon is adjusted to place a transmission peak at the target wavelength. The temperature of the second etalon is also adjusted to place a peak in its transmission curve at the same target wavelength. Because of the slightly differing periods of the two etalons the target wavelength is the only wavelength at which two transmission peaks coincide, and the transmission is a maximum at this point. Light at the target wavelength passes through the filter and is reflected by the mirror back to the laser chip [20]. Precise independent temperature control of the two silicon filters is necessary to suppress mode hopping. Such a device can achieve linewidths below 100 kHz, however the increased complexity increases the packaging cost, compared to monolithic lasers or fixed frequency ECLs.

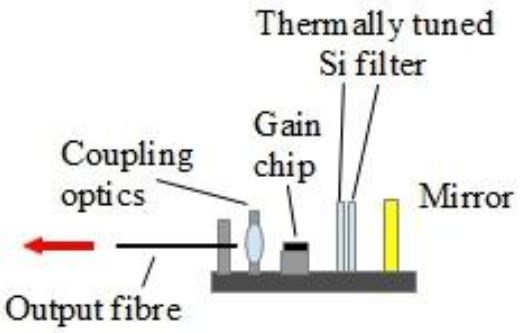

Fig. 3.11. ECL using thermally tuneable silicon etalon filters for wavelength selection.

3.4 Single mode laser characteristics

Single mode lasers are used in many different application areas in fibre optic communications. In this section some of the main parameters of interest are discussed.

3.4.1 Light-current characteristic

The light-current (L-I) characteristic is one of the most common measurements carried out on laser diodes. From it parameters such as the threshold current, slope efficiency, and linearity are extracted, which can be used to assess the quality of the laser. In uncooled applications the performance over temperature has to be considered. The efficiency of a laser diode decreases at higher temperatures, resulting in an increase in the threshold current and a decrease in the slope efficiency. Typically, the laser threshold will increase exponentially with temperature as,

$$I_{th} = \mu \exp\left(\frac{T}{T_0}\right) \tag{3.2}$$

where μ is a constant, T is the laser temperature in Kelvin and T_0 is the "characteristic temperature" of the laser. The parameter T_0 is often used to express the temperature sensitivity of a laser's threshold current [1, 21].

When a laser chip is packaged, the chip to fibre coupling efficiency achieved is a key parameter, as together with the slope efficiency from the chip it determines the overall slope efficiency of the module. The coupling efficiency can be easily determined by comparing the L-I's from the module and the chip prior to packaging. A laser package usually incorporates a monitor photodiode, which collects the light from the laser's back facet. The signal from the photodiode can be applied to a feedback circuit in the laser driver in order to control the output power from the module. In uncooled applications this is used to keep the optical power constant over the operating temperature range. Changes in the coupling efficiency can result in inaccuracies between the monitor photodiode current and the expected output power from the module. Variations which occur over temperature can be characterised by measuring a modules L-I at different temperatures, from which, an extracted parameter called the tracking error can be used to quantify the error. Causes of tracking error include instabilities in the output beam from the laser chip, such as a shift in the far field with temperature, or bias current, and changes in the mechanical alignment of the light coupling optics.

3.4.2 Side mode suppression ratio

Single mode lasers need to maintain a high SMSR under all operating conditions, which may include modulation of the bias current and operation over a specified temperature range. For most applications a minimum SMSR of 30 dB is required and this can be met by modern devices which can deliver typical values greater than 40 dB. For most applications continuous tuning, i.e. no mode hops, over the operating temperature and bias current ranges is required.

3.4.3 Relative intensity noise

When a laser is operated CW the carrier and photon densities are not constant, instead random carrier and photon recombination and generation events produce instantaneous time variations in the carrier and photon densities [2]. These random variations lead to variations in the magnitude of the output power from the laser, creating a noise source that is referred to as the relative intensity noise (RIN), defined by:

$$RIN = \frac{(\Delta P)^2}{(P_{AVG})^2} \tag{3.3}$$

where $(\Delta P)^2$ is the mean square intensity-fluctuation spectral-density of an optical signal and P_{AVG} is the average optical power. RIN can limit the performance of optical systems; therefore, low RIN is desirable for these systems.

3.4.4 Modulation bandwidth

The modulation bandwidth determines the maximum data rate that can be transmitted by a directly modulated laser. Fig. 3.12 shows the amplitude versus frequency response, or S21, for a typical single mode laser measured using a vector network analyser (VNA). The maximum achievable data rate can be estimated from the 3 dB bandwidth point, F_{3dB}, shown in the figure. It can be assumed that the minimum bandwidth required for a digital link is 75 % of the link bit rate; however, in order to optimise performance and yield most lasers are designed to exceed this minimum. At a chip level the relaxation oscillation frequency, F_r, limits the achievable bandwidth. It can be measured using a VNA, as shown in Fig. 3.12, or from the RIN spectrum. Using the RIN spectrum allows the intrinsic frequency response of the laser to be determined without the influence of electrical parasitics. F_r is given by,

$$F_r = \frac{1}{2\pi}\sqrt{\frac{\nu_g g' S}{\tau_{ph}}} \tag{3.4}$$

where ν_g is the group velocity, g' is the differential gain, S is the average photon density inside the active layer, and τ_{ph} is the photon lifetime in the cavity [6]. As evident from (3.4) increasing the photon density, by increasing the output power from the laser, is one approach to increase F_r; however, increased damping of the resonance at high powers, thermal limitations and high power facet damage set practical limitations on the output power that can be used [2]. A further consideration is that the drive current and output power levels need to meet the specification of the target application. As discussed previously, MQW lasers have a higher differential gain and provide a platform for designing high speed lasers at relatively low drive currents (< 100 mA) [6].

In a packaged device the electrical performance of both the chip and the packaging platform has to be optimised. Electrical parasitics can limit the high speed performance and steps such as minimising the size of the bond pad and using a deep ridge etch or current blocking layers in the longitudinal direction, parallel to the laser cavity can be employed to reduce the capacitance of the laser chip. When packaging high speed laser chips the packaging platform is carefully designed to optimise its high speed performance. This involves choosing materials, such as TO-can headers or high speed butterfly packages, that are designed for high speed operation. At 2.5 Gbit/s the connections within the package can be made with wire bonds, but at higher speeds of 10 Gbit/s and above the length of the wire bonds need to be minimised, in order to reduce parasitic inductance [22]. An alternative to wire bonds is to use transmission lines on specially designed submounts to distribute the high

speed signals within the package, while wirebonds are still used the length can be significantly reduced.

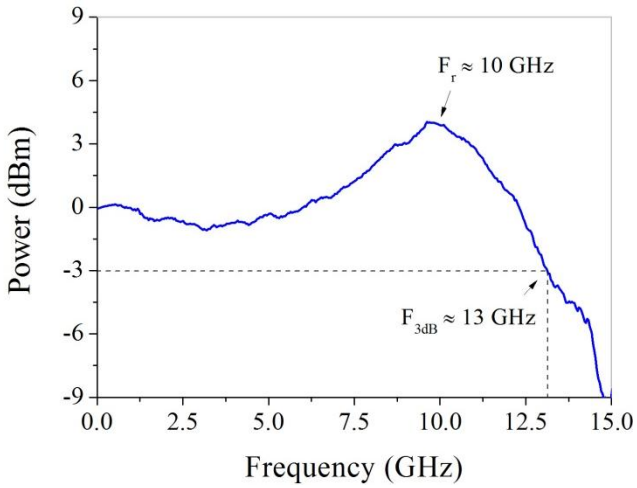

Fig. 3.12. Modulation response of a single mode laser, with an extracted 3 dB bandwidth of 13 GHz.

3.4.5 Linewidth

The spectral width of a single mode laser has a finite value, which is termed the linewidth, and is an important parameter in fibre optic communication systems employing advanced modulation formats. The emission linewidth behaviour of a semiconductor laser diode operating above threshold can be described by the modified Schawlow-Townes expression [9],

$$\Delta\nu = \frac{\hbar\omega v_g^2 g_{th}\alpha_m n_{sp}}{8\pi P_e}(1+\alpha^2) \tag{3.5}$$

where, ħ is the reduced Planck constant, ω is the angular frequency, v_g is the group velocity, g_{th} is the threshold gain, α_m is the mirror loss per unit length, n_{sp} is the spontaneous emission factor, P_e is the emitted power and α is the linewidth enhancement factor. The term $g_{th} = \alpha_m + \alpha_i$ where α_i is the intrinsic loss in the cavity. The mirror loss is obtained from,

$$\alpha_m = \frac{1}{2L} \ln\left(\frac{1}{R_1 R_2}\right) \tag{3.6}$$

where L is the cavity length, R_1 and R_2 are the front and back facet reflectivities, respectively. From these expressions it is evident that the linewidth can be reduced by (i) increasing the output power, (ii) reducing the laser linewidth enhancement factor and (iii) reducing the mirror loss. Therefore, it is desirable to operate the laser at high bias currents in order to achieve higher output powers. Also, high output power can be achieved through design of the laser and epitaxial structure. However, other design parameters, such as the maximum bias current allowable for the application, have to be taken into account. The α factor is largely dependent on the material properties. Quantum well structures have a lower α factor compared to bulk structures [1], and it can be decreased by adding strain to the quantum well active region and can be further decreased by adding p-doping in the strained active region [23]. The α factor is also dependent on the wavelength, and the value varies across the laser's gain curve with lower values being observed at shorter wavelengths [7]. Therefore, detuning the peak wavelength to the shorter side of the gain peak will reduce the linewidth. As evident from (3.6), α_m can be reduced by increasing the cavity length and, or, increasing the facet reflectivity. Using (3.5) and typical parameters for a monolithic single mode laser listed in table 3.1, the linewidth was simulated for three variables: (i) inverse power in the laser cavity, (ii) cavity length and (iii) front facet reflectivity, the results of which are plotted in Fig. 3.13, Fig. 3.14 and Fig. 3.15, respectively.

Fixed parameters		
Parameter	**Fixed Value**	**Comment**
$\hbar$	$1.0545887 \times 10^{-34}$ J·s	
λ	1550 nm	
n_g	3.6	
R_2	0.95%	
α_i	10 cm^{-1}	
n_{sp}	2	
α	3 cm^{-1}	
P_{cavity}	10 mW	Varied from 0.1 mW to 100 mW
L	1000 µm	Varied from 500 µm to 2000 µm
R_1	1%	Varied from 0.5% to 50 %

Table. 3.1. Parameters used in linewidth simulation.

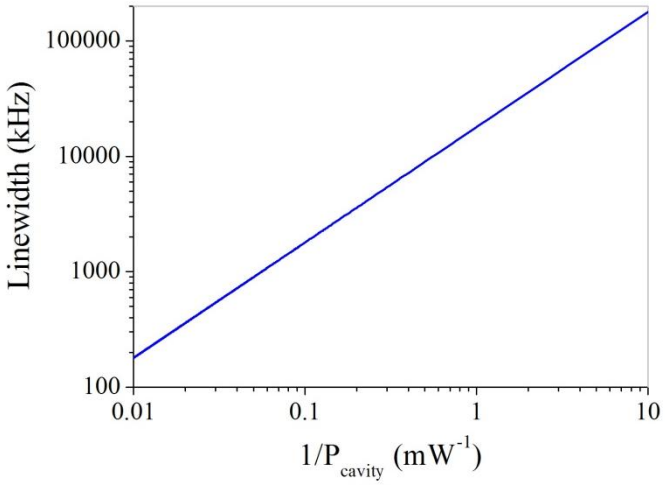

Fig. 3.13. Simulated linewidth versus inverse power.

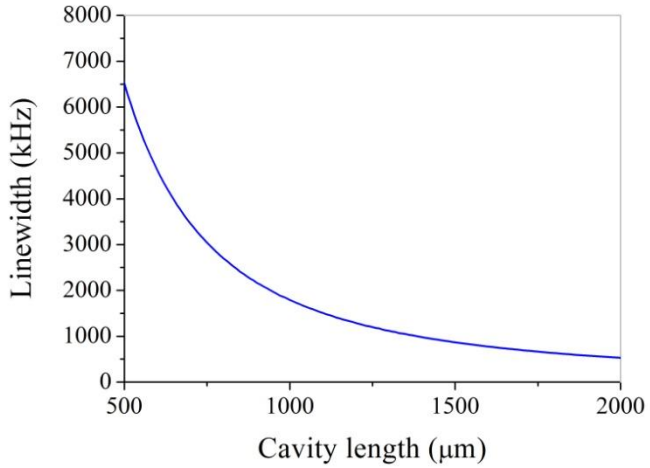

Fig. 3.14. Simulated linewidth versus cavity length.

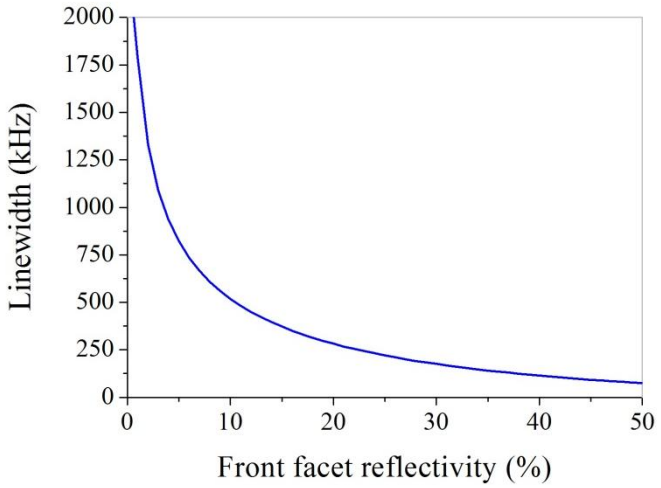

Fig. 3.15. Simulated linewidth versus front facet reflectivity.

The approach of reducing the linewidth by increasing the cavity length has been applied to DFB lasers. In [23] a linewidth of 70 kHz was demonstrated using a cavity length of 1450 μm. The device used uncoated facets, and as shown in Fig. 3.15 the linewidth can be reduced substantially by increasing the front facet reflectivity. However, it was reported that secondary modes began to appear at higher output powers. To suppress this behaviour, and improve overall performance and yield, DFBs are normally AR coated on the front facet and HR coated on the back [10]. However, the AR coating will increase the linewidth.

3.5 Conclusion

This chapter reviewed the basic structures of semiconductor lasers. Lasers used in optical communications were reviewed and approaches used to achieve single mode operation were discussed. Also, characteristics of interest for optical communications were considered. In the next chapter we describe a novel approach to producing single mode lasers.

References

[1] G. P. Agrawal, Lightwave Technology : components and devices, Hoboken: Wiley, 2004.

[2] L. A. Coldren, Diode Lasers and Photonic Integrated Circuits, Hoboken: Wiley, 2012.

[3] G. P. Agrawal and N. K. Dutta, Long wavelength Semiconductor Lasers, New York: Von Nostrand Reinhold, 1986.

[4] P. S. Zory, Quantum Well Lasers, San diego: Academic Press, 1993.

[5] J. M. Senior, Optical Fiber Communications: Principles and Practice, 3rd ed., New York: Prentice Hall, 2009.

[6] W. F. Brinkman, T. L. Koch, D. V. Lang and D. P. Wilt, "The lasers behind the communications revolution," Bell Labs Technical Journal, vol. 5, no. 1, pp. 150-167, 2002.

[7] K. Petermann, Laser Diode Modulation and Noise, London: Kluwer Academic, 1991.

[8] K. Nakahara, T. Tsuchiya, E. Nomoto and M. Mukaikubo, "Transmission Properties of 1.3-μm InGaAlAs MQW FP Lasers in 10-Gb/s Uncooled Operation," Journal of Lightwave Technology, vol. 23, no. 12, pp. 3997-4003, Dec. 2005.

[9] J. Buus, Single Frequency Semiconductor Lasers, Bellingham: SPIE Optical Engineering Press, 1990.

[10] T. Kjellberg, S. Nilsson, T. Klinga, B. Broberg and R. Schatz, "Investigation on the spectral characteristics of DFB lasers with different grating configurations made by electron-beam lithography," Journal of Lightwave Technology, vol. 11, no. 9, pp. 1405-1415, Sep. 1993.

[11] C. Chang-Hasnain, “Tunable VCSEL,” IEEE Journal of Selected Topics in Quantum Electronics, vol. 6, no. 6, pp. 978-987 , Nov. 2000.

[12] M. Muller, W. Hofmann, G. Bohm and M. C. Amann, “Short-Cavity Long-Wavelength VCSELs With Modulation Bandwidths in Excess of 15 GHz,” IEEE, Photonics Technology Letters, vol. 21, no. 21, pp. 1615-1617, Aug. 2009.

[13] D. M. Bird, J. R. Armitage, R. Kashyap, R. M. A. Fatah and K. H. Cameron, “Narrow line semiconductor laser using fibre grating,” Electronic letters, vol. 27, no. 13, pp. 1115-1116, Jun. 1991.

[14] M. Alalusi, P. Brasil, S. Lee, P. Mols and L. Stolpner, “Low noise planar external cavity laser for interferometric fiber optic sensors,” in Volume 7316 of Proceedings of Spie, Fiber Optic Sensors and Applications VI, 2009.

[15] J. Tidmarsh, S. Fasham, P. Stopford, A. Tomlinson and T. Bestwick, “A narrow linewidth laser for WDM applications using silicon waveguide technology,” in IEEE Lasers and Electro-Optics Society (LEOS) 12th Annual Meeting , San Francisco, Nov. 1999.

[16] K. Numata, J. Camp, M. A. Krainak and L. Stolpner, “Performance of planar-waveguide external cavity laser for precision measurements,” Optics Express, vol. 18, no. 22, pp. 22781-22788, Oct. 2010.

[17] C. Ye, Tunable External Cavity Diode Lasers, Singapore: World Scientific Publishing Co. Pte. Ltd., 2004.

[18] M. McDonald, A. Daiber, M. Finot and S. Xu, “Wavelength Filter with Integrated Thermal Control used as an Intracavity DWDM Laser Tuning Element,” in IEEE/LEOS International Conference on Optical MEMS and Their Applications Conference, Big Sky, Aug. 2006.

[19] A. Daiber, C. Schulz, J. C. Lo, P. Ludwig and S. Xu, “Tunable DWDM XFP with an external cavity laser transmitter and transmission performance matching 300-pin transponders,” in Optical Fiber Communication Conference (OFC), Los Angeles, Mar. 2010.

[20] M. Finot, M. McDonald, A. Daiber, W. B. Chapman, D. Li, M. Epitaux, E. Zbinden, J. Bennett, W. J. Kozlovsky and J. M. Verdiel, “Automated Optical Packaging Technology for 10 Gb/s Transceivers and its Application to a Low-Cost Full C-Band Tunable Transmitter,” Intel Technology Journal, vol. 8, no. 2, pp. 101-114, May 2004.

[21] T. Hertsens, “ILX lightwave, Application note #5, An Overview of Laser Diode Characteristics,” 2005. [Online]. Available: http://www.ilxlightwave.com/appnotes/AN%205%20REV02%20LD%20Characteristics%20Overview.pdf.

[22] W. Han, M. Rensing, X. Wang, H. Yang, F. H. Peters and P. O'Brien, “Investigation of the Packaging-Induced RF Attenuations and Resonances in a Broadband Optoelectronic Modulator Module,” Journal of Lightwave Technology, vol. 30, no. 16, pp. 2610-2617, Aug. 2012.

[23] H. Bissessur, C. Starck, J. Y. Emery, F. Pommereau, C. Duchemin, J. G. Provost, J. L. Beylat and B. Fernier, “Very narrow-linewidth (70 kHz) 1.55 um strained MQW DFB lasers,” Electronics Letters, vol. 28, no. 11, pp. 998-999, May 1992.

Chapter 4

Discrete mode laser diodes

This chapter gives an overview of discrete mode lasers and describes the operation of this type of laser, where etched features are introduced to the ridge waveguide to achieve single mode operation. A simplified model is presented, which describes how the single mode characteristics of the device can be controlled by precise control of the positions of these features. Static characterisation results are presented for devices targeted for direct modulation and optical coherent communication applications.

4.1 Single mode operation in a discrete mode laser diode

In FP laser diodes if unintended non-uniformities are introduced to the laser cavity during processing they can act as randomly distributed light scattering regions. Cassidy et al [1] demonstrated that such scattering regions can cause significant modulation in the envelope of lasing modes. This modulation is undesirable as it can compromise the transmission performance of FP transmitter lasers. However, if artificial index perturbations are introduced to the laser cavity, and the position of these perturbations is precisely controlled, the emission spectrum of an FP laser

diode can be altered in a controlled way. Index perturbations have been introduced to laser cavities using a variety of methods, with the first demonstration using a laser cutting tool to etch slots in the laser cavity [2, 3]. Significant modulation of the optical spectra was observed using this approach and even single mode behaviour, with an SMSR > 20 dB, was demonstrated. However, the single mode behaviour was accompanied by large increases in threshold currents and much reduced slope efficiencies as a result of loss introduced by the slots created using this method. Later work demonstrated that slots could be etched using focused ion beam etching (FIBE) [4] and reactive ion etching [5]. In terms of developing a process that could be applied to volume manufacture of semiconductor lasers, the latter method was the most practical. While the initial devices produced using these approaches demonstrated single longitudinal mode operation they did so under a limited range of operating conditions, displaying mode hops with variation in the bias current and temperature [6]. The laser devices used in this work build on this early work, particularly that of [5], and are referred to as discrete mode laser diodes.

4.1.1 Theory of operation

Single wavelength operation in DMLDs is achieved by introducing index perturbations in the form of shallow-etched features, or slots, positioned at a small number of sites distributed along the ridge waveguide. The slots are realized using ICP dry etching, with a typical depth in the region of 1.5 μm to 2 μm and a width of approximately 1 μm. Fig. 4.1(a) shows a SEM image where slots are etched into the ridge using this process. The slots are relatively shallow and are not etched into the active (wave guiding) region, however, they will still interact with the modes electric field (and magnetic field) as the mode profile is not fully confined to the active

region and will expand into the surrounding cladding regions. This interaction results in a proportion of the propagating light being reflected at the boundaries between the perturbed and the unperturbed sections. In effect the slots act as reflection centres and through suitable positioning the slots manipulate the mirror loss spectrum of an FP laser so that the mirror loss of a specified mode is reduced below that of the other cavity modes [7]. Using a simplified model, developed in [8, 9], a slot can be described as a one dimensional discontinuity inserted into the cavity; as most of the reflection comes from the front of the slot interface, the slot width has minimal effect on the reflection and is not considered in the model. Fig. 4.1(b) shows a schematic of a laser cavity with slots introduced into the cavity; where r_s is the slot reflectivity, t_s is the slot transmission, N is the number of slots, L is the distance between the slots, and Υ_i is the reflectivity in a section of the cavity where i is the slot number. The reflectivity from the first slot, Υ_1 is given by r_s.

The introduction of a slot into the waveguide changes its effective refractive index, so that it differs slightly from the segments of the waveguide without slots. The reflectivity from the waveguide to slot interface can be approximated using:

$$r_s \approx abs\left(\frac{n_2-n_1}{n_2+n_1}\right) \tag{4.1}$$

where n_1 is the effective refractive index of the waveguide and n_2 is the effective refractive index of the waveguide with a slot.

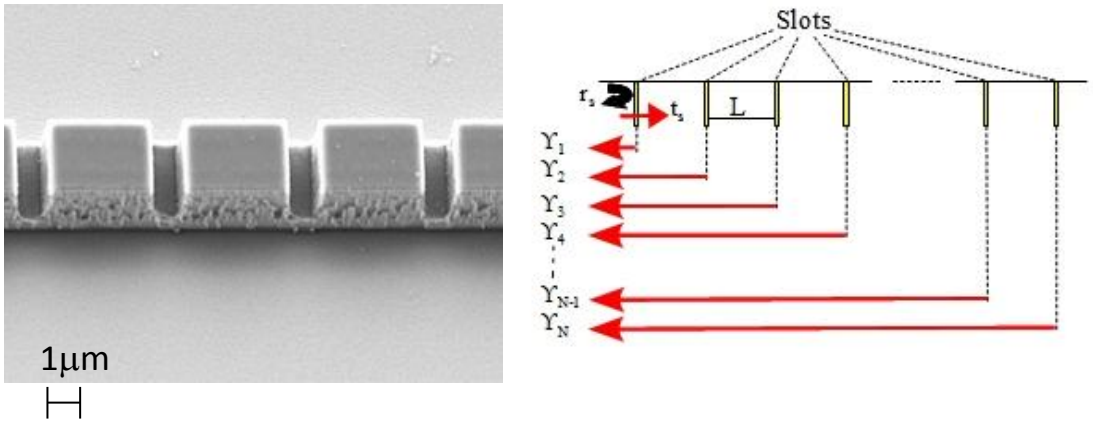

(a) (b)

Fig. 4.1. (a) SEM image of 2µm wide ridge waveguide with etched slots. The slot width is 1 µm and the spacing between the slots is 4 µm in this example. (b) Illustration of slot reflection and transmission for N slots.

Assuming no loss from the slot,

$$t_s = 1 - r_s \tag{4.2}$$

Υ_2 is the reflectivity from the second slot and is given by

$$\Upsilon_2 = r_s t_s^2 \exp(-2i\beta L) \tag{4.3}$$

where β is the complex propagation constant, and the term t_s is squared to take account of forward and backward travelling waves. The exponential term describes the medium in which the light travels, and a factor of 2 is used again to take account of forward and backward travelling waves. The complex propagation constant takes account of the gain and loss in the transmission medium and is defined in terms of

$$\beta = \beta_{re} + i\beta_i = \frac{2\pi n}{\lambda} + i\frac{g - \alpha_i}{2} \tag{4.4}$$

where n is the refractive index, λ is the wavelength, g is the optical gain and α_i is the internal cavity loss.

The reflectivities from the third and fourth slots are given by:

$$\Upsilon_3 = r_s t_s^4 \exp(-4i\beta L) \tag{4.5}$$

and,

$$\Upsilon_4 = r_s t_s^6 \exp(-6i\beta L) \tag{4.6}$$

respectively. Therefore, the reflectivity obtained from four slots is given by:

$$\Upsilon_{total} = \Upsilon_1 + \Upsilon_2 + \Upsilon_3 + \Upsilon_4$$

$$= r_s + r_s t_s^2 \exp(-2i\beta L) + r_s t_s^4 \exp(-4i\beta L) + r_s t_s^6 \exp(-6i\beta L) \tag{4.7}$$

By letting

$$X = t_s^2 \exp(-2i\beta L) \tag{4.8}$$

the total reflectivity from N slots can be expressed by the following series

$$\Upsilon_{total} = r_s(1 + X + X^2 + X^3 + \ldots\ldots + X^{N-1}) \tag{4.9}$$

Which in terms of known variables can be described as

$$\Upsilon_{total} = r_s \left[\frac{1-\left(t_s^2 exp(-2i\beta L)\right)^N}{1-t_s^2 exp(-2i\beta L)} \right] \tag{4.10}$$

The power reflection is related to the reflection amplitude by,

$$R = abs(\Upsilon_{total}^2) \tag{4.11}$$

Using this model the power reflection versus wavelength was simulated for different slot patterns in the 1550 nm window. The refractive indices were set to $n_1 = n = 3.1838$ and $n_2 = 3.1808$. The following simplifications were used in the model: changes in the refractive index due to changes in the carrier density were not taken in to account, the loss introduced by the slots and the internal cavity loss were set to zero, and the gain was set to 1 and showed no dependence on wavelength. With N = 30, Fig. 4.2 plots the overlapped results of a simulation where the slot spacing is varied from 3.31 μm to 3.46 μm in increments of 0.03 μm. Using a fixed slot spacing of 3.4 μm, Fig. 4.3 plots the overlapped results of a simulation where N equals 10, 20, 25 and 30. The overlapped results show that the power reflection increases as the number of slots introduced into the cavity is increased. While it is desirable to have the power reflection as large as possible, there are practical limitations for a real device that limit the number of slots that are introduced into the cavity, such as the cavity length. Also, the slots introduce loss and therefore to optimise the efficiency of the device only the requisite number required to achieve a given performance level should be introduced into the cavity.

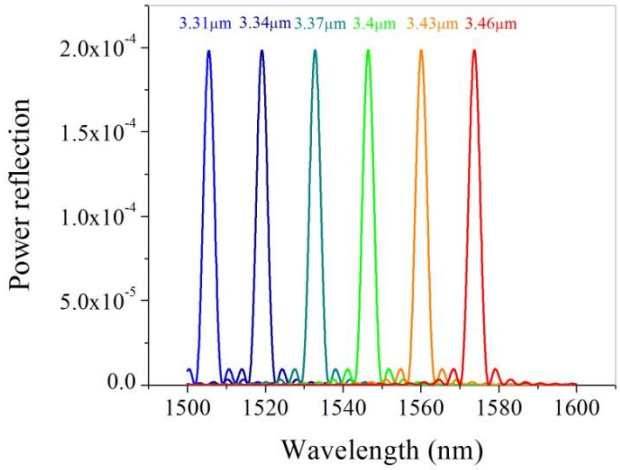

Fig. 4.2. Overlapped power reflection versus wavelength simulation results, for slot spacing ranging from 3.31 μm to 3.46 μm.

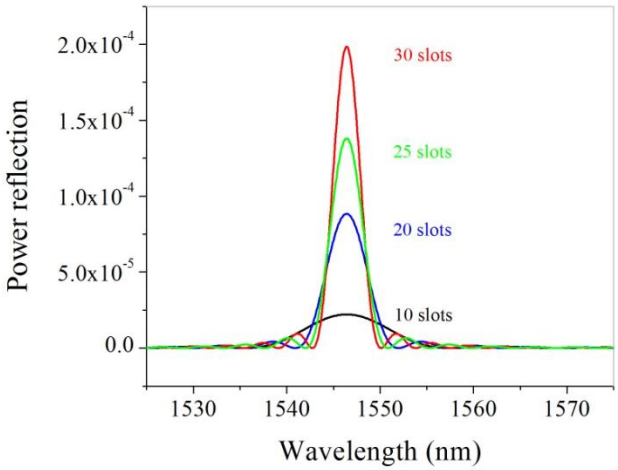

Fig. 4.3. Overlapped power reflection versus wavelength simulation results, for slot numbers ranging from 10 to 30.

In semiconductor lasers once threshold is reached the carrier density clamps at that value and any increase in injected carriers does not lead to an increase in carrier density but rather the generation of photons through stimulated emission [10]. Another effect of increasing the level of injected carriers is the generation of heat within the active region as a result of Joule heating [11]. The amount of heat generated depends on a number of factors including the laser resistance, cavity length, chip thickness, metal thickness on the chip and the quality of the eutectic bonding of the chip to the submount. The refractive index of the semiconductor material is dependent on its temperature, so any changes in temperature due to Joule heating, or in the ambient temperature, will change the refractive index resulting in a corresponding change in the peak reflection wavelength. The change in peak wavelength versus temperature for single mode semiconductor lasers is typically 0.1 nm/°C [12]. As stated previously the heat generated as a result of injected current depends on the laser design and packaging, and a typical value for a 1 mm cavity device would be 4 pm/mA. Fig. 4.4 plots the peak reflection wavelength versus refractive index for a slot spacing of 3.4 μm and N = 30. The refractive indices of the

waveguide with and without slots will change at the same rate versus temperature and in the simulation $n_2 = n_1 - 0.003$.

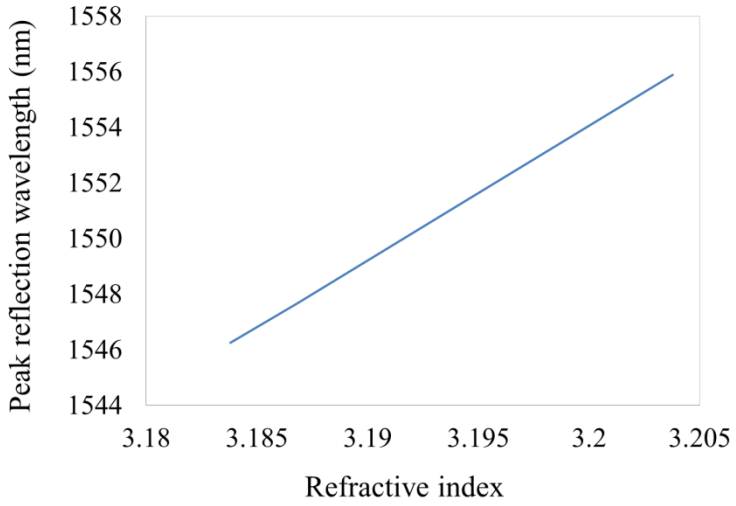

Fig. 4.4. Simulated reflection peak wavelength versus refractive index.

The main focus of this chapter is DMLDs designed for fibre optic communication applications. However, the DMLD process can be used with other material systems to produce single mode lasers operating from the visible [13] to the mid-infrared [14, 15] regions of the optical spectrum. Single mode lasers are important components for use in other application areas such as gas sensing, atomic clocks and LIDAR. Fig. 4.5 shows examples of optical spectra measured from DMLDs designed for non-telecom applications. The devices have peak wavelengths of (a) 684 nm (AlGaInP/GaAs), (b) 779 nm (AlGaAs/GaAs), (c) 1276 nm (InGaAlAs/InP), (d) 1393 nm (InGaAlAs/InP), (e) 1645 nm (InGaAlAs/InP), and (f) 2002 nm (InGaAs/InP).

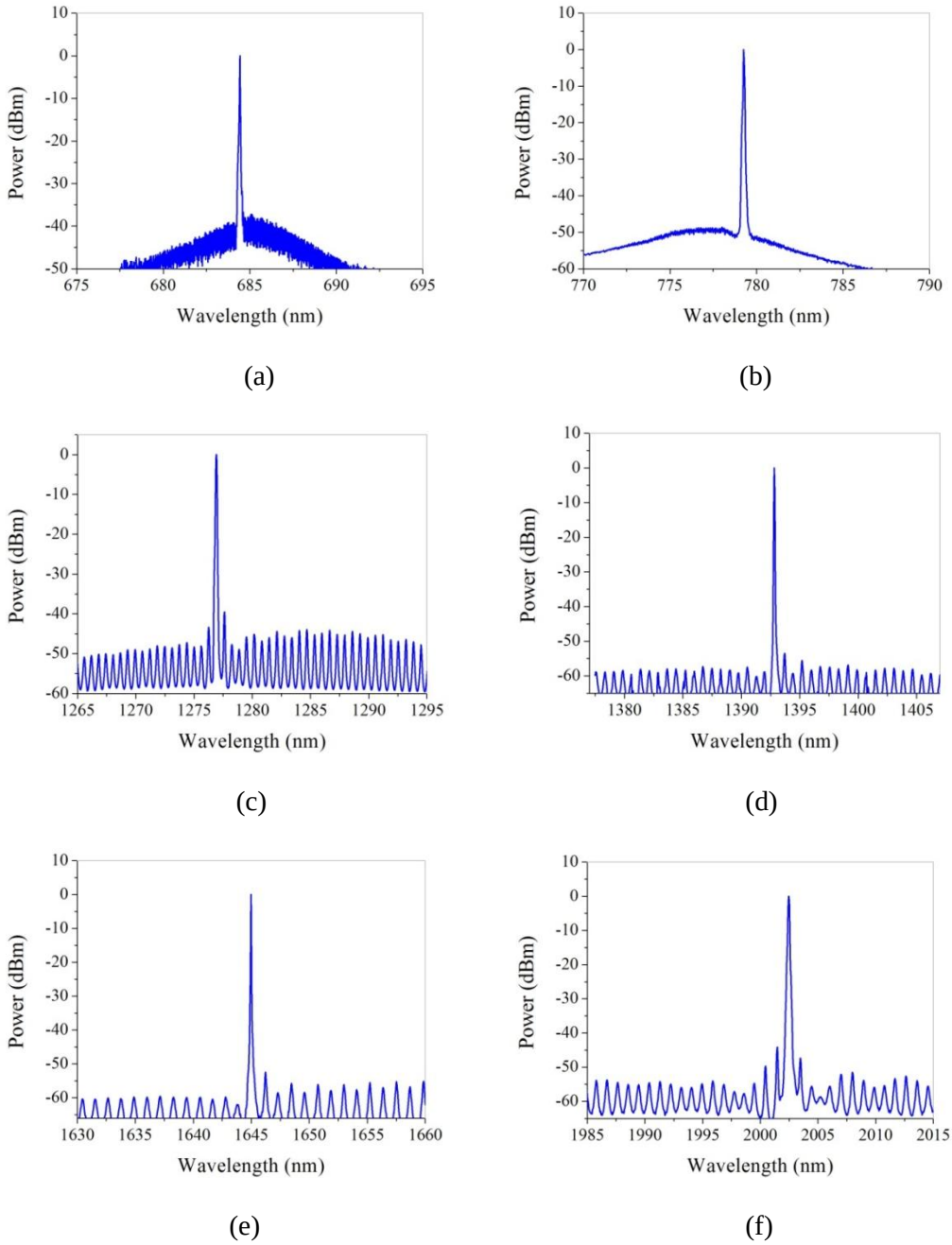

Fig. 4.5. Spectra measured for DMLDs with operating wavelengths of (a) 684 nm, (b) 779 nm, (c) 1276 nm, (d) 1393 nm, (e) 1645 nm, and (f) 2002 nm.

In [15] a DMLD was fabricated using InGaAs/AlAsSb on InP quantum cascade epitaxial materials and demonstrated single mode laser emission at $\lambda \approx 3.3$ μm. Fig. 4.6 shows the measured spectrum with emission wavelength of 3.3 μm and a minimum SMSR of 25 dB, the value of which was limited by the noise floor of the

Fourier transform infrared (FTIR) spectrometer. For comparison the emission spectrum of an FP laser fabricated on the same wafer is also shown.

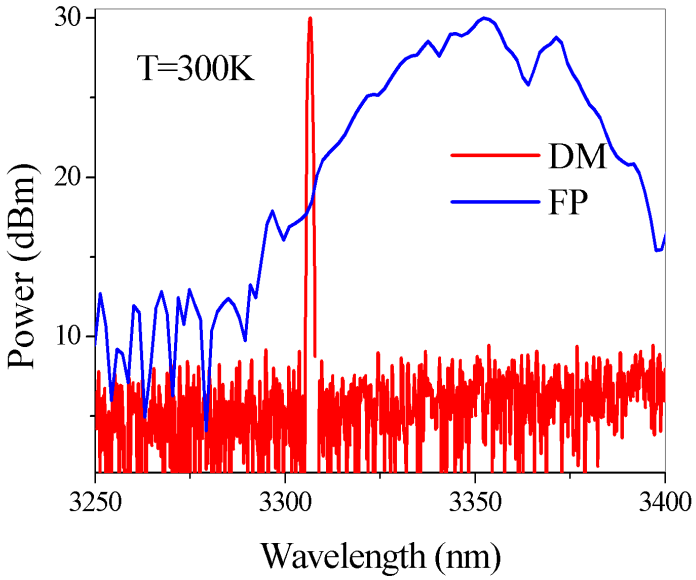

Fig. 4.6. Single mode wavelength emission spectrum of a DMLD fabricated on InGaAs/AlAsSb quantum cascade materials showing an SMSR of 25dB, also overlapped is the broad emission spectrum from an FP laser from the same wafer.

4.2 Characterisation of DMLDs for fibre optic communications

Lasers used in fibre optic communications are designed to meet target specifications determined by the specific application. Access and enterprise markets require directly modulated lasers capable of operating without a thermoelectric cooler (TEC), while still operating in a predictable fashion over the specified temperature range [16]. Similar to the electronics industry, fibre optic components are also graded by operating temperature with temperature (T) ranges of -0 ˚C ≤ T ≤ 70 ˚C specified for the standard or commercial grade and -40 ˚C ≤ T ≤ 85 ˚C specified for industrial grade devices [17]. Single mode lasers designed for these applications are required to maintain single mode operation over the temperature range while still maintaining

high output powers in excess of 5 mW from the chip, even at the upper temperature in the range. In applications where precise wavelength control is required a TEC is incorporated into the package to maintain the temperature of the laser chip at a set point. Because temperature control is employed, the operating temperature range of the laser chip can be relaxed. However, other parameters can be important for these applications, such as the linewidth in coherent communications for example.

The DMLDs described in the rest of this chapter used an AlGaInAs MQW epitaxial structure. The structure was grown on an n-type (100)-InP substrate in an OMVPE reactor at low pressure. The MQW active region was sandwiched between two InGaAsP SCH guide layers, which also acted as an etch stop layer for the ridge waveguide. A p-InP layer was grown on top of the SCH followed by a highly p-doped InGaAs contact layer. Electrical contacting was achieved using conventional metals (Ti/Pt/Au) and SiO2 as an insulator for contact definition on the cap layer. Finally the wafers were thinned by mechanical polishing, n-metal (Ti/Pt/Au) deposited, the devices cleaved into the designed cavity length and the front and back facets coated.

4.2.1 Directly modulated lasers

DMLDs for uncooled directly modulated applications were designed at both 1310 nm and 1550 nm. Static characterisation of the devices was performed and the results are presented here.

4.2.1.1 1310 nm window

The structure of a 1310 nm DMLD designed for direct modulation at 2.5 Gbit/s is as follows. The undoped laser active region consists of five compressively strained AlGaInAs quantum wells with a well thickness of 5 nm whose composition is chosen to give an emission wavelength centred at λ = 1.3 μm. The ridge width is approximately 2.5 μm and the slots in the ridge had a width of around 1 μm. A pattern of index perturbations was calculated to give single mode emission at λ = 1295 nm at 25 ˚C. The slot pattern featured 20 index perturbations distributed along the laser cavity [7]. The device had a cavity length of 350 μm and the front and back facets were coated to have reflectivities of 30 % and 95 %, respectively. Fig. 4.7 shows the CW L-I characteristics measured over the range -40 ˚C ≤ T ≤ 97 ˚C. The extracted threshold currents were 7 mA, 12 mA and 38 mA at -40 ˚C, 25 ˚C and 87 ˚C, respectively. The characteristic temperature of threshold current between -40 ˚C to 25 ˚C and 25 ˚C to 95 ˚C is calculated to be 78 K and 70 K, respectively. The measured slope efficiency at 25 ˚C and 87 ˚C was 0.3 W/A and 0.2 W/A, respectively. An output power > 5 mW was achieved at 97 ˚C. Fig. 4.8 shows the emission spectrum of the laser operating at 25 ˚C, at an output power of 5 mW, together with the emission spectrum of the base ridge waveguide FP laser fabricated in the same process run. The laser was designed to operate single mode over a wide range of temperatures; Fig. 4.9 shows the lasing spectra for a number of operating temperatures in the range -40 ˚C ≤ T ≤ 97 ˚C. The lasing wavelength shows a linear dependence with temperature, with a tuning rate $\Delta\lambda/\Delta T$ of approximately 0.1 nm / ˚C, which is consistent with the expected mode shift due to the temperature-induced change in the refractive index. An SMSR > 40 dB was measured across the full temperature range. Fig. 4.10 shows the far field plots measured in (a) the parallel

and (b) perpendicular directions, at 25 ˚C and 85 ˚C, with an output power from the chip of 5 mW. The measurement shows that the beam remains relatively stable over the temperature range, with values of 24.4 degrees and 25.5 degrees measured in the parallel direction at 25 ˚C and 85 ˚C, respectively. In the perpendicular direction values of 27.1 degrees and 27.4 degrees were measured at 25 ˚C and 85 ˚C, respectively. The far field was measured using a Photon Inc. far field tester. Due to limitations in the test fixture it was not possible to measure the far field at lower temperatures. However, similar devices packaged in fiberized packages displayed low tracking error, less that 1 dB, over the range -40 ˚C ≤ T ≤ 85 ˚C indicating that the far field remains stable with temperature.

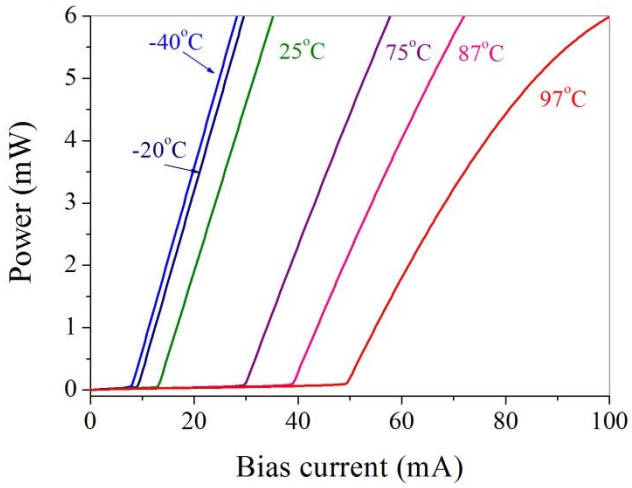

Fig. 4.7. 1310 nm DMLD L-I plots over the range -40 ˚C ≤ T ≤ 97 ˚C.

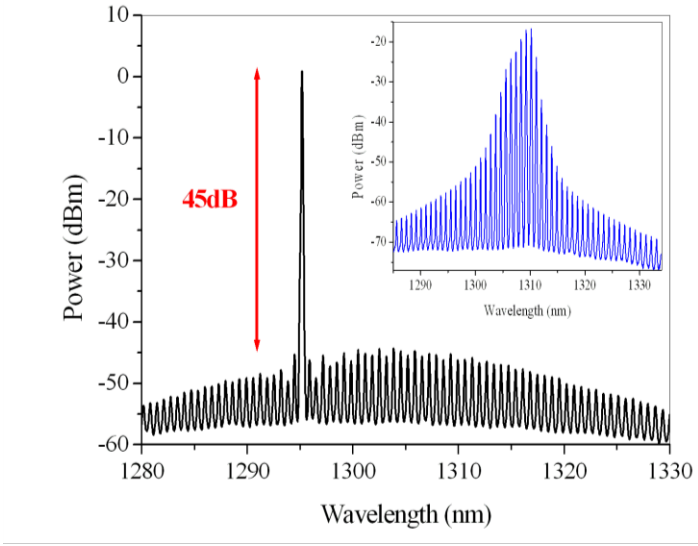

Fig. 4.8. Measured emission spectrum of a DMLD biased for 5 mW emission, showing a high SMSR of 45 dB. Inset: Typical multimode emission spectrum of an FP laser fabricated on the same wafer (i.e. a DMLD fabricated without any index perturbing features) under the equivalent operating conditions.

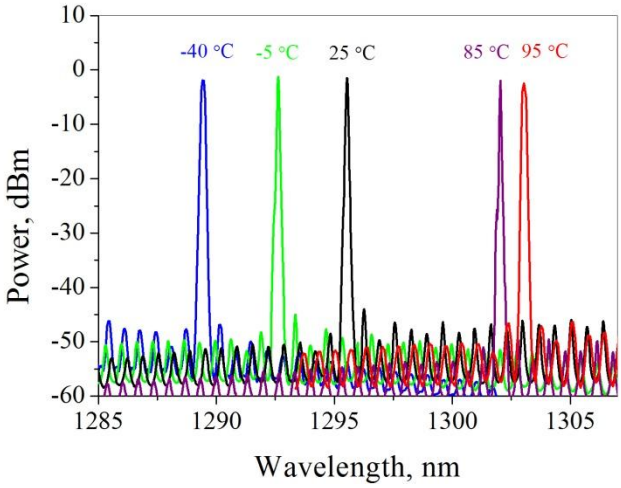

Fig. 4.9. 1310 nm DMLD optical spectra measured over the range -40 ˚C ≤ T ≤ 95 ˚C.

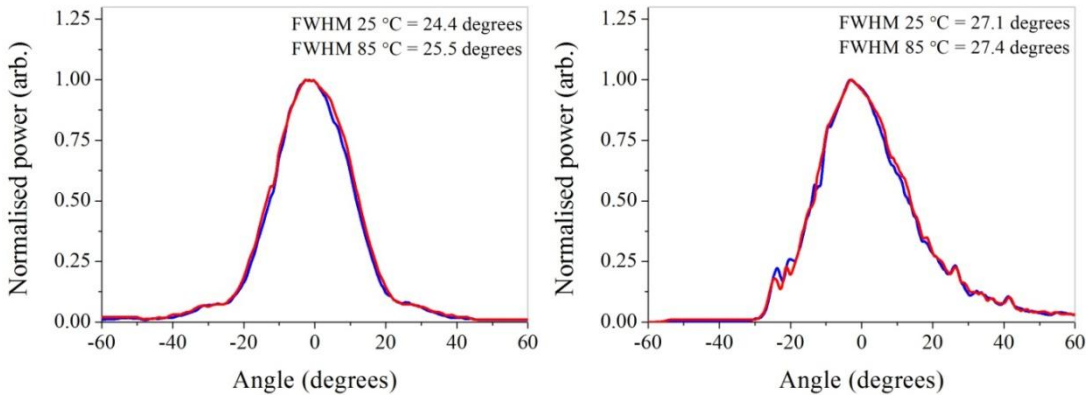

(a) (b)

Fig. 4.10. Far field measurement at 25 ˚C and 85 ˚C, in (a) the parallel direction and in (b) the perpendicular direction.

A structure consisting of nine quantum wells was designed for high speed operation under direct modulation at bit rates up to 10 Gbit/s. Process limitations for this lot meant that the devices produced were limited to an upper temperature limit of 60 ˚C. A DMLD with a cavity length of 250 μm, and front and back facet reflectivities of 16 % and 87 % respectively, was characterised at 25 ˚C. Fig. 4.11 shows the CW L-I characteristic measured at 25 ˚C. The extracted threshold current was 12.5 mA and the measured slope efficiency was 0.19 W/A. Fig. 4.12 shows the emission spectrum of the laser operating at 25 ˚C, at an output power of 5 mW, where a peak wavelength of 1318.5 nm and SMSR of 44 dB was measured.

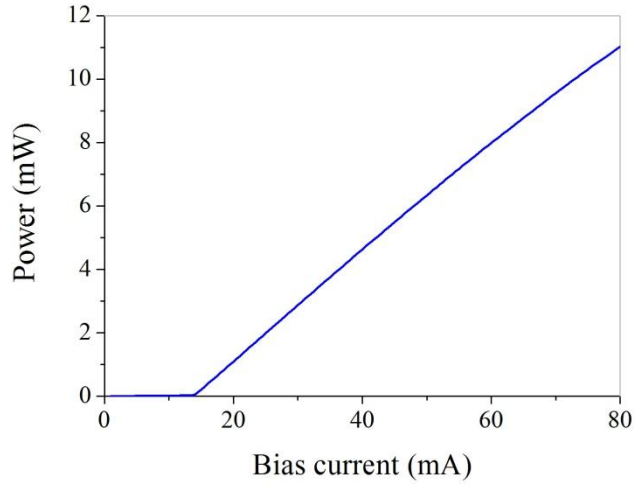

Fig. 4.11. 1310 nm DMLD L-I characteristic measured at 25 ˚C.

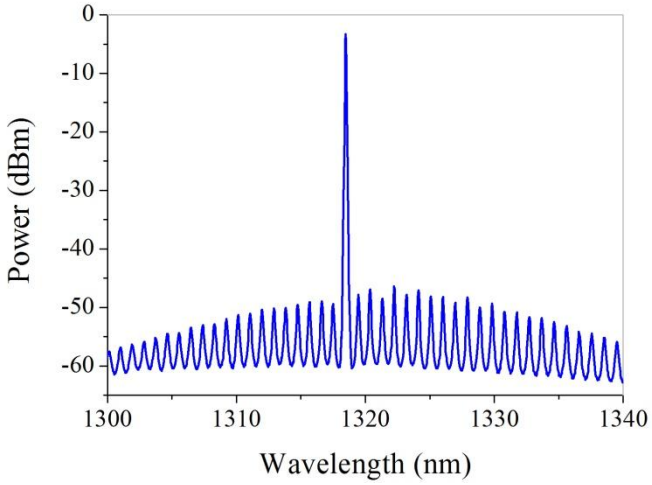

Fig. 4.12. 1310 nm DMLD optical spectra measured at 25 ˚C.

The device's modulation bandwidth was extracted by measuring the electro-optic response, or S21, using a VNA, and is shown in Fig. 4.13. The device was packaged in a high speed TO-can with a matching resistor to match the overall impedance to 50 Ω. From the S21 plot the 3 dB bandwidth value was extracted to give a value of 9 GHz at 20 mA and this increased to 15.1 GHz at 60 mA, indicating that the device has the requisite bandwidth for operation at 10 Gbit/s.

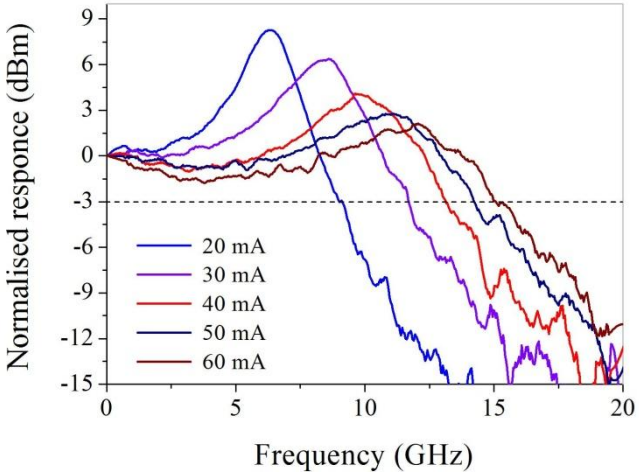

Fig. 4.13. Modulation response of a 1310 nm DM laser showing the modulation bandwidth over current ranging from 20 mA to 60 mA.

4.2.1.2 1550 nm window

The 1550 nm MQW structure consisted of five compressively strained (1%) 5 nm thick AlGaInAs quantum wells and six slightly tensile strained (0.2%) 8 nm thick AlGaInAs barriers. The DMLD had a cavity length of 300 μm with front and back facet reflectivities of 30 % and 95 %, respectively. It was packaged in a TO-56 based fiberized coaxial package with a chip to fibre coupling efficiency of 25 % and was characterised over a case temperature range -20 ˚C ≤ T ≤ 95 ˚C. The overlapped L-I plots measured in the fibre are shown in Fig. 4.14, over the temperature range. At 25 ˚C and 85 ˚C the threshold currents were 12.3 mA and 37.1 mA, respectively. The slope efficiencies, measured in the fibre, at 25 ˚C and 85 ˚C were 0.085 W/A and 0.058 W/A, respectively. Taking account of the coupling efficiency an output power from the chip > 5 mW was achieved at 97 ˚C. Fig. 4.15 shows the overlapped optical spectra, measured over the range -20 ˚C ≤ T ≤ 95 ˚C. The power in the fibre was set to 2 mW over the range -20 ˚C ≤ T ≤ 85 ˚C, at 95 ˚C the bias current was set to 100 mA corresponding to an emitted power of 1.8 mW. An SMSR in excess of

40 dB was measured over the range -20 ˚C ≤ T ≤ 95 ˚C. The lasing wavelength displayed a linear dependence with temperature corresponding to a tuning rate Δλ/ΔT of 0.11 nm/˚C.

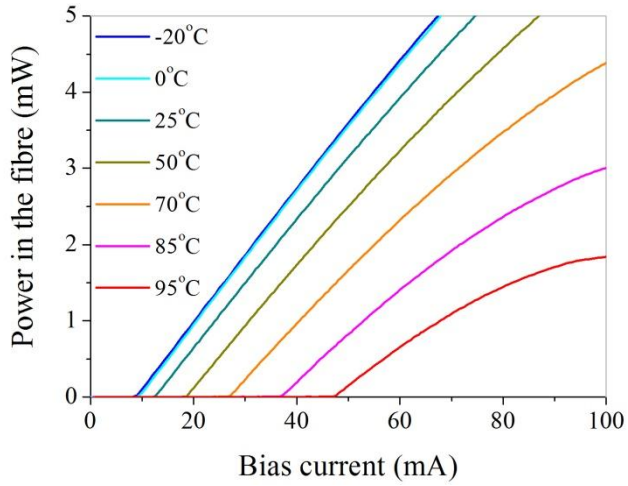

Fig. 4.14. 1550 nm DMLD module L-I plots over the range -20 ˚C ≤ T ≤ 95 ˚C.

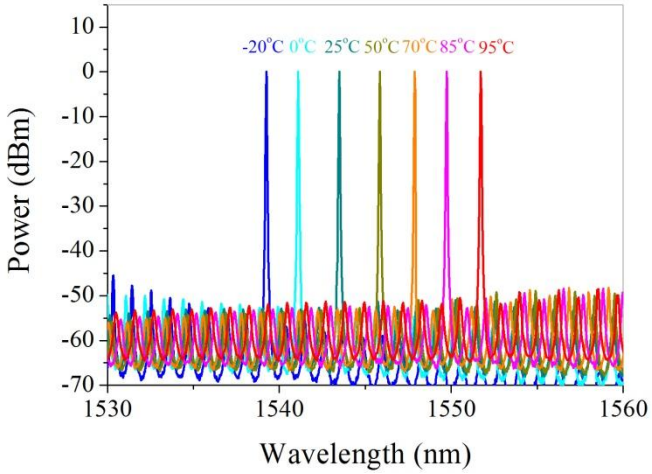

Fig. 4.15. 1550 nm DMLD optical spectra measured over the range -20 ˚C ≤ T ≤ 95 ˚C.

Fig. 4.16 shows the far field in (a) the parallel and (b) perpendicular directions, measured prior to packaging at 25 ˚C and 85 ˚C, with an output power from the chip of 5 mW. The measurement shows that the beam remains stable over the temperature range, with a value of 25.8 degrees measured in the parallel direction at both 25 ˚C and 85 ˚C. In the perpendicular direction values of 29.1 degrees and 28.9 degrees

were measured at 25 ˚C and 85 ˚C, respectively. The far field was measured using a Photon Inc. far field tester. In the packaged device a tracking error less than 1 dB was measured over the range -20 ˚C ≤ T ≤ 95 ˚C confirming the stability of the far field over temperature.

The device's coaxial package was designed for 2.5 Gbit/s operation and did not have the requisite bandwidth to fully characterise the bandwidth of the device. In order to estimate the bandwidth of the laser, independent of any limitations introduced by the package, the relaxation oscillation frequency was obtained by measuring the noise spectrum of the laser. Fig. 4.17 shows the measured relaxation oscillation frequency versus $\sqrt{I - I_{th}}$. Slopes of 1.7 GHz / √mA, 1.5 GHz / √mA, 1.3 GHz / √mA and 1.1 GHz / √mA were obtained at -20 ˚C, 25 ˚C, 70 ˚C and 85 ˚C, respectively, indicating the device has the requisite optical bandwidth for 10 Gbit/s direct modulation.

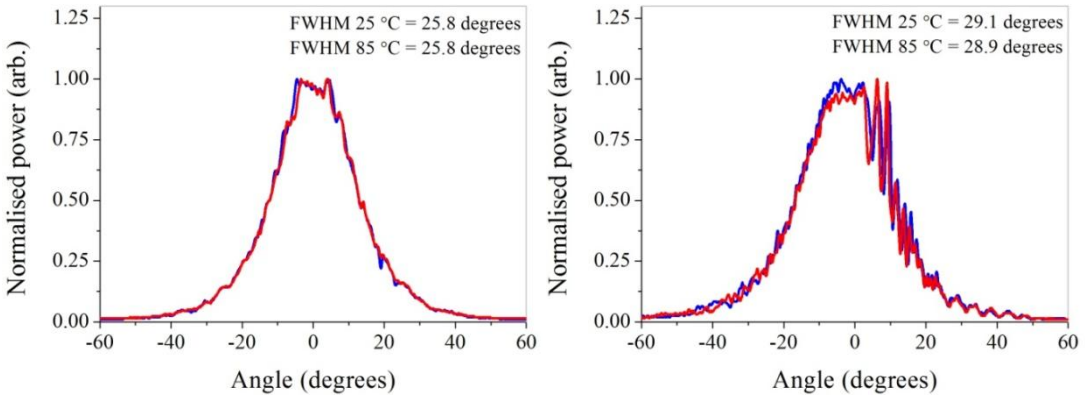

(a) (b)

Fig. 4.16. Far field measurement at 25 ˚C and 85 ˚C, in (a) the parallel direction and in (b) the perpendicular direction.

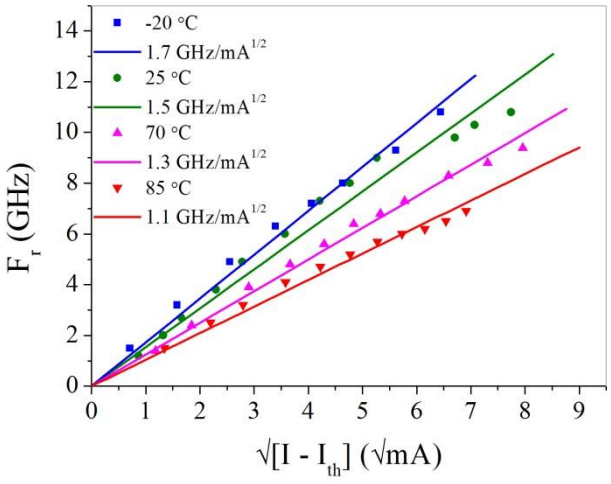

Fig. 4.17. Relaxation oscillation frequency versus $\sqrt{I - I_{th}}$ over the range -20 ˚C ≤ T ≤ 85 ˚C.

4.2.2 Narrow linewidth lasers

Using design rules derived from the modified Schawlow-Townes expression, (3.5), DMLDs were designed for narrow linewidth operation. An application of narrow linewidth lasers in optical communications is in systems employing advanced modulation formats, and these mainly operate in the 1550 nm window.

The same epitaxial structure used for the direct modulation lasers was used for the two subsequent 1550 nm low linewidth designs presented here. To lower the emission linewidth a device was designed with a cavity length of 1000 μm and a front facet coating of 30 %, with the back facet coated at 95 %. The device was packaged in a 14-pin butterfly module, which contained a TEC, thermistor and dual stage optical isolator with 60 dB isolation. A chip to fibre coupling efficiency of 63 % was obtained. The device was characterised over temperature by controlling the chip temperature using the butterfly module's internal TEC. The overlapped L-I plot measured in the fibre is shown in Fig. 4.18, over the range 0 ˚C ≤ T ≤ 85 ˚C. At 25 ˚C and 85 ˚C the threshold currents were 33 mA and 96 mA, with slope efficiencies in the fibre of 0.033 W/A and 0.017 W/A, respectively. Fig. 4.19 shows

the overlapped optical spectra measured at a bias current of 250 mA over the range -10 ˚C ≤ T ≤ 110 ˚C. The peak wavelength and SMSR values versus temperature are plotted in Fig. 4.20. An SMSR in excess of 40 dB was measured over the temperature range. The continuous wavelength tuning range was 11.6 nm and displayed a linear dependence with temperature corresponding to a tuning rate $\Delta\lambda/\Delta T$ of 0.097 nm/˚C. Fig. 4.21 shows the peak wavelength and SMSR versus bias current at 25 ˚C. Mode hop free operation, with a wavelength shift versus bias current of approximately 4 pm/mA, was observed.

Using the setup shown in Fig. 4.22 linewidth spectra were measured using a standard delayed self-heterodyne (DS-H) technique [18, 19]. The fibre delay length in one arm of the interferometer set-up was 6 km (corresponding to a linewidth measurement resolution ≈ 17 kHz). To enhance measurement accuracy light propagating in the short arm of the set-up was modulated using a $LiNbO_3$ phase modulator to frequency shift the detected heterodyne beat signal to 1 GHz away from the zero Hertz response of the radio frequency (RF) spectrum analyser.

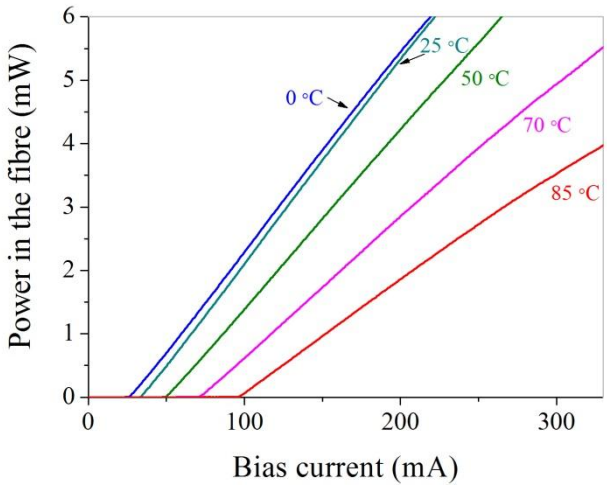

Fig. 4.18. 1550 nm DMLD module L-I plots over the range 0 ˚C ≤ T ≤ 85 ˚C.

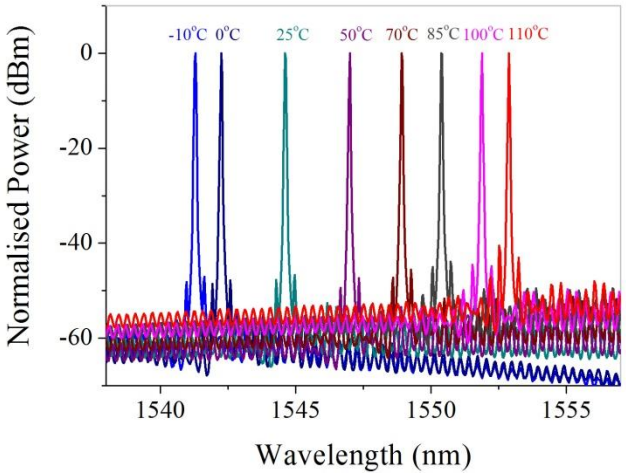

Fig. 4.19. 1550 nm DMLD measured optical spectra over the range -10 ˚C ≤ T ≤ 110 ˚C.

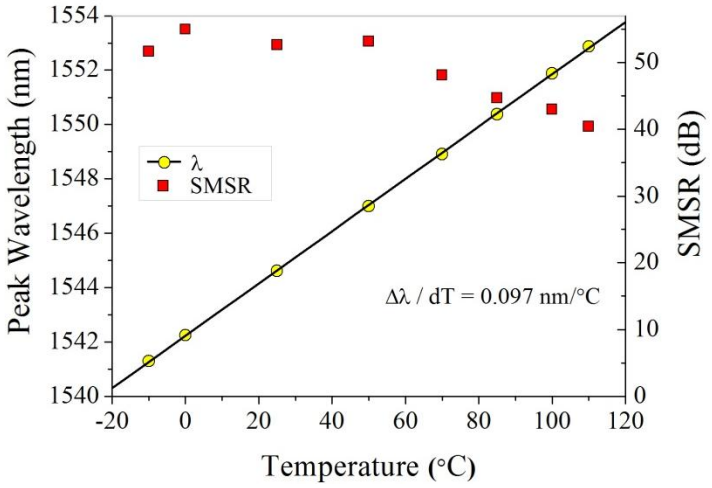

Fig. 4.20. Peak wavelength and SMSR versus temperature.

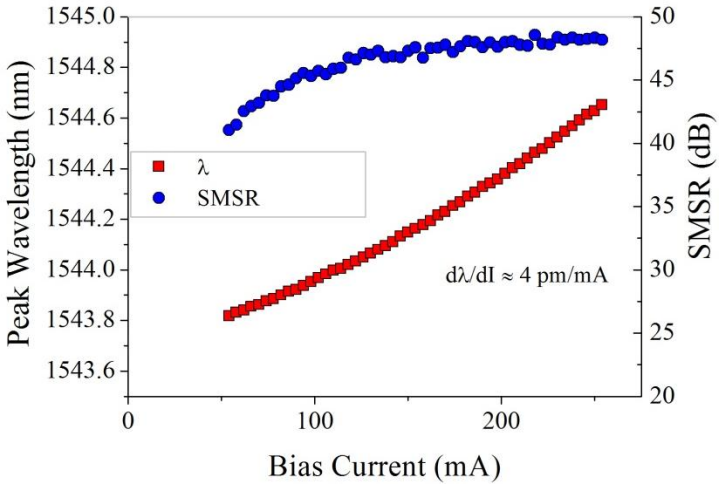

Fig. 4.21 Peak wavelength and SMSR versus bias current at 25 ˚C.

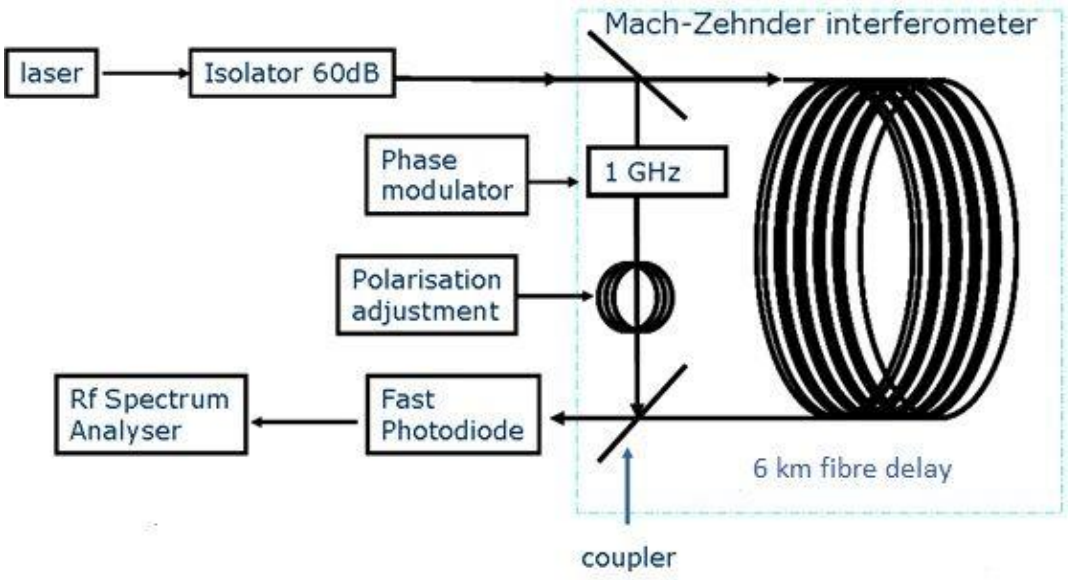

Fig. 4.22. Delayed self-heterodyne experimental set-up.

Fig. 4.23 shows the extracted Lorentzian component of the emission linewidth versus inverse power in the fibre. A minimum linewidth of 138 kHz was measured at an output power of 8.4 mW, and a corresponding bias current of 300 mA. The measured DS-H spectrum was fitted to a Lorentzian lineshape to extract the half-width at half maximum value, and is shown in Fig. 4.24, with the bias current set to 300 mA. Fig. 4.25 shows the extracted Lorentzian component of the emission linewidth versus temperature for two operating conditions; the first where the power in the fibre is kept constant at 4 mW and the second where the bias current is kept constant at 250 mA. At a constant power of 4 mW a maximum linewidth of 235 kHz was measured at 85 ˚C, and a minimum value of 212 kHz was measured at 25 ˚C, corresponding to a variation in the linewidth of only 23 kHz over the range 0 ˚C ≤ T ≤ 85 ˚C. When the device is operated at a constant bias current of 250 mA a linewidth below 200 kHz was measured over the range 0 ˚C ≤ T ≤ 60 ˚C. The increase in linewidth at higher temperatures is due to the reduction in the optical power for a given input current, leading to a reduction in the photon density in the laser cavity. At temperatures below 0 ˚C and above 85 ˚C it was not possible to

achieve the temperature stability necessary to accurately measure the linewidth using the internal TEC as it was being driven beyond its normal operating limits at these temperatures. Controlling the chip temperature can be used to tune the wavelength; a limitation is that using temperature to tune the peak wavelength is relatively slow. However, in applications where high speed tuning rates are not required it could provide a cost effective tuneable source with linewidth comparable to an ECL. A potential application of this device is as a low cost backup laser source for fixed wavelength WDM systems employing advanced modulation formats. By temperature tuning the wavelength a single device could cover multiple channels, thereby reducing inventory costs. In a DWDM system with 50 GHz spacing 20 channels could be covered by a device with an operating temperature range of 0 ˚C to 85 ˚C.

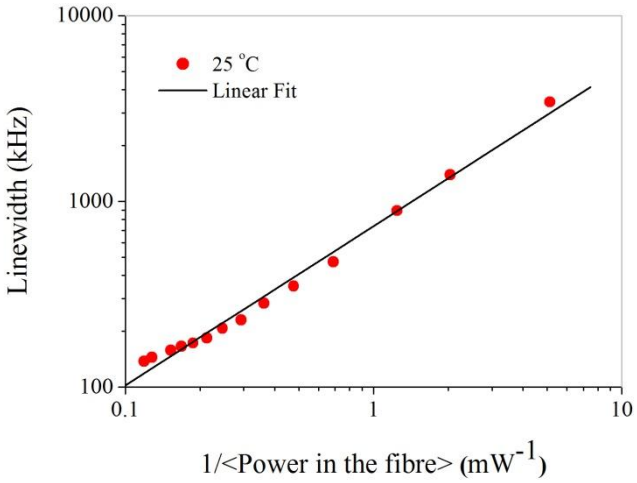

Fig. 4.23. Extracted linewidth versus optical power at T = 25 ˚C.

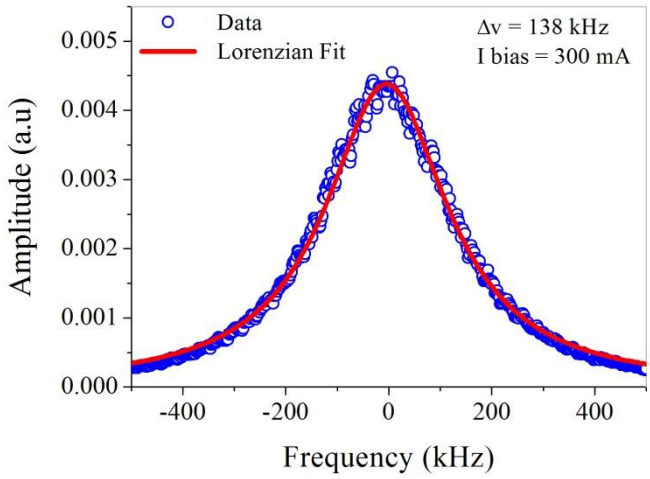

Fig. 4.24. D-SH spectrum at I = 300mA with Lorentzian fit linewidth = 138 kHz.

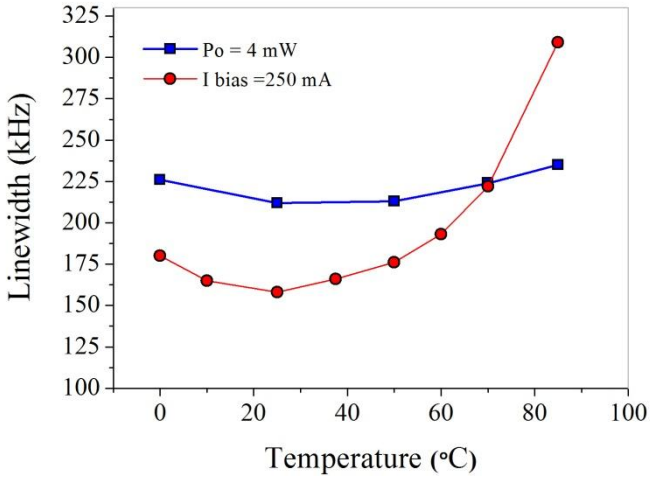

Fig. 4.25. Linewidth versus temperature at constant power in the fibre of 4 mW and also at a constant bias current of 250 mA.

To reduce the linewidth further a device was produced where the cavity length was doubled to 2000 μm. The device was also packaged in a butterfly module where a chip to fibre coupling efficiency of 73 % was obtained. The overlapped L-I plot measured in the fibre is shown in Fig. 4.26, at temperatures of 0 ˚C, 20 ˚C and 50 ˚C. At 20 ˚C and 50 ˚C the threshold currents were 45 mA and 71 mA, with slope efficiencies in the fibre of 0.019 W/A and 0.016 W/A, respectively. At 0 ˚C a slope efficiency of 0.018 W/A was measured, the decrease in slope efficiency, compared to

that obtained at 20 ˚C, is due to a slight change in the alignment of the coupling optics in the butterfly package at 0 ˚C, and a result of the TEC being operated below the recommended operating temperature for this package. Fig. 4.27 shows the overlapped optical spectra measured at a bias current of 300 mA over the range -5 ˚C ≤ T ≤ 50 ˚C. An SMSR in excess of 40 dB was measured over the temperature range. The peak wavelength and SMSR values versus temperature are plotted in Fig. 4.28. An SMSR in excess of 40 dB was measured over the temperature range. The continuous wavelength tuning range was 5.5 nm and displayed a linear dependence with temperature corresponding to a tuning rate $\Delta\lambda/\Delta T$ of 0.1 nm/˚C. Fig. 4.29 shows the peak wavelength and SMSR versus bias current at 20 ˚C. Mode hop free operation, with a wavelength shift versus bias current of approximately 2 pm/mA, was observed. The reduction in this value, compared to the 1000 μm device, is due to the longer cavity.

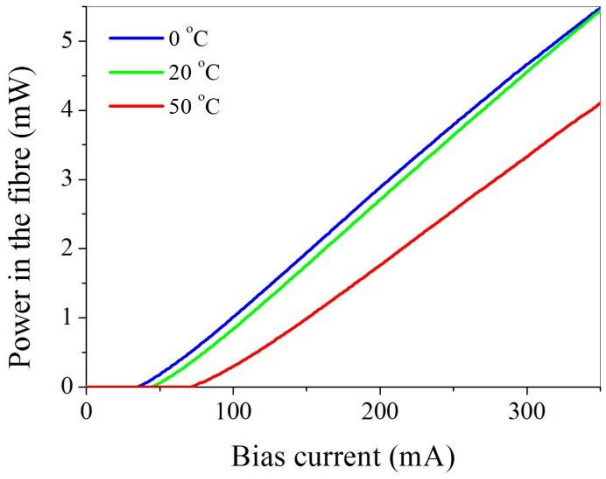

Fig. 4.26. 1550 nm DMLD module L-I plots measured at 0 ˚C, 20 ˚C and 50 ˚C.

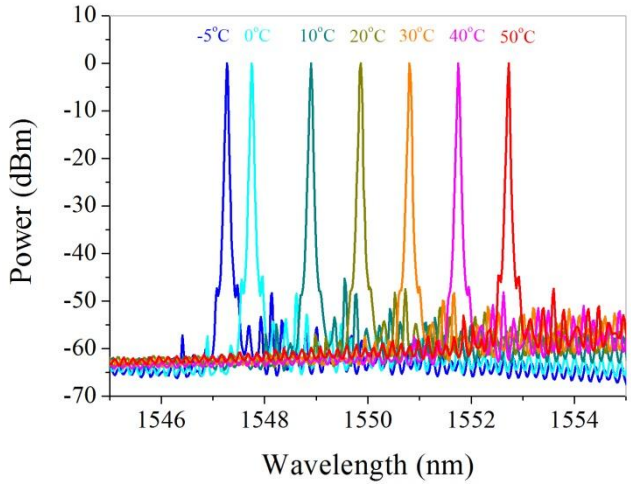

Fig. 4.27. 1550 nm DMLD measured optical spectra over the range -5 ˚C ≤ T ≤ 50 ˚C.

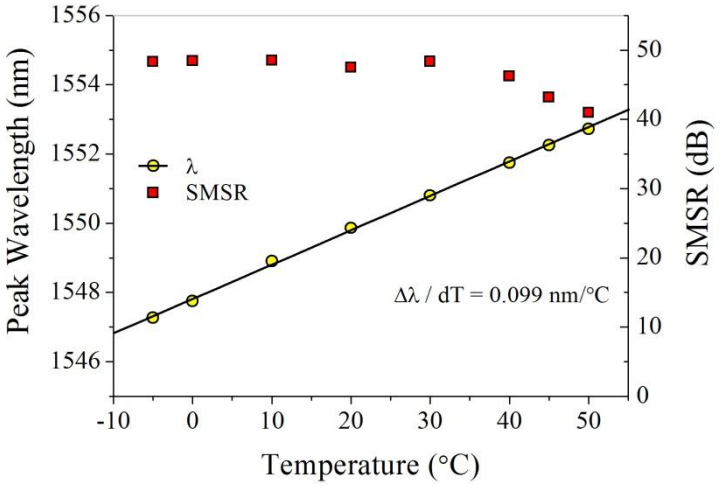

Fig. 4.28. Peak wavelength and SMSR versus bias current at 20 ˚C.

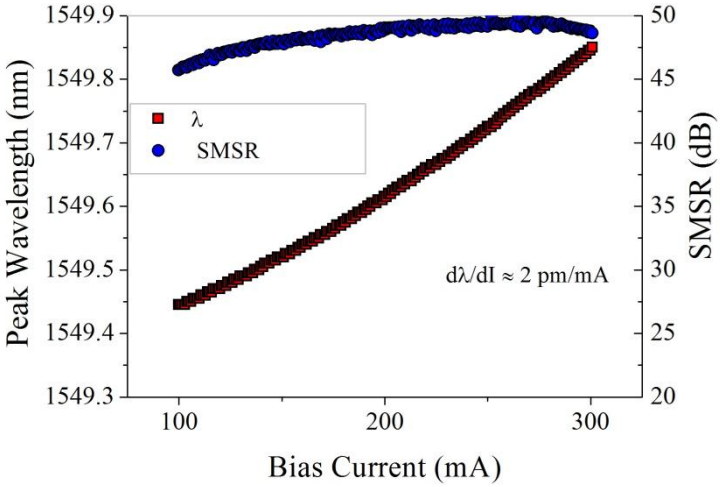

Fig. 4.29. Peak wavelength and SMSR versus bias current at 20 ˚C.

Linewidth spectra were measured using the DS-H technique. Fig. 4.30 shows the extracted Lorentzian component of the emission linewidth versus inverse power in the fibre. A minimum linewidth of 70 kHz was obtained at an output power of 6.3 mW, and a corresponding bias current of 400 mA. The measured DS-H spectrum fitted to a Lorentzian lineshape is shown in Fig. 4.31, with the bias current set to 400 mA. Fig. 4.32 shows the extracted Lorentzian component of the emission linewidth versus temperature at a constant bias current of 300 mA. Over the measured temperature range a maximum linewidth of 99 kHz was measured at -5 ˚C and a minimum value of 93 kHz was measured at 5 ˚C, corresponding to a variation in the linewidth of only 6 kHz over the range -5 ˚C ≤ T ≤ 50 ˚C.

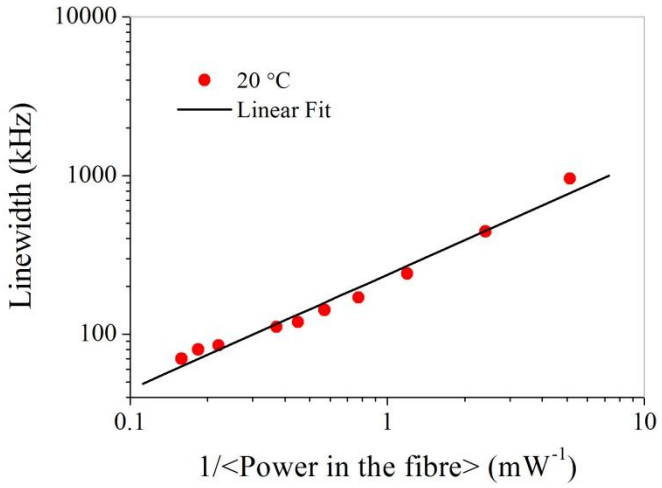

Fig. 4.30. Extracted linewidth versus optical power at T = 20 ˚C.

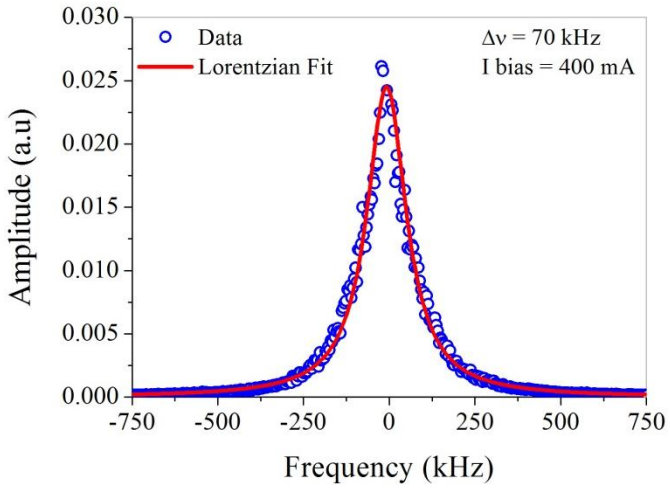

Fig. 4.31. D-SH spectrum at I = 400 mA with Lorenztian fit linewidth = 70 kHz.

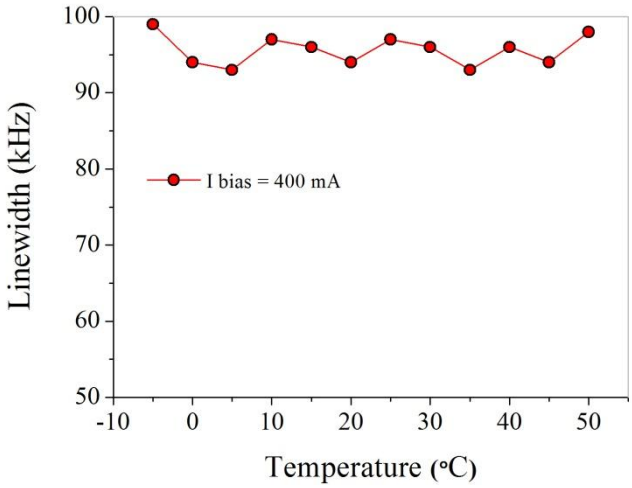

Fig. 4.32. Linewidth versus temperature at a constant bias current of 300 mA.

From a coherent detection viewpoint having a knowledge of the frequency noise spectrum is preferred over a simple linewidth number as it allows the source of the noise to be identified and allows assessment of the extent to which detection electronics can compensate for the phase noise. The phase noise power spectral density (S_ν (f), PSD) [20], was also measured for this laser. This measurement was carried out in the optical communications optoelectronics research centre, University of Southampton. The accuracy of the results obtained using this setup was verified using other commercially available lasers, and in [21] this setup was used to

characterise four different types of lasers. A second reason for carrying out this measurement was to compare the linewidth result obtained using this technique with that obtained using the D-SH technique.

The experimental set-up for measuring S_v (f) is shown in Fig. 4.33. It consists of a delayed balanced MZI that acts as a sensitive frequency-to-amplitude converter followed by a DC-coupled photodetector and a fast Fourier transform (FFT) spectrum analyser. The PSD measured with FFT spectrum analyser, (expressed in V^2/Hz), is related to S_v (f) by [20]:

$$S_v(f) = S_{SA}(f) \cdot \frac{f^2}{A^2 \sin^2(\pi f \tau)} \tag{4.12}$$

Here, *f* is the Fourier frequency, τ is the MZI time delay and *A* is the maximum peak-to-peak (p-p) amplitude (in Volts) of the fringes seen on the interferometer. This equation assumes that the intensity noise of the laser, the shot noise, and electronic thermal noise are negligible compared to the converted frequency noise. The highest sensitivity is obtained when $\sin(\pi f \tau) = 0$, which occurs when signal power at this frequency is split equally into both arms of the output MZI coupler. During the measurement the laser carrier frequency was maintained at this condition by feedback control of a piezoelectric fibre stretcher placed inside one arm of the MZI that allows for fine tuning of the time delay τ. The coarse setting of the time delay τ is realized by inserting a length of fibre inside one arm of the MZI. The whole set-up is implemented with polarization maintaining (PM) components in order to avoid polarization fading/drift. A time delay τ of 6.5 ns (1.3 m fibre length) was chosen, which was small enough to make the approximation

$$\sin(\pi f \tau) \approx \pi f \tau \tag{4.13}$$

over the whole frequency range of interest (e.g., 0-10 MHz). Practically, this means that there is constant sensitivity over the whole measurement range, which can be easily appreciated by inserting (4.13) into (4.12) giving:

$$S_\nu(f) = S_{SA}(f) \big/ (A\pi\tau)^2 \cdot \tag{4.14}$$

$S_\nu(f)$, measured in Hz/√Hz, is shown in Fig. 4.34, over the frequency ranges 100 Hz to 10 MHz in (a) and 1 kHz to 100 kHz in (b). It was measured by converting the laser frequency noise into amplitude noise with the interferometer maintained in quadrature. At low frequencies (1Hz-10kHz) the PSD has a 1/f behaviour. For higher frequencies (10kHz-10MHz) the frequency noise forms a plateau. The white frequency noise decreases as the bias current is increased as shown in Fig. 4.34 (a). These measurements were processed to calculate the laser linewidth at the points shown in Fig. 4.34 (b), values of 91 kHz and 67 kHz were extracted at bias currents of 300 mA and 400 mA, respectively. This compares favourably with the D-SH measurement where values of 94 kHz and 70 kHz were extracted at 300 mA and 400 mA, respectively.

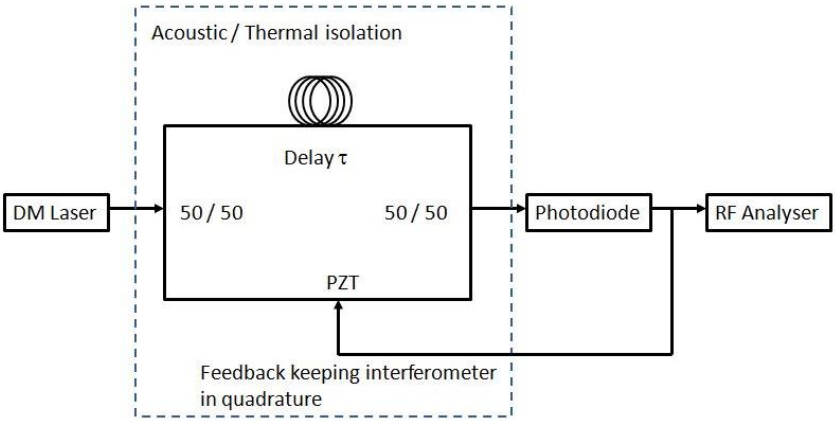

Fig. 4.33. Measurement set-up for frequency noise PSD measurement based on frequency-to-amplitude converter.

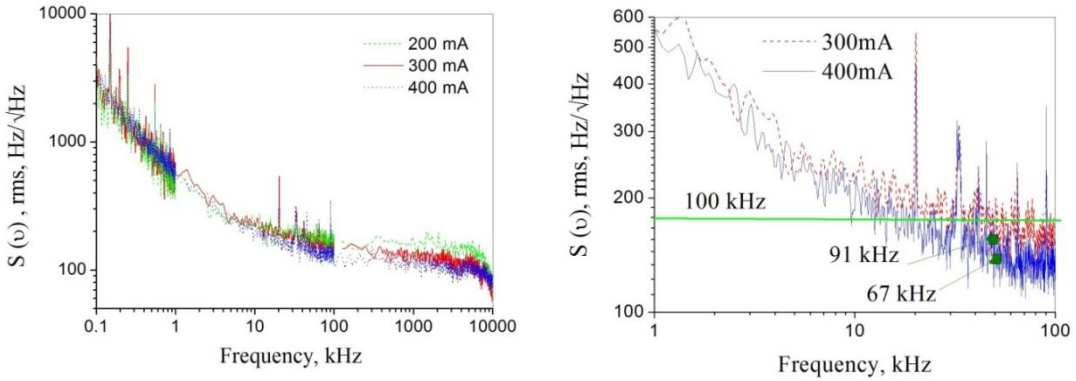

(a) (b)

Fig. 4.34. Overlapped frequency noise spectrum measured at (a) 200 mA, 300 mA and 400mA, over a frequency range of 0.1 kHz to 10 MHz and (b) 300 mA and 400mA, over a frequency range of 1 kHz to 100 kHz and showing extracted linewidth values.

4.2.3 Higher power lasers

DMLDs designed for higher output power, as well as low linewidth, were also fabricated. In order to increase the optical power the number of quantum wells was reduced to three and the thickness of the SCH was increased to expand the optical mode at the facets, thereby reducing the optical intensity. Details of the layer structure are as follows: the MQW structure consisted of three compressively strained (1%) 6 nm-thick AlGaInAs quantum wells and four slightly tensile strained (0.2%) 8 nm thick AlGaInAs barriers. The MQW was sandwiched between two 400 nm-thick InGaAsP SCH layers with a bandgap wavelength of λg = 1.3 μm, which also acted as an etch stop layer for the ridge waveguide and slot definition. A 1.8 μm thick p-InP layer was grown on top of the SCH, followed by a 200 nm thick highly p-doped InGaAs contact layer. The ridge waveguide width was 3 μm and the laser had a cavity length of 1000 μm. Increased output power was also achieved by reducing the front facet coating to 7 %, with the back facet coated at 95 %. The DMLD was mounted p-side up on a C-mount. Light was coupled from the laser chip

to the fibre using a lensed fibre focuser assembly. To minimise reflections back to the laser chip the focuser assembly was designed to provide low back reflection of less than -60 dB. To achieve low back reflection the lens was coated with an antireflection coating, and an optical isolator was incorporated into the assembly to prevent reflections from the fibre tip. The overlapped L-I plot, measured ex-facet, is shown in Fig. 4.35 over the range 0 ˚C ≤ T ≤ 85 ˚C. At 25 ˚C and 85 ˚C the threshold currents were 30.8 mA and 84 mA, with slope efficiencies of 0.102 W/A and 0.070 W/A, respectively. At 25 ˚C an output power of 32.6 mW was measured at a bias current of 400 mA. Placing this device in a package with a coupling efficiency > 62 % would allow a power in the fibre > 20 mW to be achieved.

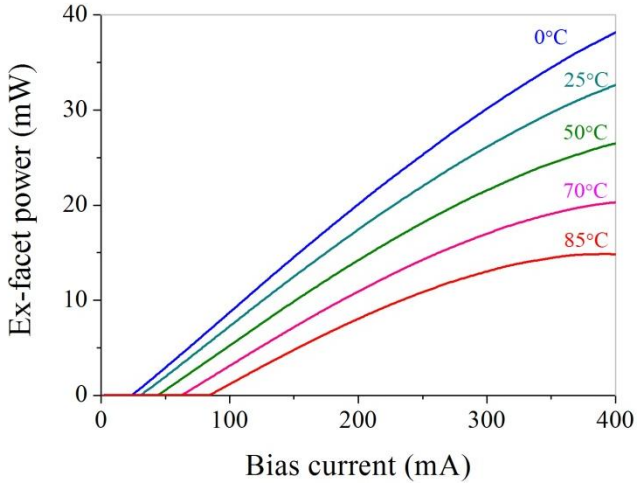

Fig. 4.35. Overlapped L-I plot measured ex-facet over the range 0 ˚C ≤ T ≤ 85 ˚C.

Fig. 4.36 shows the overlapped optical spectra measured at a bias current of 300 mA over the range 0 ˚C ≤ T ≤ 95 ˚C. The peak wavelength and SMSR versus temperature is plotted in Fig. 4.37. An SMSR in excess of 45 dB was measured over the temperature range. The continuous wavelength tuning range was 9.5 nm, and displayed a linear dependence with temperature corresponding to a tuning rate $\Delta\lambda/\Delta T$ of 0.1 nm/˚C. Fig. 4.38 shows the measured DS-H spectrum fitted to a Lorentzian

lineshape to extract the half-width at half maximum value. A value of 194 kHz was obtained at 25 ˚C at a bias current of 300 mA.

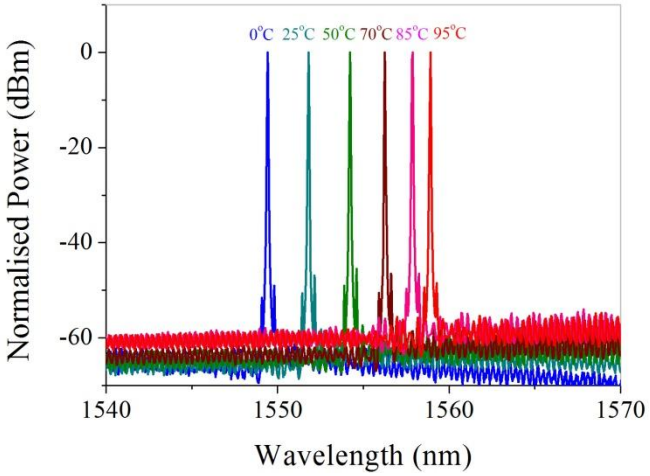

Fig. 4.36. 1550 nm DMLD measured optical spectra over the range 0 ˚C ≤ T ≤ 95 ˚C.

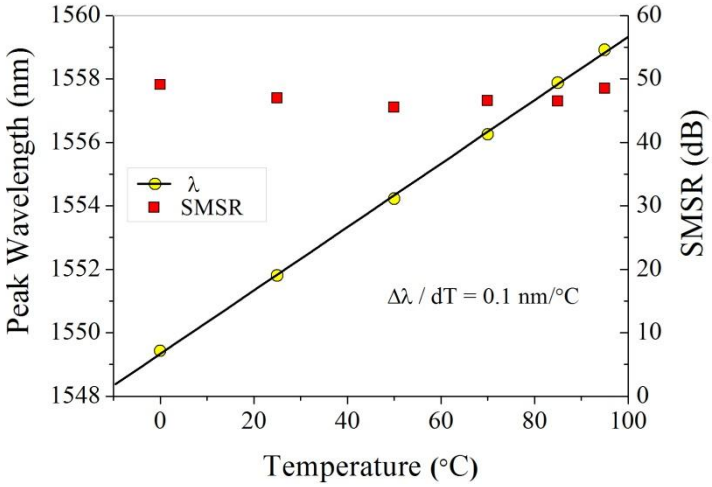

Fig. 4.37. Peak wavelength and SMSR versus temperature.

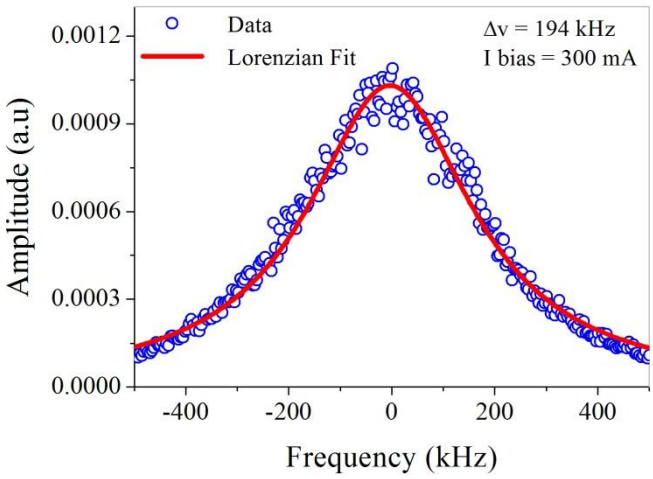

Fig. 4.38 D-SH spectrum at I = 300mA with Lorentzian fit linewidth = 194 kHz.

4.3 Conclusion

This chapter gave an overview of discrete mode laser diodes and showed how using this potentially economic approach lasers can be designed for wavelengths used in fibre optic communications and also other wavelengths, ranging from the visible to the mid-infrared regions of the optical spectrum. Characterisation results were presented for lasers operating in the 1310 nm and 1550 nm windows. Tables 4.1 and 4.2 summarise the characteristics of DMLDs targeted for direct modulation applications at 1310 nm and 1550 nm, respectively. The 1310 nm device operated over a temperature range of -40 ˚C ≤ T ≤ 97 ˚C and the 1550 nm device operated over a temperature range of -20 ˚C ≤ T ≤ 95 ˚C. Over these temperature ranges both devices operated single mode with SMSRs in excess of 40 dB. Also, the output power from the chip exceeded 5 mW for both devices at 85 ˚C. The static characteristics of these devices demonstrate their suitability for use in uncooled applications. DMLDs also show potential for use in next generation access networks, the optical bandwidth of DMLDs operating in the 1310 nm and 1550 nm windows

was also characterised and the devices have the requisite bandwidth for direct modulation applications up to 10 Gbit/s.

Temperature	Ith(mA)	SE(W/A)	Wavelength (nm)	SMSR (dB)
-40	7	0.3	1289.7	42.8
25	12	0.3	1295.5	43.5
85	38*	0.2*	1302	44

* measured at 87 °C

Table 4.1. Summary of a 1310 nm DMLD characteristics measured over the temperature range -40 ˚C ≤ T ≤ 97 ˚C.

Temperature	Ith(mA)	SE(W/A)*	Wavelength (nm)	SMSR (dB)
-20	9	0.1	1539.2	42
25	12.3	0.09	1543.5	51.04
85	37.1	0.06	1549.725	45.02

* measured from the fibre, coupling efficiency 25 %.

Table 4.2. Summary of a 1550 nm DMLD characteristics measured over the temperature range -40 ˚C ≤ T ≤ 97 ˚C.

DMLDs were also designed to achieve low linewidth emission at 1550 nm. Table 4.3 summarises the characteristics for three variations on the low linewidth design. The first device in the table was designed to achieve low linewidth and demonstrated a value as low as 70 kHz. The second device was designed to achieve low linewidth and operate over a wide temperature range. A linewidth as low as 138 kHz was demonstrated and single mode operation was demonstrated over a temperature range -10 ˚C ≤ T ≤ 110 ˚C. The third device was designed for low linewidth while achieving higher output power, and minimum linewidth of 194 kHz and an output power from the chip in excess of 30 mW was demonstrated. Low linewidth devices such as these could be used in optical systems employing higher order modulation formats.

Number of Quantum wells	Coating front/back (%)	Cavity length (μm)	Minimum Linewidth @ 25 °C (kHz)
5	30/95	2000	70
5	30/95	1000	138
3	7/95	1000	194

Table 4.3. Summary of low linewidth DMLDs design parameters and the corresponding minimum linewidth values demonstrated.

The next two chapters will focus on the characterisation of DMLDs in system level experiments, utilising direct modulation and advanced modulation formats, respectively.

References

[1] D. T. Cassidy and F. H. Peters, "Spontaneous emission, scattering, and the spectral properities of semiconductor diode lasers," IEEE Journal of Quantum Electronics, vol. 28, no. 4, pp. 785-791, Aprl. 1992.

[2] L. F. DeChiaro, "Damage-Induced Spectral Perturbations in Multilongitudinal-Mode Semiconductor Lasers," Journal of Lightwave Technology, vol. 8, no. 11, pp. 1659-1669, Nov. 1990.

[3] L. F. DeChiaro, "Spectral width reduction in multilongitudinal mode lasers by spatial loss profiling," Journal of Lightwave Technology, vol. 9, no. 8, pp. 975-986, Aug. 1991.

[4] D. A. Kozlowski, J. S. Young, J. M. C. England and R. G. S. Plumb, "Longitudinal mode control in 1.3 μm Fabry-Perot lasers by mode suppression," IEE Proceedings-Optoelectronics, vol. 143, no. 1, pp. 71-76, Feb. 1996.

[5] B. Corbett and D. McDonald, " Single longitudinal mode ridge waveguide 1.3 μm Fabry-Perot laser by modal perturbation," Electronics Letters, vol. 31, no. 25, pp. 2181-2182, Dec. 1995.

[6] V. Weldon, J. O'Gorman, J. J. Perez-Camacho, D. McDonald, J. Hegarty and B. Corbett, "Methane sensing with a novel micromachined single-frequency Fabry-Perot laser diode emitting at 1331 nm," IEEE Photonics Technology Letters , vol. 9, no. 3, pp. 357-359, Mar. 1997.

[7] J. Patchell, D. Jones, B. Kelly and J. O'Gorman, "Specifying the wavelength and temperature tuning range of a Fabry-Perot laser containing refractive index perturbations," Proceedings of SPIE, vol. 5825, pp. 1-13, Aprl. 2005.

[8] D. C. Byrne, PhD Thesis: An experimental investigation of tunable laser diodes based on multiple etched slots, Dublin: Trinity College, 2010.

[9] D. C. Byrne, J. P. Engelstaedter, W. H. Guo, Y. L. Qiao, B. Corbett, B. Roycroft, J. O'Callaghan, F. H. Peters and J. F. Donegan, "Discretely Tunable Semiconductor Lasers Suitable for Photonic Integration," IEEE Journal of Selected Topics in Quantum Electronics, vol. 15, no. 3, pp. 482-487, Jun. 2009.

[10] L. A. Coldren, Diode Lasers and Photonic Integrated Circuits, Hoboken: Wiley, 2012.

[11] M. Fukuda, T. Mishima, N. Nakayama and T. Masuda, "Temperature and current coefficients of lasing wavelength in tunable diode laser spectroscopy," Applied Physics B, vol. 100, no. 2, pp. 377-382, Aug. 2010.

[12] H. Lu, C. Blaauw and T. Makino, "Single-mode operation over a wide temperature range in 1.3 μm InGaAsP/InP distributed feedback lasers," Journal of Lightwave Technology, vol. 14, no. 5, pp. 851-859, May 1996.

[13] F. Gruet, T. Bandi, G. Mileti, R. Phelan, J. O'Carroll, B. Kelly and J. O'Gorman, "Development and spectral characterisation of discrete mode laser diodes (DMLDs) emitting at 780 nm for Rubidium atomic clocks," in Lasers and Electro-Optics Europe Conference (CLEO), Munich, May 2011.

[14] R. Phelan, J. O'Carroll, D. Byrne, C. Herbert, J. Somers and B. Kelly, "In0.75Ga0.25As/InP Multiple Quantum Well Discrete Mode Laser Diode Emitting at 2 um," IEEE Photonics Technology Letters, vol. 24, no. 8, pp. 652-654, Aprl. 2012.

[15] R. Phelan, T. J. Slight, B. Kelly, J. O'Carroll, A. McKee, D. G. Revin, S. Y. Zhang, A. B. Krysa, K. L. Kennedy, J. W. Cockburn, C. N. Ironside, W. Meredith and J. O'Gorman, "Room-Temperature Operation of Discrete-Mode InGaAs–AlAsSb Quantum-Cascade Laser With Emission at λ =3.3 μm," IEEE Photonics Technology Letters, vol. 22, no. 17, pp. 1273-1275, Sept. 2010.

[16] H. Venghaus and N. Grote, Fibre Optic Communication key devices, Berlin: Springer, 2012.

[17] Integra Networks, "News articles: operating temperatures for fiber optic devices," May 2012. [Online]. Available: http://integranetworks.net/2012/05/operating-temperatures-for-fiber-optic-devices/.

[18] T. Okoshi, K. Kikuchi and A. Nakayama, “Novel method for high resolution measurement of laser output spectrum,” Electronics Letters, vol. 16, no. 16, pp. 630-631, Jul. 1980.

[19] M. O. van-Deventer, P. Spano and S. K. Nielsen, “Comparison of DFB laser linewidth measurement techniques results from COST 215 round robin,” Electronics Letters, vol. 26, no. 24, pp. 2018-2020, Nov. 1990.

[20] G. M. Stéphan, T. T. Tam, S. Blin, P. Besnard and M. Têtu, “Laser line shape and spectral density of frequency noise,” Physical Review A, vol. 71, no. 4, pp. 0438091-0438099, Aprl. 2005.

[21] R. Slavík, Y. Liao, E. Austin, P. Petropoulos and D. J. Richardson, “Full characterization and comparison of phase properties of narrow linewidth lasers operating in the C-band,” in International Conference on Optical Fiber Sensors, Ottawa, May. 2011.

Chapter 5

Direct modulation of discrete mode laser diodes

This chapter looks at the performance of discrete mode laser diodes under direct modulation at a bit rate of 10 Gbit/s. Results are presented for lasers operating in both the 1310 nm and 1550 nm wavelength windows, and includes the transmission performance over single mode fibre.

5.1 1310 nm DMLD

1310 nm directly modulated single mode lasers capable of operating at 10 Gbit/s are of interest for next generation access networks. Transmission distances of 10 km and 20 km are specified for Ethernet 10GBase-LR and 10GBase-LW, respectively. The performance of a 1310 nm DMLD is characterised and its performance is evaluated for use in 10 Gbit/s applications.

The nine quantum well 1310 nm DMLD presented in 4.2.1.1 was packaged in a high speed TO-can package, where an internal resistor matched the impedance to 50 Ω and single-ended modulation was used. Light was coupled to a fibre via a lensed

coupler on a precision x, y, z translation stage and a coupling efficiency of approximately 10 % was achieved. The laser was modulated at 10 Gbit/s using a pseudo random binary sequence (PRBS) pattern of 2^{23}-1. PRBS patterns of 2^{15}-1 and 2^{23}-1 have been adopted by international standards [1], and 2^{23}-1 was chosen as longer patterns contain more frequency components, due to longer sequences of continuous '1's and '0's. The DC bias current was set to 40 mA and the modulation current was set to 40 mA p-p. An average optical power of 5.5 mW was measured ex-facet and an extinction ratio of 6 dB was obtained. Fig. 5.1 shows the overlapped spectra with the modulation on (white trace) and off (black trace) measured at a span of (a) 40 nm and (b) 1 nm. The resolution of the optical spectrum analyser (OSA) was set to 0.02 nm for the measurement. A peak wavelength of 1318.68 nm and 1318.64 nm was measured with the modulation on and off, respectively, and an SMSR of 44.7 dB was measured for both conditions, demonstrating the stability of the laser's spectrum under modulation. The width of the peak, measured 20 dB down, was 0.078 nm for the modulation turned off, and this increased to 0.172 nm when the modulation was turned on. The value taken with the modulation turned off was limited by the resolution of the OSA.

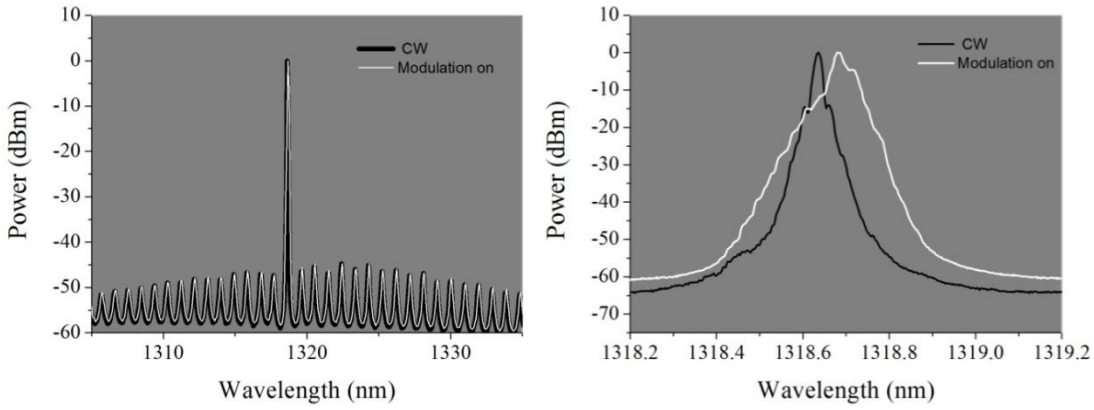

Fig. 5.1. Overlapped optical spectra for a 1310 nm DMLD at 25 ˚C, with modulation current on and off, measured at a wavelength span of (a) 40 nm and (b) 1 nm.

Using the setup shown in Fig. 5.2, the device was characterised back-to-back and after transmission through 10 km and 22 km of SSMF, at a temperature of 25 ˚C. The receiver used an unamplified PIN photo-detector with a 7.46 GHz low pass Bessel Thompson filter applied to the output. Clock recovery was used for the transmission experiments. Fig. 5.3 shows the eye diagram measured back-to-back, and a clear eye opening is shown. Fig. 5.4 shows the BER versus received optical power measured back-to-back and after transmission through 10 km and 22 km of SSMF. Relatively low power penalties of 0.25 dB and 0.3 dB were measured after transmission through 10 km and 22 km, respectively, and no error floor was observed. The experiment confirms that the laser is capable of achieving 10 Gbit/s transmission. The device was not tested at 85 ˚C as it did not maintain single mode operation at higher temperatures.

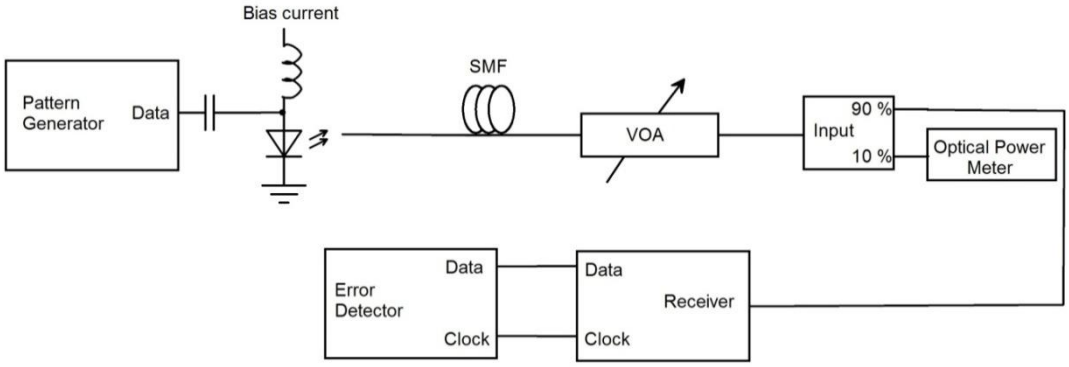

Fig. 5.2. Experimental setup for 10 Gbit/s transmission experiments at 1310 nm.

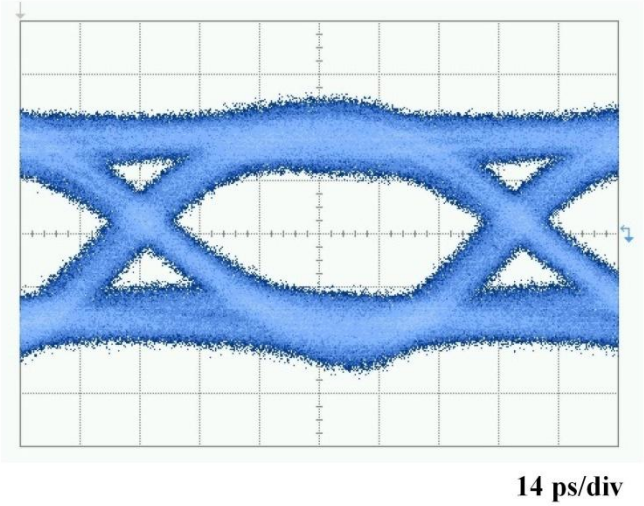

Fig. 5.3. Back-to-back eye diagram for a 1310 nm DMLD directly modulated at 10 Gbit/s at 25 ˚C.

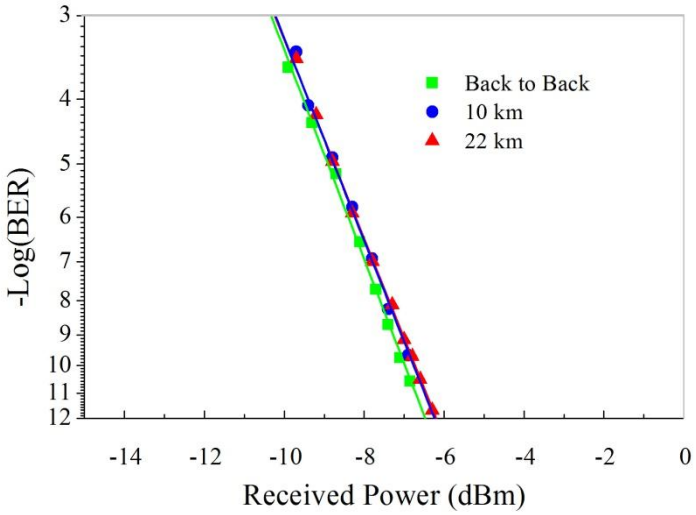

Fig. 5.4. BER versus received optical power, measured back-to-back and after transmission through 10 km and 22 km of SSMF for a 1310 nm DMLD directly modulated at 10 Gbit/s at 25 ˚C.

As the DMLD is based on an FP structure a prerequisite to achieving 10 Gbit/s operation over a wide temperature range is that the FP lasers made from the same epitaxial structure can achieve the requisite high speed performance. An FP laser taken from the same wafer as the DMLD was characterised at 10 Gbit/s at 25 ˚C and 85 ˚C. The laser had a cavity length of 250 μm, with front and back facet reflectivities of 16 % and 87 %, respectively. The device was mounted on a high speed submount and the light was coupled to a fibre using a lensed coupler on a precision x y z translation stage. The DC bias current was set to 40 mA and 45 mA at 25 ˚C and 85 ˚C, respectively, and a modulation current of 40 mA p-p was used at both temperatures. An extinction ratio of approximately 5 dB was obtained at both temperatures. Centre wavelengths of 1326 nm and 1358 nm were measured at 25 ˚C and 85 ˚C, respectively. The S21 was measured at these DC bias levels and 3 dB bandwidths of 11 GHz and 8.5 GHz were obtained at 25 ˚C and 85 ˚C, respectively, which should be sufficient to achieve 10 Gbit/s operation at both temperatures. The device was characterised back-to-back and after transmission through 1 km and 2 km of SSMF. Fig. 5.5 shows the back-to-back eye diagrams measured at (a) 25 ˚C and (b) 85 ˚C. Fig. 5.6 shows the BER versus received optical power measured back-to-back and after transmission through 1 km and 2 km of SSMF at (a) 25 ˚C and (b) 85 ˚C. After transmission through 2 km a power penalty less than 0.3 dB was measured at both temperatures, and such a device can be used in short reach applications. Operation at 10 Gbit/s was demonstrated at 25 ˚C and 85 ˚C, with open eyes being measured, also the BER measurements displayed no error floors. However, the eyes were not optimum, in that significant jitter was observed. To investigate the source of this jitter, and determine if it was related to the package or the laser chip, a similar FP laser from the same batch was packaged in a high speed

TOSA package. A commercial laser driver was used instead of applying the output signal from the pattern generator to the laser via a matching resistor.

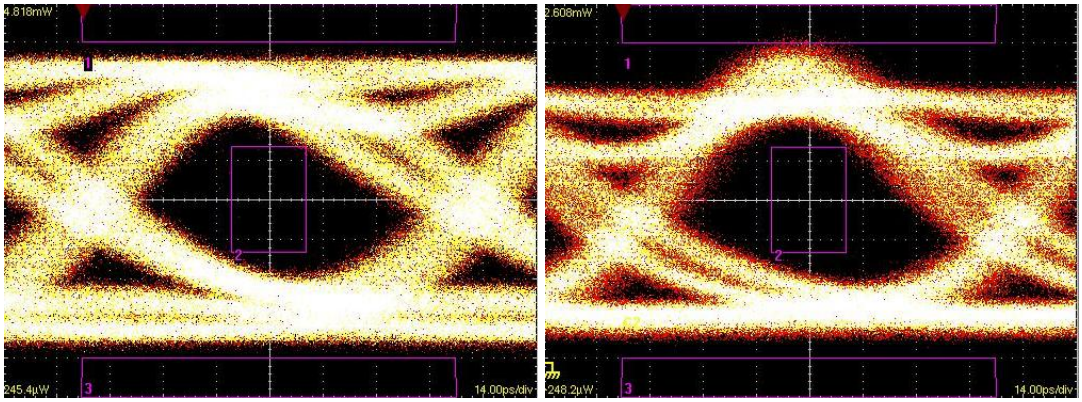

(a) (b)

Fig. 5.5. Eye diagram for a 1310 nm FP directly modulated at 10 Gbit/s, at (a) 25 ˚C and (b) 85 ˚C.

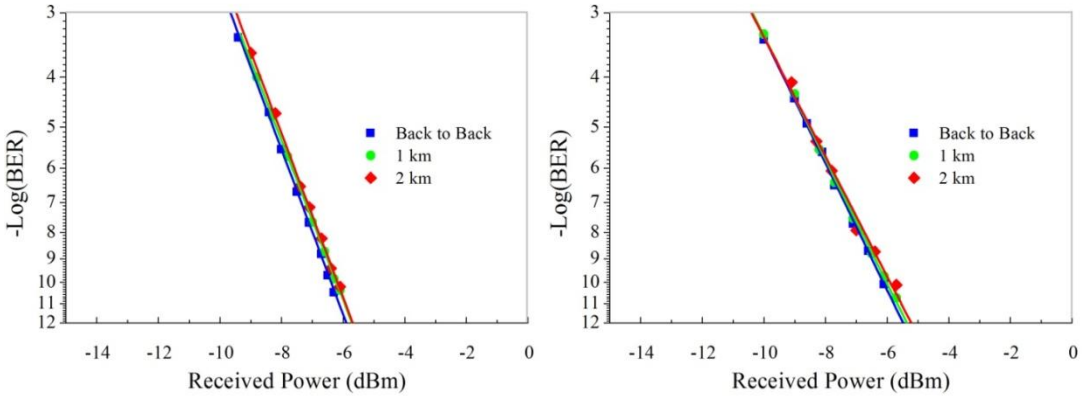

(a) (b)

Fig. 5.6. BER versus received optical power, back-to-back and after transmission through 1 km and 2 km of SSMF for a 1310 nm FP directly modulated at 10 Gbit/s at (a) 25 ˚C and (b) 85 ˚C.

Fig. 5.7 shows the back-to-back eye diagram from the TOSA measured at room temperature with the bias current set 40 mA, where an extinction ratio of approximately 5 dB was obtained. Comparing Fig. 5.7 with Fig. 5.5 (a), there is a clear improvement in the eye with the jitter being significantly reduced, indicating that the packaging of the previous device was the source of the jitter, it also demonstrates the importance of the packaging to the overall performance. The TOSA

was not used for the initial work as this was carried out on a small number of devices and the TOSA process is geared towards higher volumes.

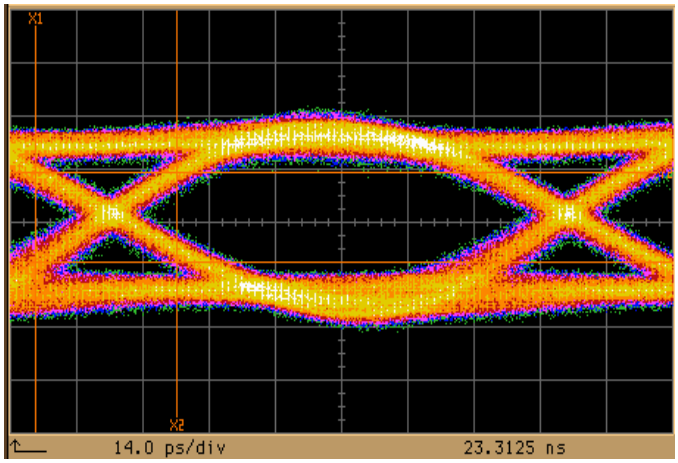

Fig. 5.7. Eye diagram for a 1310 nm FP TOSA directly modulated at 10 Gbit/s, at room temperature.

5.2 1550 nm DMLD

The 1550 nm DMLD presented in 4.2.1.2 was packaged in a TO-56 based package; however, this package did not have the required electrical bandwidth to investigate the dynamic performance at 10 Gbit/s. To characterise the performance at 1550 nm a DMLD in a more advanced package was used. The device had the same epitaxial structure as the device presented in 4.2.1.2 but had a cavity length of 400 μm with front and back facet reflectivities of 30 %. The package was a fiberized high speed butterfly package with the modulation signal applied via a K type connector. An internal resistor in the RF transmission line matched the impedance to 50 Ω, and single-ended modulation was used. The laser chip temperature was set to 25 ˚C and the device was modulated at a bit rate of 10 Gbit/s using a PRBS 2^{23}-1 pattern. The DC bias current was set to 60 mA and a modulation current of 40 mA p-p was used to obtain an extinction ratio of 5.5 dB. Fig. 5.8 shows the overlapped spectra with the modulation turned on (white trace), and off (black trace), at a wavelength span of

(a) 50 nm and (b) 3 nm. The 50 nm span was measured with a Yokogawa AQ6370 OSA with the resolution set to 0.02 nm, and the 3 nm span was measured with an Apex technologies high resolution OSA, with the resolution set to 0.16 pm. Peak wavelengths of 1540.95 nm and 1540.87 nm, and SMSR values of 36.1 dB and 38.3 dB nm were measured for the modulation on and off, respectively. The width of the peak measured 20 dB down was 0.6 pm with the modulation turned off, and this increased to 0.19 nm with the modulation turned on. The value with the modulation turned off is limited by the resolution of the OSA, which is illustrated in the difference between the traces of Fig. 5.1 (b) and Fig. 5.8 (b), for resolution settings of 0.02 nm and 0.16 pm, respectively.

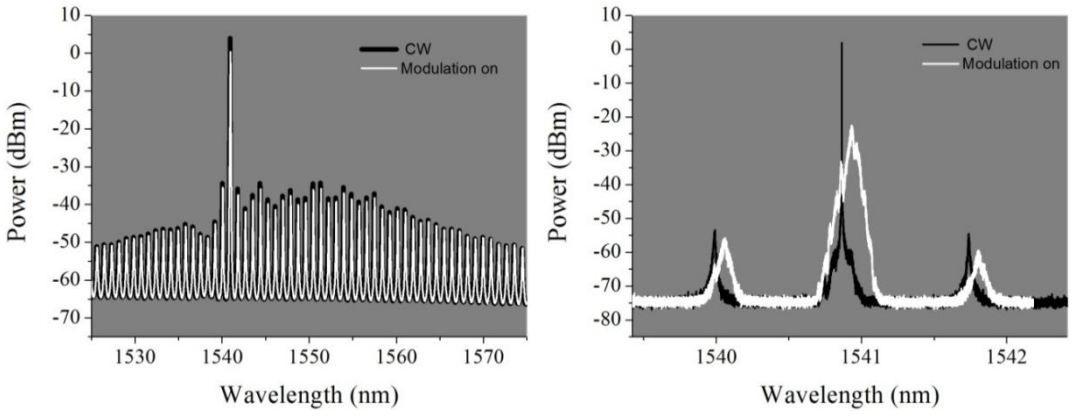

Fig. 5.8. Overlapped optical spectra for a 1550 nm DMLD at 25 ˚C, with modulation current on and off, measured at a span of (a) 40 nm (resolution 0.02 nm) and (b) 3 nm (0.16 pm resolution).

The BER versus received power was measured using the setup shown in Fig. 5.9. The optical signal was detected using a single stage optically pre-amplified receiver and clock recovery was used in the transmission experiments. Fig. 5.10 shows the measured eye diagram with a clear eye opening shown. The BER versus received optical power was measured back-to-back and after transmission through 10 km and 20 km of SSMF. After 10 km a power penalty, measured at a BER of 1×10^{-9}, of

0.8 dB was observed. After transmission through 20 km this increased to 5.3 dB, also, the change in the slope of the 20 km data indicates the presence of an error floor. The degradation in performance is the result of dispersion effects after transmission through SSMF.

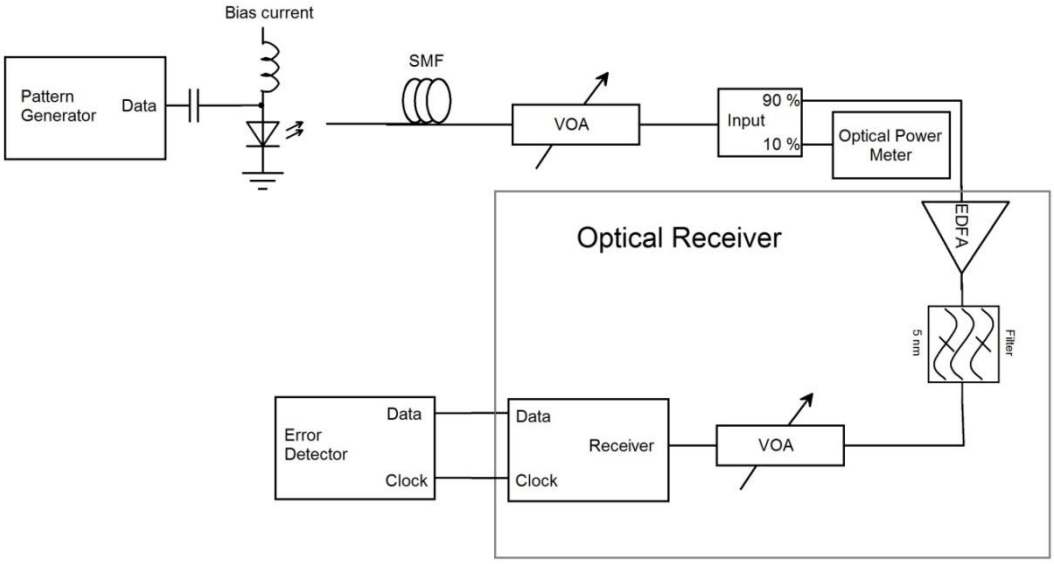

Fig. 5.9. Experimental setup for 10 Gbit/s transmission experiments at 1550 nm.

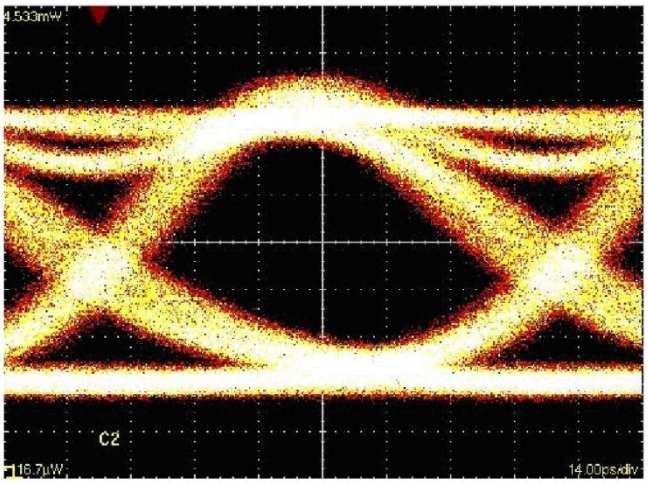

Fig. 5.10. Back-to-back eye diagram for a 1550 nm DMLD directly modulated at 10 Gbit/s at 25 ˚C.

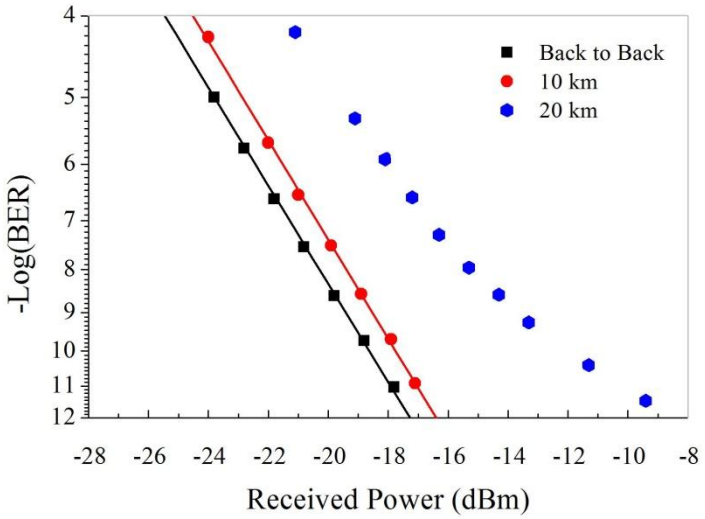

Fig. 5.11. BER versus received optical power, measured back-to-back and after transmission through 10 km and 20 km of SSMF for a 1550 nm DMLD directly modulated at 10 Gbit/s at 25 ˚C.

5.2.1 10 Gbit/s transmission at 1550 nm with dispersion compensation

Dispersion compensation modules can be used to extend the reach of directly modulated lasers. In this experiment a dispersion compensation module with a dispersion value of -681 ps/nm was introduced to the setup shown in Fig. 5.9, and was placed directly after the laser. This provided pre-compensation for dispersion at the transmitter allowing the reach to be extended. Fig. 5.12 shows the BER versus received optical power measured back-to-back and after transmission through SSMF for distances of 10 km, 22 km, 37 km, 49 km and 60 km. The back-to-back BER measurement was taken at the output of the dispersion compensating module, and in this case the laser together with the dispersion compensating module is considered to be the transmitter. A maximum power penalty of 3.6 dB was measured at 60 km and an increase in sensitivity, compared to the back-to-back measurement, was observed at 10 km and 22 km indicating that the received signal was close to an optimum value. Also, comparing the back-to-back case with dispersion compensation to that

of Fig. 5.11 for the laser on its own, there was an improvement in sensitivity of 2.2 dB. Previous work has shown that negative dispersion can lead to an improvement in receiver sensitivity, as a result of pulse shaping due to the combined effect of the chirp introduced by the laser and negative dispersion [2, 3]. Fig. 5.13 shows the BER versus received power measured after transmission through 37 km of SSMF using dispersion pre-compensation and also using post compensation, where the dispersion compensation module was moved and placed before the receiver; negligible differences in the BER performance was observed between both cases.

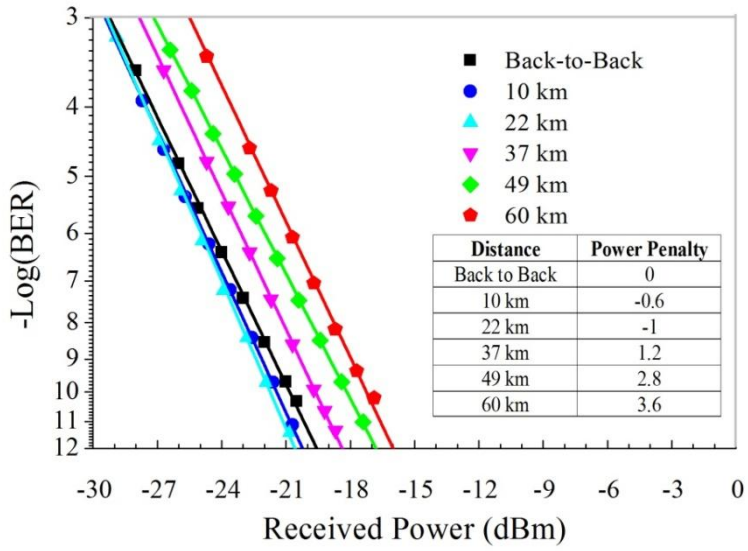

Fig. 5.12. BER versus received optical power with dispersion pre-compensation of -681 ps/nm, measured back-to-back and after transmission through 10, 22, 37, 49 and 60 km of SSMF. Inset: table listing the power penalties at the transmission distances measured.

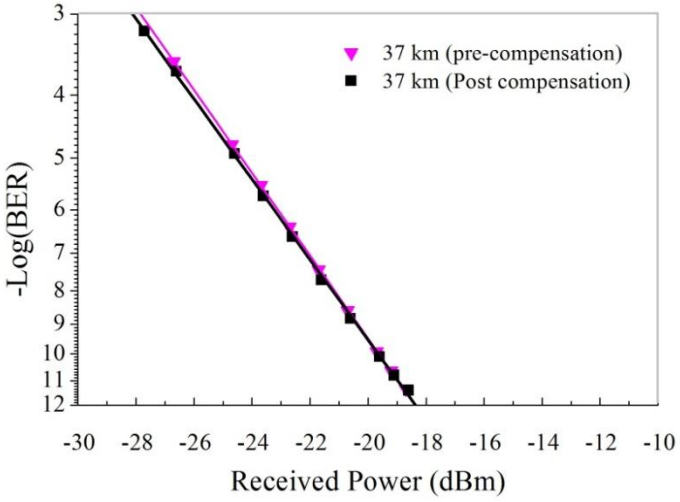

Fig. 5.13. BER versus received optical power measured after transmission through 37 km of SSMF, using dispersion pre-compensation and post compensation.

5.3 Discussion

The 1310 nm DMLD demonstrated 10 Gbit/s operation at 25 ˚C. Transmission over 10 km and 22 km was demonstrated, without error floors being observed and a power penalty of only 0.3 dB was measured after 22 km. The low power penalty is primarily due to the lower dispersion of SSMF in the 1310 nm window, which is why directly modulated lasers, even at bit rates as high as 10 Gbit/s, are the transmitter of choice for access applications at this wavelength. In order for these DMLDs to be considered for access applications at 10 Gbit/s the temperature range would have to be extended, ideally to cover the range -40 ˚C to 85 ˚C. Process limitations for this batch of lasers meant that the devices produced were limited to an upper temperature limit of 60 ˚C. In terms of future development, a critical step necessary to develop a high speed DMLD is having an FP structure with the requisite bandwidth, something which is more challenging at higher temperatures. An FP laser from the same wafer demonstrated 10 Gbit/s operation and displayed no error floor

in the BER measurement at both 25 ˚C and 85 ˚C, and this structure could be used in future 10 Gbit/s DMLD development runs.

The 1550 nm DMLD demonstrated 10 Gbit/s operation at 25 ˚C. An open eye was measured and the BER versus received optical power was measured back-to-back and after transmission through 10 km and 20 km of SSMF. The power penalties, measured at a BER of 1×10^{-9}, were 0.8 dB and 5.3 dB after transmission through 10 km and 20 km of SSMF, respectively. The increase in the power penalty after 20 km was due to chirp from the laser in combination with increased dispersion in SSMF in the 1550 nm window. No error floor was observed in the back-to-back or the 10 km measurement. The device could potentially be used as a transmitter laser in links up to 10 km, but for transmission distances of 20 km, and beyond, more advanced solutions need to be used for operation at 10 Gbit/s. One approach is to use dispersion compensation, where negative dispersion is used to compensate for the positive dispersion introduced by the SSMF. Negative dispersion can be introduced to a link by adding dispersion compensating fibre (DCF) or lumped elements, such as fibre Bragg gratings [4]. A dispersion compensating module, consisting of DCF, was introduced to the setup and enabled the transmission distance to be extended to 60 km. In the experiment transmission over distances ranging from 10 km to 60 km with a maximum power penalty of 3.6 dB was demonstrated. As the dispersion compensation was placed in a pre-compensation configuration, such a scheme could be used in a point to multi-point link. However, such a scheme may find limited applications in access networks operating at 10 Gbit/s, as an EML with its lower chirp may be a more practical solution. However, the use of directly modulated lasers and dispersion compensation may be viable in an access system employing WDM, as the dispersion compensation module would be shared between multiple channels [5].

Another development which could make the use of 1550 nm directly modulated lasers a viable solution is electronic dispersion compensation. Pre-compensation pre-distorts the drive signal applied to the laser and has the potential to extend the reach significantly [6]. Electronic dispersion compensation can also be applied at the receiver, where it could potentially double the transmission distance achievable [7].

The DMLD used at 1550 nm was primarily chosen because it was in a suitable high speed package. The design was not optimum for high speed operation and it would have been desirable to have used a device with a shorter cavity and a high reflectivity coating on the back facet, as this would have increased the relaxation oscillation frequency. The SMSR for the device exceeded 30 dB; however, as demonstrated in 4.2.1.2, it is possible to achieve an SMSR in excess of 40 dB from a 1550 nm DMLD. Despite this, the device demonstrated 10 Gbit/s operation, showing that the structure is capable of high speed operation. Also, optimised devices have the potential to achieve improved performance, and this is an objective for future work in this area. High speed lasers are also essential components for other applications, in one example demonstrated in other work, a DMLD was gain switched at a frequency of 10.7 GHz in order to generate a coherent optical multicarrier signal with a frequency spacing between the side bands of 10.7 GHz [8]. Such a device could potentially be used in a range of applications including optical arbitrary waveform generation, photonic microwave signal generation, optical signal processing and multicarrier spectrally efficient transmission techniques with the sub-channel spacing equal to the symbol rate of each sub-channel [9].

5.4 Conclusion

10 Gbit/s operation was demonstrated using DMLDs at wavelengths in the 1310 nm and 1550 nm windows. Transmission distances up to 22 km and 10 km were demonstrated at 1310 nm and 1550 nm, respectively, without dispersion compensation. Table 5.1 summarises the results after transmission through SSMF at 1310 nm. A maximum power penalty of only 0.3 dB was observed after 22 km and the device shows potential for use in future access networks operating at 10 Gbit/s. Table 5.2 summarises the results after transmission through SSMF at 1550 nm. A maximum power penalty of 0.8 dB was observed after 10 km and this increased to 5.3 dB after transmission through 20 km. Such a device may find application in short reach applications at 10 km, or less, operating at 10 Gbit/s. To increase the transmission distance dispersion compensation would be necessary and it was shown that the transmission distance could be extended to 60 km at 1550 nm using dispersion compensation.

The next chapter will look at another application of single mode laser in fibre optic communications, namely coherent communications, where the laser is operated CW and external modulation is used.

Distance (km)	Power penalty (dB)	Comment
Back-to-back	-	Error free
10	0.25	Error free
22	0.3	Error free

Table 5.1. Summary of the transmission experiment results at 1310 nm.

Distance (km)	Power penalty (dB)	Comment
Back-to-back	-	Error free
10	0.8	Error free
20	5.3	Error floor observed

Table 5.2. Summary of the transmission experiment results at 1550 nm.

References

[1] D. Derickson, Fiber Optic Test and Measurement, New Jersey: Prentice Hall, 1998.

[2] Y. Miyamoto, K. Hagimoto, F. Ichikawa, M. Yamamoto and T. Kagawa, "10 Gbit/s, 50 km dispersive fibre transmission experiment using strained multiquantum-well DFB laser diode," Electronics Letters, vol. 27, no. 10, pp. 853-855, May 1991.

[3] K. Sato, S. Kuwahara and Y. Miyamoto, "Chirp Characteristics of 40-Gb/s Directly Modulated Distributed-Feedback Laser Diodes," Journal of Lightwave Technology, vol. 23, no. 11, pp. 3790-3797, Nov. 2005.

[4] J. M. Senior, Optical Fiber Communications: Principles and Practice, 3rd ed., New York: Prentice Hall, 2009.

[5] X. Cheng, Y. J. Wen, Z. Xu, X. Shao, Y. Wang and Y. Yeo, "10-Gb/s WDM-PON transmission using uncooled, directly modulated free-running 1.55-μm VCSELs," in European Conference on Optical Communication (ECOC), Brussels, Sept. 2008.

[6] A. S. Karar, J. C. Cartledge, J. Harley and K. Roberts, "Electronic Pre-Compensation for a 10.7-Gb/s System Employing a Directly Modulated Laser," Journal of Lightwave Technology, vol. 29, no. 13, pp. 2069-2076, Jul. 2011.

[7] M. D. Feuer, H. Sun-Yuan, S. L. Woodward, O. Coskun and M. Boroditsky, "Electronic dispersion compensation for a 10-Gb/s link using a directly modulated laser," IEEE Photonics Technology Letters, vol. 15, no. 12, pp. 1788-1790, Dec. 2003.

[8] P. M. Anandarajah, R. Maher, Y. Q. Xu, S. Latkowski, J. O'Carroll, S. G. Murdoch, R. Phelan, J. O'Gorman and L. P. Barry, "Generation of Coherent Multicarrier Signals by Gain Switching of Discrete Mode Lasers," IEEE Photonics Journal, vol. 3, no. 1, pp. 112-122, Feb. 2011.

[9] R. Zhou, S. Latkowski, J. O'Carroll, R. Phelan, L. P. Barry and P. Anandarajah, "40nm wavelength tunable gain-switched optical comb source," in European Conference and Exhibition on Optical Communication (ECOC), Geneva, Sept. 2011.

Chapter 6

Characterisation of discrete mode laser diodes in advanced modulation format systems

In this chapter discrete mode laser diodes designed for narrow linewidth emission are characterised in a test bed employing advanced modulation formats. Two formats are considered, QPSK and 16-QAM, and the performance achieved using low linewidth discrete mode laser diodes and an external cavity laser is compared. QPSK was chosen as it has been widely used in current state of the art commercially deployed systems [1, 2]. Compared to QPSK, 16-QAM has the potential to double capacity while maintaining the same baud rate making it attractive for use in future coherent systems [3]. Increasing the order of the modulation format places more stringent requirements on the phase noise of the lasers used in these systems. The performance of low linewidth DMLDs is evaluated through system experiments employing both modulation formats and the results compared with those obtained using an ECL. The

effect of increased linewidth on the performance of these systems is also investigated.

6.1 Experimental setup

The back-to-back coherent transmission setup is shown in Fig. 6.1. To generate the electrical QPSK modulation signal, the data and data-bar outputs from a pattern generator were used. The output for the pattern generator was 2 V p-p, however this was insufficient to drive the IQ modulator which required a minimum drive voltage of 3.5 V p-p [4]. Modulator drivers were used to amplify the pattern generator's outputs. The data pattern used was PRBS 2^9-1. A delay of 5.2 ns, corresponding to 13 symbols at 2.5 Gbaud, was applied to the data-bar signal decorrelating the data patterns in order to emulate two independent channels. The data and data-bar signals were then applied to the I and Q inputs of a dual parallel MZM, respectively. The IQ modulator is a polarisation sensitive device, therefore, a polarisation controller was placed at the modulators input to optimise the polarisation of the input light from the transmitter laser. The output optical signal from the modulator was applied to a single-stage optically pre-amplified coherent receiver. The function of EDFA was to increase the sensitivity of the receiver. The EDFA used was a JDSU MEDFA-A15500. The EDFA was followed by a 2 nm optical bandpass filter to reduce ASE noise. The coherent receiver consisted of a 90˚ hybrid and a pair of balanced photo-detectors with integrated transimpedance amplifiers, which were manufactured by Teleoptix and had a bandwidth of up to 32.5 GHz. Polarisation controllers were placed at both inputs of the 90˚ hybrid, in order to match the polarisations of the received signal and the local oscillator. Also, variable optical attenuators (VOAs) were placed at both inputs of the 90˚ hybrid in order to control the power levels

applied to the receiver. In the setup either self-homodyning with the TX laser or heterodyning with a second LO laser could be implemented by switching the signal applied to the second input of the 90˚ hybrid. In the self-homodyne configuration, the optical signal from the TX laser was split using a 90:10 splitter, with 90 % and 10 % being applied to the TX, and LO paths, respectively. The TX and LO were decorrelated by passing the LO through 12 km of SSMF. This emulates a system using lasers at the TX and the LO matched in frequency but with uncorrelated phase. In the heterodyne configuration, a second LO laser was introduced to the setup. In this configuration both the phase and frequency of the lasers were uncorrelated. The I and Q outputs of the balanced receivers were captured using a real-time scope for post processing.

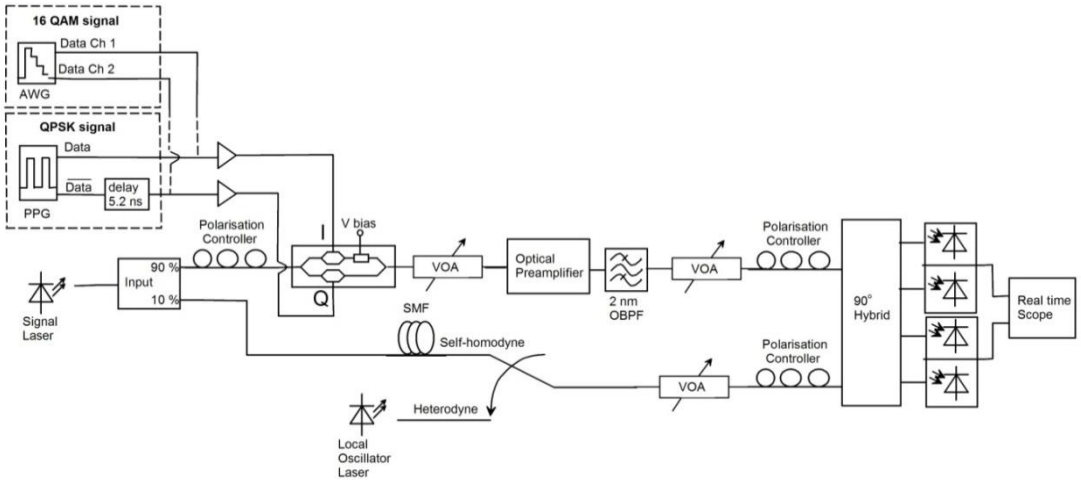

Fig. 6.1. Coherent transmission setup, QPSK or 16-QAM modulation can be generated by applying the appropriate electrical drive signals to the IQ modulator. By switching between a decorrelated portion of the TX laser, or a separate LO laser, the receiver can be setup as a self-homodyne or heterodyne receiver.

The pattern generator used in the QPSK setup was replaced with a dual-channel arbitrary waveform generator (AWG), which provided the multi-level electrical signals used to generate 16-QAM. The outputs from the AWG were amplified and

applied to the I and Q inputs of the modulator. At the receiver, improved sensitivity was achieved using a dual-stage EDFA as an optical preamplifier, as opposed to the single-stage EDFA used in the QPSK setup. The first stage EDFA was a MPB communications Inc. EFA-R35 and the second stage was a JDSU MEDFA-A15500. A 2nm optical bandpass filter was placed after the first EDFA to reduce ASE noise. Also, in comparison to the QPSK setup, further optimisation of the setup was performed. Low-pass filters were applied directly after the outputs of the arbitrary waveform generator to reduce electrical noise. Linearity is very important in the generation of multi-level formats, such as 16-QAM, therefore, the drive signals were carefully optimized to cope with the nonlinearity of the electrical amplifiers and the I/Q modulator. Table 6.1 lists some of the main specifications of components used at the transmitter and in the optically pre-amplified coherent receiver [4, 5, 6, 7, 8, 9].

6.1.1 Digital signal processing

In the reception of phase-modulated signals in an optical system, as described here, the DSP is responsible for some major tasks such as the resolving, correcting and tracking of the phase error between the received signal and the LO [10]. Additionally, the task of symbol timing falls to the DSP function. In this experimental setup, these tasks are accomplished by off-line processing conducted in Matlab™, using the DSP algorithms described in [11]. An Agilent real-time scope captured the optical beating between the received signal and the LO at the detector outputs. The I & Q samples were normalized by RMS value for balanced I/Q components. In the heterodyne configuration, a non-data-aided frequency correction [12] was performed to eliminate the frequency offset between the lasers. This was not needed for the homodyne experiments.

Component	Parameter	Min.	Typ.	Max.	Unit
JDSU IQ Modulator, Part number: 21090286-010	Wavelength range	1528		1564	nm
	Optical Insertion loss			6	dB
	RF drive voltage (@ 2GHz)	3.5		6.5	V
	RF Bandwidth		11		GHz
	DC input Vπ			6	V
JDSU Modulator driver/RF Amplifier, Part number: H301-1210	Data rate	2.488		12.2	Gbit/s
	Output amplitude			7.5	V
	Gain	24	26		dB
	Noise figure		11		dB
Optoplex 90 degree Hybrid, Part number: HB-C0GFA5001	Wavelength range	1527		1567	nm
	Insertion loss (with connectors)				
	Received signal port (polarization scrambled) to all outputs	9.5		11	dB
	LO port (45° linear polarized) to all outputs	9.5		11	dB
	Max. input optical power			300	mW
Teleoptix PD, Part number: T43G-DPN-DTLNR-xx	Wavelength range	1525		1560	nm
	Optical input power		3	7	dBm
	Photodetector responsivity		0.6		A/W
	Small signal differnetial conversion gain		150		V/W
	3 dB Bandwidth		32.5		GHz
JDSU MAP EDFA, Part number: MEDFA-A15500	Wavelength range	1528		1565	nm
	Saturated output power	14			dBm
	Noise figure	3.5		4	dB
	Small signal gain	37			dB
MPB communications Inc. EDFA, Part number: EFA-R35	Wavelength range	1542		1560	nm
	Saturated output power	13.5			dBm
	Noise figure	3		3.5	dB
	Small signal gain		37		dB

Table. 6.1. Specifications for components used in coherent transmission setup.

Symbol timing and initial phase error (Φ_0) computation is accomplished by the use of a known pilot sequence, of length equal to 20 symbols, arranged to appear at the beginning of the captured received data. A cross-correlation between the received samples and the known pilot sequence is conducted and the correlation peak identified. The position of this peak indicates the optimum sampling position and hence symbol timing. The phase of the correlation peak provides an estimate of the initial phase error Φ_0. Many carrier phase recovery algorithms have been proposed to cope with the pronounced issue of laser phase noise in coherent detection [13, 14]. In

this work, a standard phase-tracking algorithm is used where tentative decisions are made and the phase of the instantaneous error between these decisions and the actual received constellation point is computed. This phase error is used to drive a first-order control loop that strives to track the evolving phase error.

Reliably computing the BER using offline processing, especially if the signal quality is high, is very time consuming. An alternative is to measure the constellation diagram, which is a relatively quick measurement, and extract the error vector magnitude (EVM). The EVM describes the effective distance of the received complex symbol from its ideal position in the constellation diagram [15, 16]. The EVM was calculated from the following:

$$EVM_{RMS}[\%] = \sqrt{\frac{\frac{1}{N}\sum_{n=1}^{N}\left|S_{Rx,n} - S_{Tx,n}\right|^2}{\frac{1}{N}\sum_{n=1}^{N}\left|S_{Tx,n}\right|^2}} \times 100\% \tag{6.1}$$

Here $S_{Tx,n}$ and $S_{Rx,n}$ are the n^{th} transmitted and received symbols, respectively, and N is the number of symbols. Error counting was also performed on the received data and an estimate of the BER was calculated based on a total of 10^5 bits captured. When no errors were counted it was not possible to obtain a BER value.

6.2 QPSK

A low linewidth DMLD, which will be identified as DMLD A in subsequent sections, was placed in the QPSK setup. The device had an active region consisting of five quantum wells, a cavity length of 1000 μm and front and back facet reflectivities of 30 % and 95 %, respectively. The device was packaged in a butterfly module. The laser temperature and bias current were set to 25 ˚C and 200 mA, respectively, to give an emission linewidth of 190 kHz and a peak wavelength of

1551.3 nm. Fig. 6.2 shows the transmitted eye diagrams measured at (a) 10 Gbaud, (b) 5 Gbaud and (c) 2.5 Gbaud. The other lasers used in the experiment were also measured and produced similar eye diagrams for a given baud rate. This was because direct detection was used to measure the eye diagram and parameters, such as the laser linewidth, have no influence on the measurement. The TX performance was optimised through adjustment of parameters, such as the bias points for the IQ modulator and the delay between the I and Q channels, while observing their effects on the eye.

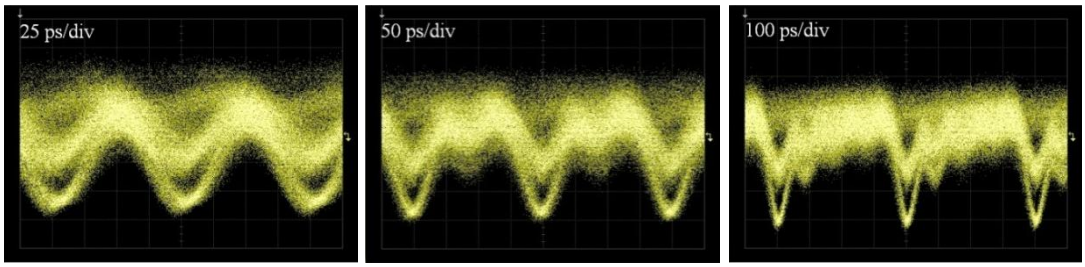

(a) (b) (c)

Fig. 6.2. Transmitted QPSK eye diagram measured at (a) 10 Gbaud, (b) 5 Gbaud and (c) 2.5 Gbaud, using a DMLD with a linewidth of 190 kHz as the TX laser.

6.2.1 QPSK self-homodyne receiver

Using the operating conditions outlined in the preceding section, DMLD A was placed in the QPSK setup. The EVM versus received power was measured at three baud rates, 10 Gbaud, 5 Gbaud and 2.5 Gbaud. The experiment was repeated using an ECL with a linewidth of 100 kHz. Fig. 6.3 plots EVM versus received power for the DMLD and the ECL. Similar performance was achieved at the three baud rates between both lasers with measured EVM values within 1 % at a received power of -24 dBm. As outlined in chapter 2, coherent communication systems have a lower tolerance to phase noise at lower baud rates. In this setup, improved EVM

performance was measured at lower baud rates indicating that noise sources, such as thermal noise at the detector and noise added by the RF amplifiers at the modulator inputs, were a limiting factor rather than the linewidth of the laser sources. The effect of increased linewidth on system performance was investigated by decreasing the DMLD bias current to 80 mA, to obtain an emission linewidth of 460 kHz; also a DFB with a linewidth of 1.5 MHz and a peak wavelength of 1550.4 nm was used. Fig. 6.4 plots EVM versus received power for the DMLD with emission linewidths of 190 kHz and 460 kHz and the DFB with a linewidth of 1.5 MHz. At the highest baud rate, 10 Gbaud, an increase in the EVM of 5.3 % was measured at a linewidth of 1.5 MHz and a received power of -20 dBm, compared to the value measured at a linewidth of 190 kHz. At 2.5 Gbaud, an increase in EVM was also measured by increasing the DMLDs linewidth to 460 kHz; at a received power of -20 dBm an increase of 5.5 % was measured, compared to the value measured at a linewidth of 190 kHz. At 2.5 Gbaud, the phase noise from the DFB laser was too high to even determine the EVM. Fig. 6.5 shows the constellation diagrams measured at 2.5 Gbaud and a received power of -20 dBm for (a) the ECL with a linewidth of 100 kHz, (b) DMLD A with a linewidth of 190 kHz, (c) DMLD A with a linewidth of 460 kHz and (d) a DFB with a linewidth of 1.5 MHz. The constellation obtained using the DMLD, with an emission linewidth of 190 kHz, was similar to that obtained using the ECL, with the extracted EVM value within 0.5 %; however, when the linewidth was increased to 460 kHz, broadening was observed in the constellation, which is characteristic of increased phase noise [17]. At a linewidth of 1.5 MHz, the broadening increases further with the constellation almost circular in appearance. When the same laser is used as the TX and LO, any increase in linewidth is seen in both the TX and LO. For most of the measurements presented the error rate

was low, with no errors being counted. While it is not possible to obtain a BER value, we can say that it was less than the FEC threshold of 3.8×10^{-3} at a received power of -24 dBm. The only exception was at 2.5 Gbaud and a linewidth of 1.5 MHz, where a BER worse than 10^{-1} was calculated. Simulated values for BER versus EVM were presented in [15], and it was shown that an EVM of approximately 32 % was required to achieve a BER of 10^{-3}. In all the measurements taken using the DMLD and the ECL, EVMs below 32 % were obtained, at received power levels greater than -32 dBm. An EVM of 15.3 % was measured at 2.5 Gbaud, at a received power of -24 dBm using a DMLD with a linewidth of 190 kHz, based on the simulated results this would correspond to a BER of approximately 10^{-10}.

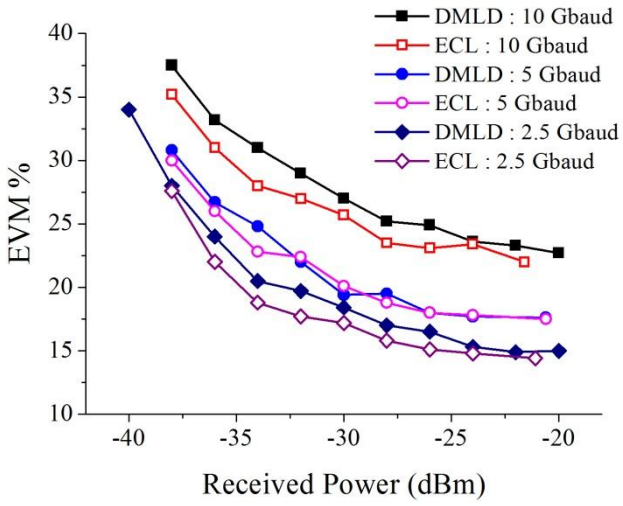

Fig. 6.3. EVM versus received power measured with the QPSK setup using a self-homodyne receiver at 10 Gbaud, 5 Gbaud and 2.5 Gbaud, for a DMLD with a linewidth of 190 kHz and an ECL with a linewidth of 100 kHz.

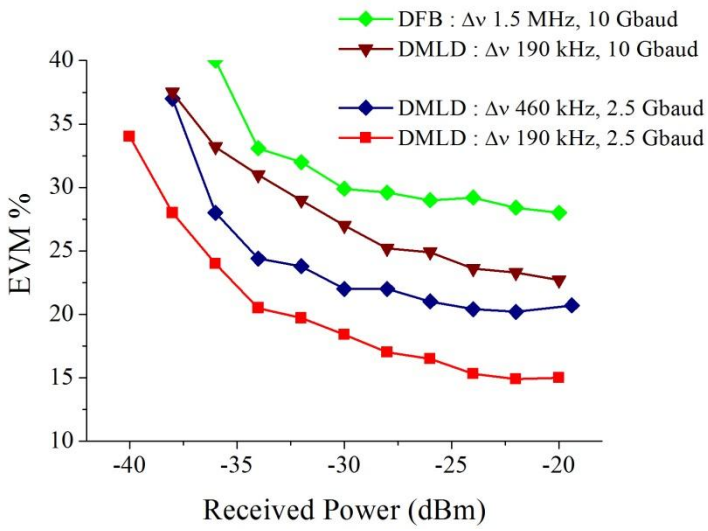

Fig. 6.4. EVM versus received power measured with the QPSK setup using a self-homodyne receiver at 10 Gbaud, for a DMLD with the linewidth of 190 kHz and a DFB with a linewidth of 1.5 MHz, and also at 2.5 Gbaud for a DMLD with linewidth of 190 kHz and a DMLD with a linewidth of 460 kHz.

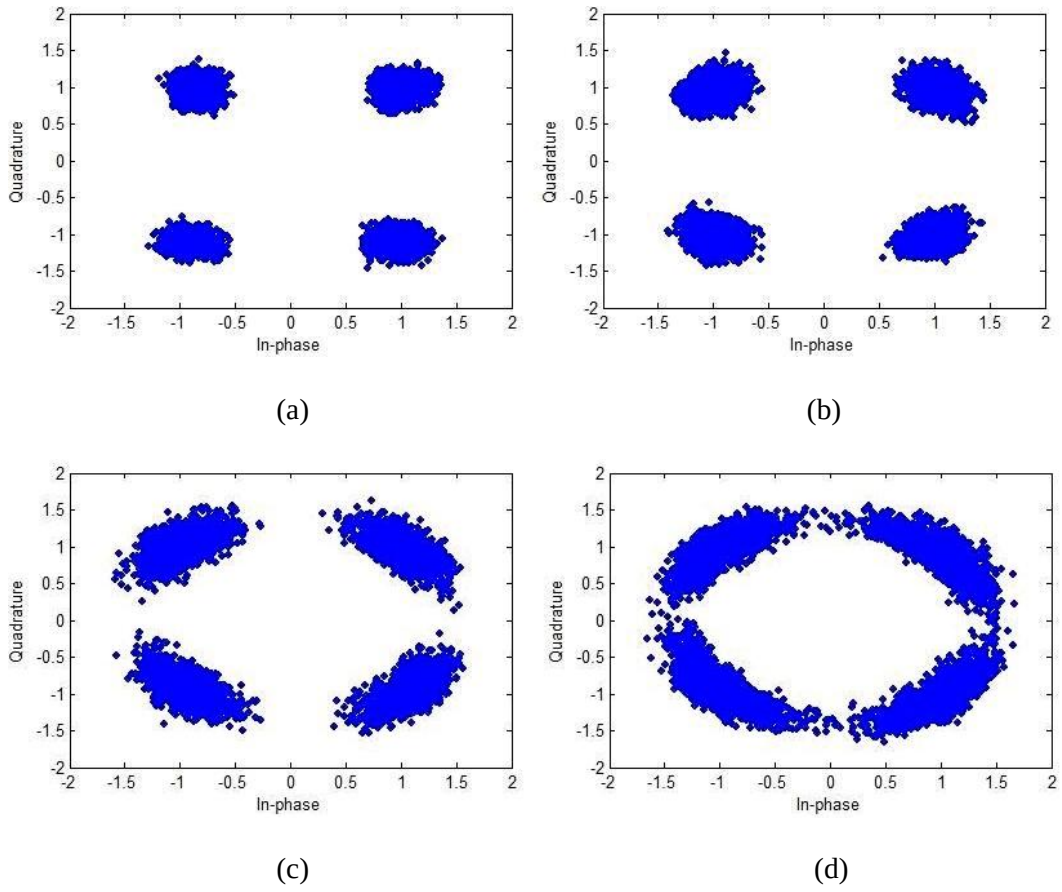

Fig. 6.5. Constellation diagrams measured with the QPSK setup using a self-homodyne receiver at 2.5 Gbaud and a received power of -20 dBm for (a) ECL, linewidth 100 kHz, (b) DMLD, linewidth 190 kHz, (c) DMLD, linewidth 460 kHz and (d) DFB, linewidth 1.5 MHz.

6.2.2 QPSK heterodyne receiver

Using a heterodyne receiver setup, DMLD A was used as the TX laser and a second DMLD, DMLD B, was used as the LO laser. DMLD B had an active region consisting of five quantum wells, a cavity length of 2000 μm and front and back facet reflectivities of 30 % and 95 %, respectively. The device was packaged in a butterfly module with internal TEC, which was used to control the chip temperature. The laser temperatures were set to 25 ˚C and 36.7 ˚C for DMLD A and DMLD B, respectively. The peak wavelength of DMLD B was tuned via the chip temperature, so that it matched the wavelength of the received signal. Both lasers were operated at a bias current of 200 mA. The emission linewidths were 190 kHz and 120 kHz for DMLD A and DMLD B, respectively, and a peak wavelength of 1551.3 nm was measured for both. Fig. 6.6 plots EVM versus received power measured at 10 Gbaud, 5 Gbaud and 2.5 Gbaud. For comparison, the values measured using the ECL in the self-homodyne receiver setup are also plotted. This was equivalent to using TX and LO lasers with linewidths of 100 kHz. Similar performance was achieved using the DMLDs in the heterodyne and an ECL in the self-homodyne receiver setup at the three baud rates, with measured EVM values within 0.5 % at a received power of -24 dBm. This demonstrates that narrow linewidth DMLDs can achieve similar performance to an ECL at baud rates as low as 2.5 Gbaud, and can be used as both TX and LO lasers in a QPSK system. Fig. 6.7 shows the constellation diagrams measured using the heterodyne receiver setup at a received power of -20 dBm at (a) 10 Gbaud, (b) 5 Gbaud and (c) 2.5 Gbaud.

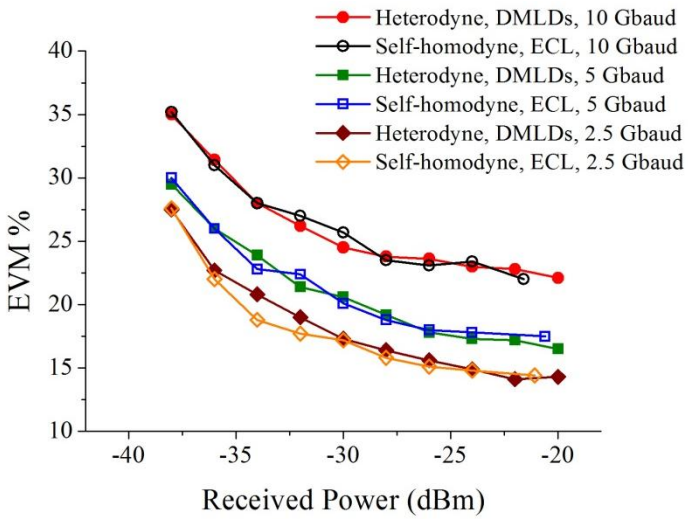

Fig. 6.6. EVM versus received power measured with the QPSK setup using a heterodyne receiver at 10 Gbaud, 5 Gbaud and 2.5 Gbaud, for DMLDs as the TX and LO lasers with linewidths of 190 kHz and 120 kHz, respectively. Also plotted an ECL with a linewidth of 100 kHz measured with a self-homodyne receiver setup.

The improvement in performance at lower baud rates shows that the performance was not limited by the linewidth, but rather the performance at higher baud rates was limited by additional noise sources in the setup, such as thermal noise at the detector and noise added by the RF amplifiers at the modulator inputs. It was not possible to calculate a BER value as no errors were counted in the captured data; however, we can say that the BER was better than 10^{-3} in all cases, at a received power of -24 dBm. At a received power of -24 dBm the EVM values measured using the heterodyne setup at 10 Gbaud and 2.5 Gbaud, where 23 % and 14.9 %, respectively. Based on the simulations of EVM versus BER presented in [15], these EVM values correspond to BERs of approximately 10^{-5} and 10^{-10} at 10 Gbaud and 2.5 Gbaud, respectively. While some degradation in performance was observed at 10 Gbaud, which is primarily due to intensity noise in the setup, the BER obtained at 10 Gbaud still exceeds the FEC threshold.

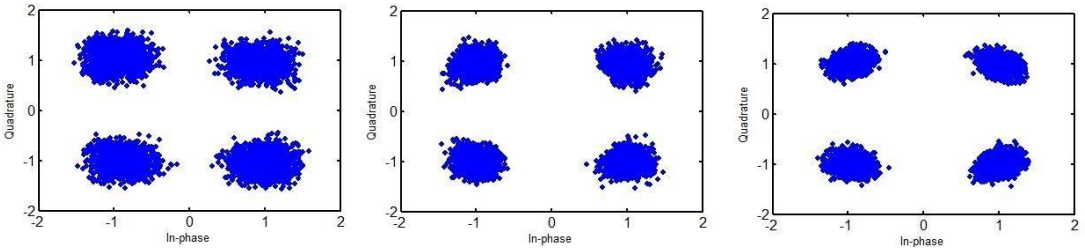

(a) (b) (c)

Fig. 6.7. Constellation diagrams measured with the QPSK setup using a heterodyne receiver at (a) 10 Gbaud, (b) 5 Gbaud and (c) 2.5 Gbaud, at a received power of -20 dBm for DMLDs as the TX and LO lasers with linewidths of 190 kHz and 120 kHz, respectively.

6.3 16-QAM

Using DMLD A, with a linewidth of 190 kHz, the 16-QAM transmitted eye diagram was measured at 5 Gbaud, and is shown in Fig. 6.8. Other lasers used in the experiment were also measured and produced similar eye diagrams. Similar to the QPSK setup, the transmitted optical signal was optimised while observing the eye diagram.

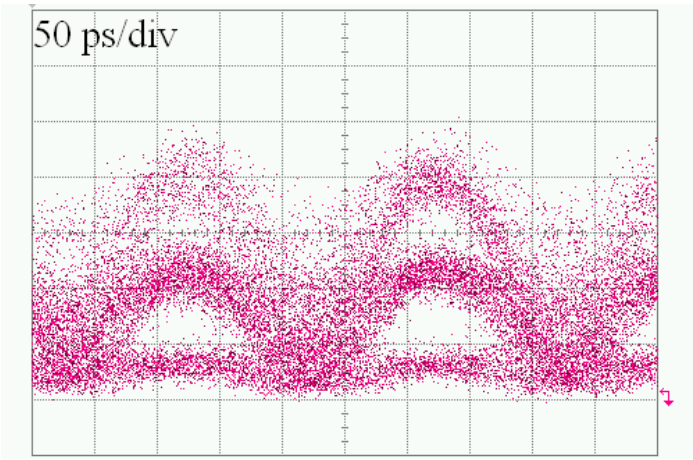

Fig. 6.8. Transmitted 16-QAM eye diagram measured at 5 Gbaud, using a DMLD with a linewidth of 190 kHz as the TX laser.

6.3.1 16-QAM self-homodyne receiver

An ECL, DMLD B and DMLD A were characterised in the 16-QAM transmission setup using a self-homodyne receiver. EVM versus received power was measured at a baud rate of 5 Gbaud. The temperature and bias current of DMLD B was set to 25 ˚C and 350 mA, respectively, to give an emission linewidth of 80 kHz and a peak wavelength of 1550.4 nm. DMLD A was also operated at 25 ˚C and the laser was characterised at two emission linewidths, 190 kHz and 300 kHz, by setting the bias current to 200 mA and 110 mA, respectively. EVM versus received power for DMLD B, DMLD A and the ECL are plotted in Fig. 6.9. Similar performance was achieved using the ECL and DMLD B, with EVMs of 14 % and 14.4 % measured at a received power of –23 dBm, respectively. Fig. 6.10 (a) and (b) show the corresponding constellation diagrams measured at a received power of -23 dBm using the ECL and DMLD B, respectively; a BER better than 10^{-3} was measured for both devices. The effect of increased linewidth on system performance was investigated using DMLD A. At 190 kHz and 300 kHz, EVM values of 17 % and 20 % were measured at a received power of –23 dBm, respectively; a BER worse than 10^{-3} was measured in both cases. In the simulation results of EVM versus BER presented in [15], an EVM of approximately 15 % was required to achieve a BER of 10^{-3}, and this shows a close correlation with the BER and EVM results measured here. The constellation diagrams measured at 190 kHz and 300 kHz are shown in Fig. 6.10 (c) and (d), respectively, and show degradation in performance due to the increased linewidth.

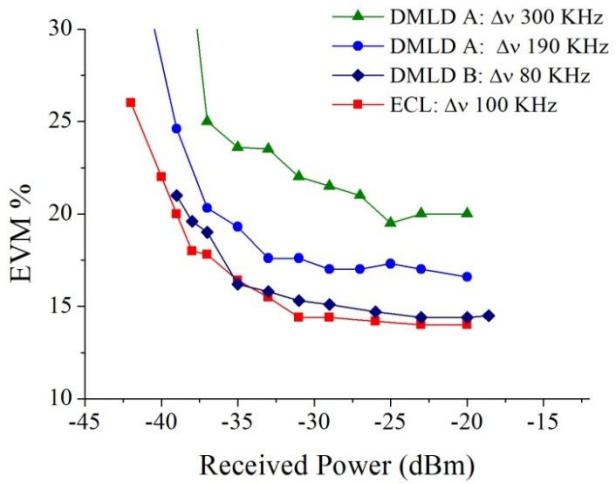

Fig. 6.9. EVM versus received power measured with the 16-QAM setup using a self-homodyne receiver at 5 Gbaud, for an ECL with a linewidth of 100 kHz, a DMLD with a linewidth of 80 kHz, a DMLD with a linewidth of 190 kHz and a DMLD with a linewidth of 300 kHz.

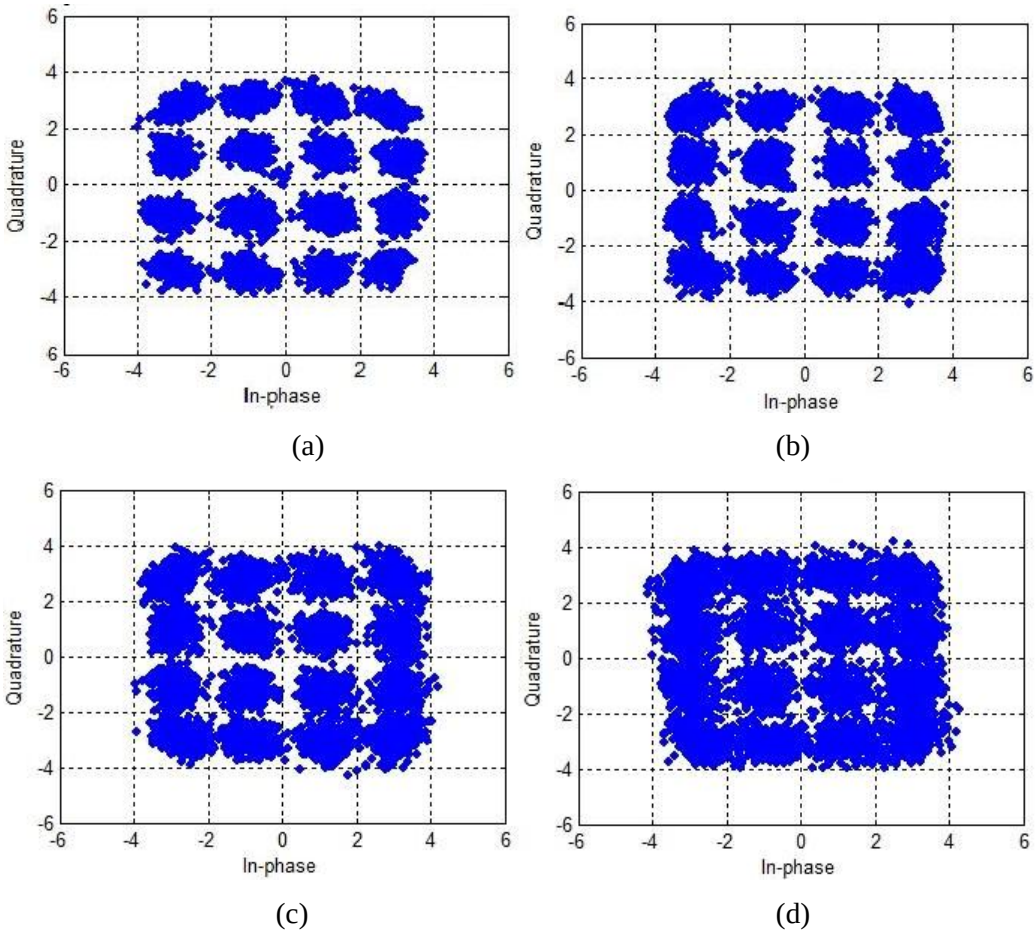

Fig. 6.10. Constellation diagrams measured with the 16-QAM setup using a self-homodyne receiver at 5 Gbaud and a received power of -23 dBm for (a) ECL, linewidth 100 kHz, (b) DMLD, linewidth 80 kHz, (c) DMLD, linewidth 190 kHz and (d) DMLD, linewidth 300 kHz.

In comparison to the QPSK setup, where similar performance was demonstrated at baud rates as low as 2.5 Gbaud for linewidths of 190 kHz and 100 kHz, the degradation in performance observed using the 16-QAM setup confirms that higher order modulation formats have more stringent linewidth requirements.

6.3.2 16-QAM heterodyne receiver

The lasers were also characterised using a heterodyne receiver setup. Fig. 6.11 plots the EVM versus received power for three cases, first using DMLD A with a linewidth of 190 kHz as the TX laser and DMLD B with a linewidth of 85 kHz as the LO, second using DMLD A with a linewidth of 190 kHz as the TX laser and an ECL with a linewidth of 100 kHz as the LO, and third using DMLD B with a linewidth of 80 kHz as the TX laser and an ECL with a linewidth of 100 kHz as the LO. The DMLD operating conditions were as follows: the temperature and bias current of DMLD A was set to 25 ˚C and 200 mA, respectively. When used as the LO the temperature and bias current of DMLD B was set to 34 ˚C and 350 mA, respectively, and when used as the TX the temperature and bias current was set to 25 ˚C and 350 mA, respectively. When used as the LO the temperature of DMLD B was used to tune the wavelength to match that of the received signal. The performance achieved in the first and second case was similar, with EVM values of 15.4 % and 15.1 % measured at a received power of -23 dBm, respectively. In the third case an EVM of 14 % was measured at a received power of -23 dBm. The constellation diagrams for the three cases measured at a received power of -23 dBm are shown in Fig. 6.12 (a), (b) and (c), respectively. Because the error rate was higher it was possible to estimate the error rate, in the first and second case a BER slightly worse that 10^{-3} was measured. In the third case the combined linewidth was 180 kHz,

compared to 275 kHz and 290 kHz for the first and second cases, respectively, and a BER better than 10^{-3} was measured. The BER and EVM values showed a close correlation to the simulated values presented in [15], where and EVM of approximately 15 % was shown to be required to achieve a BER of 10^{-3}.

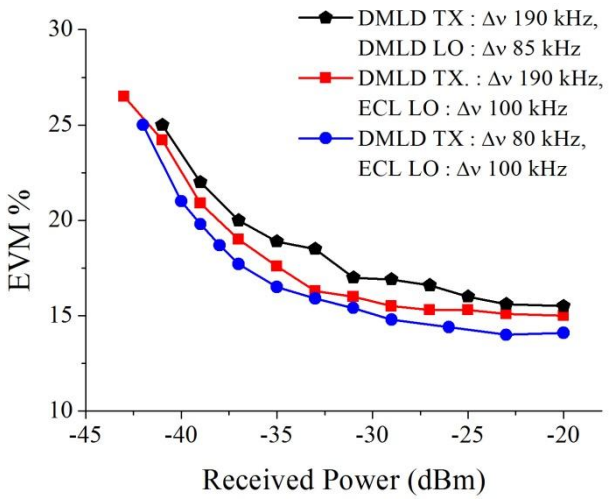

Fig. 6.11. EVM versus received power measured with the 16-QAM setup using a heterodyne receiver at 5 Gbaud for the following: DMLD TX linewidth 190 kHz, ECL LO linewidth 100 kHz; DMLD TX linewidth 190 kHz, DMLD LO linewidth 85 kHz; and DMLD TX linewidth 80 kHz, ECL LO linewidth 100 kHz.

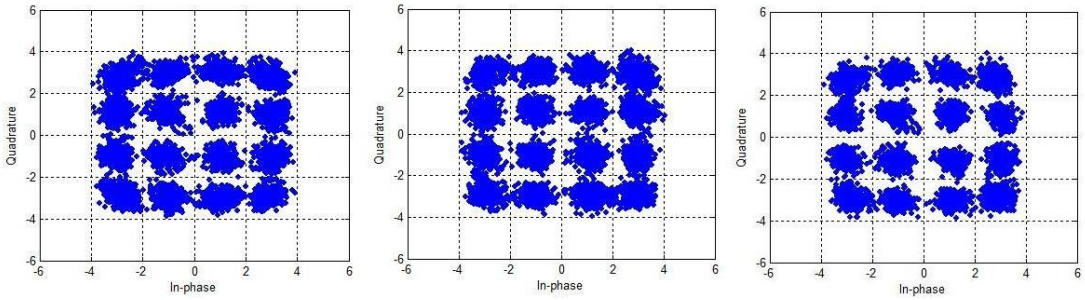

(a) (b) (c)

Fig. 6.12. Constellation diagrams measured using the 16-QAM setup with a heterodyne receiver, at 5 Gbaud and a received power of -23 dBm for (a) DMLD TX linewidth 190 kHz, ECL LO linewidth 100 kHz, (b) DMLD TX linewidth 190 kHz, DMLD LO linewidth 85 kHz and (c) DMLD TX linewidth 80 kHz, ECL LO linewidth 100 kHz.

6.4 Discussion

Characterisation results on low linewidth DMLDs were presented in chapter 4, demonstrating linewidths as low as 70 kHz. In optical coherent communication systems the linewidth is an important parameter, as the performance of phase modulated signals can be limited if the phase noise of the laser sources is too high. The level of phase noise that is tolerable depends on a number of factors, including, the order of the modulation format used, the baud rate, the architecture of the receiver and the DSP algorithms used. The objective of these experiments was to compare the performance of different lasers in a coherent transmission test bed, and to confirm that low linewidth DMLDs could achieve performance levels comparable to an ECL.

In these experiments the main figure of merit used was the EVM. The EVM is a standard metric used in wireless and wireline communications and it is increasingly being used to assess the quality of optical signals employing advanced modulation formats, with the latest optical test instruments, designed for analysing phase modulated signals, incorporating EVM analysis tools [18]. In [15] it was demonstrated that good agreement could be obtained between simulated values of EVM versus BER and values obtained experimentally using six different modulation formats, B/Q/8PSK and 16/32/64 QAM, at symbol rates of 20 Gbaud and 25 Gbaud. While the ultimate system performance measurement is the BER, the EVM presents a powerful tool for analysing the performance of phase modulated systems.

In the transmission setup using a self-homodyne receiver, EVM values within 1 % of those obtained using an ECL were demonstrated. This was achieved in the QPSK setup using a DMLD with a linewidth of 190 kHz, and in the 16-QAM setup using a

DMLD with a linewidth of 80 kHz. The effect of increased linewidth was also investigated using the self-homodyne receiver setup. In the QPSK setup an increase in EVM of approximately 5.5 % was measured at both 10 Gbaud and 2.5 Gbaud for linewidths of 1.5 MHz and 460 kHz, respectively, compared to the values obtained at a linewidth of 190 kHz. In the 16-QAM setup an increase in EVM of approximately 3 % and 6 % was measured at 5 Gbaud for linewidths of 190 kHz and 300 kHz, respectively, compared to the values obtained at a linewidth of 100 kHz. These measurements confirm that lower baud rates and higher order modulation formats require lasers with lower linewidths. Using more advanced DSP, where feedforward algorithms are used, it is possible to achieve greater tolerance to laser phase noise, allowing lasers with higher linewidths to be used in these systems, potentially a linewidth of 200 kHz could support higher order modulation formats up to 64 QAM at 10 Gbaud [13].

Experiments were also carried using a heterodyne receiver setup, which demonstrated that DMLDs could be used as TX and LO lasers in a coherent communications setup. The measurements taken using the ECL with a self-homodyne receiver setup were used as a benchmark; EVM values within 0.5 % were measured in the QPSK setup, at the three baud rates, using DMLDs as the TX and LO with a combined linewidth of 310 kHz. EVM values were also measured using the 16-QAM setup, where DMLDs with a combined linewidth of 275 kHz were used at the TX and LO; because of the higher combined linewidth, compared to the self-homodyne case using the ECL, an increase in the EVM of 1.4 % was measured. This was still a relatively small increase and demonstrates that similar performance can be achieved using DMLDs in a heterodyne setup. To investigate whether the observed increase was a limitation of the heterodyne setup used, a DMLD and ECL with a

combined linewidth of 180 kHz were placed in the setup, and an EVM of 14 % was measured, which was the same value measured using the ECL in the self-homodyne setup. Ideally two DMLDs with a linewidth of 100 kHz, or less, would have been used in the heterodyne experiment, but only one such device was available at the time this work was carried out.

For the QPSK measurements carried out on the DMLD and the ECL the error rate was low, with no errors being counted in 10^5 acquired bits. Also, using simulated results of BER versus EVM presented in [15] to estimate the BER, values better than 10^{-5} are estimated for all the measurements taken using DMLDs or the ECL. The improved performance demonstrated at lower baud rates with lower EVM values being measured, indicates that noise sources, such as thermal noise at the detector and noise added by the RF amplifiers at the modulator inputs, limited the performance rather than the linewidth of the laser sources.

For the 16-QAM measurements it was possible to estimate the BER as the error rate was higher. Using the self-homodyne receiver setup, a BER better than 10^{-3} was obtained using both a DMLD with a linewidth of 80 kHz and an ECL. For linewidths of 190 kHz and 100 kHz, a BER worse than 10^{-3} was measured. In the 16-QAM heterodyne setup using a TX laser with a linewidth of 190 kHz, BERs worse than 10^{-3}, but better than 10^{-2}, were obtained using LOs with linewidths of 100 kHz and 85 kHz, obtained from an ECL and a DMLD, respectively. A BER better that 10^{-3} was achieved using a DMLD with a linewidth of 80 kHz as the TX and an ECL as the LO. The results obtained were also consistent with simulations presented in [15], which showed that an EVM of approximately 15 % was required to achieve a BER of 10^{-3}, which exceeds the FEC threshold.

A limitation in this setup, which limited the BER performance, was additional noise sources in the setup, and improved performance should be possible through optimisation of the setup. The objective of the experiments was to compare the performance of different lasers in a coherent transmission setup and this was achieved as the lasers were tested under the same conditions.

In chapter 4, it was demonstrated that the wavelength of low linewidth DMLDs could be tuned over temperature, without a significant change in the measured linewidth value, this property was utilised in the heterodyne experiments to provide a degree of wavelength tuneabilty at the LO.

6.5 Conclusion

Similar performance to an ECL has been demonstrated using low linewidth DMLDs in a coherent transmission system. Table 6.2 summarises the performance achieved using the QPSK modulation format at 10 Gbaud, 5 Gbaud and 2.5 Gbaud using both the self-homodyne and the heterodyne receiver setups measured at a received power of -24 dBm. Comparing the results obtained using DMLDs with those obtained using an ECL, where the ECL was measured using the self-homodyne receiver setup, very similar performance was obtained at the three baud rates, with measured EVM values within 0.5 % for both receiver setups. Table 6.3 summarises the performance achieved using the 16-QAM modulation format at 5 Gbaud using both the self-homodyne and the heterodyne receiver setups measured at a received power of -23 dBm. In the self-homodyne receiver setup an 80 kHz DMLD showed similar performance to an ECL, with a measured EVM values within 0.4 % for both lasers. In the heterodyne receiver setup where DMLDs with a combined linewidth of 275 kHz were used at both the receiver and the transmitter, similar performance to an

ECL was demonstrated, with a measured EVM value within 1.4 % of that obtained using an ECL. By decreasing the combined linewidth to 180 kHz in the heterodyne setup this produced the same EVM value as was obtained using the ECL in the homodyne setup. Because these DMLDs have the linewidths required for use in advanced modulation format systems and present an economic approach for the manufacture of semiconductor lasers they are an important component to consider in the transmitters and receivers of coherent systems. The next chapter provides a conclusion to the thesis and discusses the potential for future work in this area.

Baud rate (Gbaud)	EVM %		
	100 kHz ECL self-homodyne receiver	190 kHz DMLD self-homodyne receiver	DMLD (TX 190 kHz, LO 120 kHz) heterodyne receiver
10	23.4	23.6	23
5	17.8	17.7	17.3
2.5	14.8	15.3	14.9

Table. 6.2. EVM values measured using the QPSK setup at 10 Gbaud, 5 Gbaud and 2.5 Gbaud, for an ECL and a DMLD measured using the self-homodyne receiver setup and two DMLDs measured using the heterodyne receiver setup.

EVM %			
100 kHz ECL self-homodyne receiver	80 kHz DMLD self-homodyne receiver	DMLD (TX 190 kHz, LO 85 kHz) heterodyne receiver	DMLD TX 80 kHz, ECL LO 120 kHz heterodyne receiver
14	14.4	15.4	14

Table. 6.3. EVM values measured using the 16-QAM setup at 5 Gbaud, for an ECL and a DMLD measured using the self-homodyne receiver setup, two DMLDs measured using the heterodyne receiver setup and a DMLD as the TX and an ECL as the LO measured using the heterodyne receiver setup.

References

[1] K. Roberts, M. O'Sullivan, K. T. Wu, H. Sun, A. Awadalla, D. J. Krause and C. Laperle, "Performance of Dual-Polarization QPSK for Optical Transport Systems," Journal of Lightwave Technology, vol. 27, no. 16, pp. 3546-3559, Aug. 2009.

[2] K. Roberts, D. Beckett, D. Boertjes, J. Berthold and C. Laperle, “100G and beyond with digital coherent signal processing,” IEEE Communications Magazine, vol. 48, no. 7, pp. 62-69, Jul. 2010.

[3] F. Buchali, K. Schuh, D. Rosener, E. Lach, R. Dischler, W. Idle, L. Schmalen, A. Leven, R. P. Braun, A. Ehrhardt, C. Gerlach and L. Schurer, “512-Gb/s DP-16-QAM field trial over 734 km installed SSMF with co-propagating 10 Gb/s NRZ neighbors incorporating soft-FEC decoding,” in Optical Fiber Communication Conference (OFC), Los Angeles, Mar. 2012.

[4] JDS Uniphase Corporation, “Dual parallel Mach-Zehnder modulator data sheet,” 2008. [Online]. Available: http://www.jdsu.com/ProductLiterature/dpmzmod_ds_cc_ae.pdf.

[5] JDS Uniphase Corporation, Model H301 10 Gbit/s Optical modulator driver, data sheet.

[6] Optoplex Corporation, “2x8 Coherent Mixer, data sheet,” 2009. [Online]. Available: http://www.optoplex.com/download/Optoplex%20Datasheets_2x8.pdf.

[7] Teleoptix, “43 Gbit/s balanced photoreceiver with linear TIA, data sheet,” 2009. [Online]. Available: http://www.linkra.it/images/ot/pdf/40Gb-components/Teleoptix_DualPIN-DTLIN-v1.0.pdf.

[8] JDS Uniphase Corporation, “MAP Erbium doped fiber amplifier, data sheet,” 2011. [Online]. Available: http://www.jdsu.com/ProductLiterature/mapedfa_ds_lab_tm_ae.pdf.

[9] MPB Communications Inc., Bench top pre-amplifier, EFA-R35-PAR, specification sheet, 2009.

[10] I. P. Kaminow, Optical fiber telecommunications V: B: systems and networks, Boston: Academic Press, 2008.

[11] T. N. Huynh, F. Smyth, L. Nguyen and L. P. Barry, “Effects of phase noise of monolithic tunable laser on coherent communication systems,” Optics Express, vol. 20, no. 26, pp. B244-B249, Nov. 2012.

[12] T. Nakagawa, M. Matsui, T. Kobayashi, K. Ishihara, R. Kudo, M. Mizoguchi and Y. Miyamoto, “Non-data-aided wide-range frequency offset estimator for QAM optical coherent receivers,” in Optical Fiber Communication Conference (OFC), Los Angeles, Mar. 2011.

[13] T. Pfau, S. Hoffmann and R. Noe, “Hardware-Efficient Coherent Digital Receiver Concept With Feedforward Carrier Recovery for M-QAM Constellations,” Journal of Lightwave Technology, vol. 27, no. 8, pp. 989-999, April 2009.

[14] M. Seimetz, High-Order Modulation for Optical Fiber Transmission, Berlin: Springer, 2009.

[15] R. Schmogrow, B. Nebendahl, M. Winter, A. Josten, D. Hillerkuss, S. Koenig, J. Meyer, M. Dreschmann, M. Huebner, C. Koos, J. Becker, W. Freude and J. Leuthold, "Error Vector Magnitude as a Performance Measure for Advanced Modulation Formats," IEEE Photonics Technology Letters, vol. 24, no. 1, pp. 61-63, Jan. 2012.

[16] R. A. Shafik, S. Rahman and A. H. M. R. Islam, "On the Extended Relationships Among EVM, BER and SNR as Performance Metrics," in International Conference on Electrical and Computer Engineering (ICECE), Dhaka, Dec. 2006.

[17] O. Funke and B. Nebendahl, Short Course 369, Test and measurement of complex modulated optical signals, Los Angeles: Optical Fiber Communication Conference (OFC), Mar. 2012.

[18] Agilent Technologies, "Agilent N4391A, Optical Modulation Analyzer, Data sheet," 2011. [Online]. Available: http://cp.literature.agilent.com/litweb/pdf/5990-3509EN.pdf.

Chapter 7

Conclusion and future work

7.1 Conclusion

The demand for optical networks with higher capacity looks set to continue, with global IP traffic forecast to grow at a compound annual rate of 32 % up to 2015 [1]. Factors such as the availability of new services, customer demands and policy initiatives by governments are all pushing for the delivery of higher speed broadband connections. The delivery of higher speed connections is dependent on extending the reach of fibre in the field and increasing the cumulative capacity of the network infrastructure. In the access network the bit rate of next generation systems is likely to increase to 10 Gbit/s, making high speed transmitters a requirement. The latest systems being deployed in core and long haul applications are employing advanced modulation formats to cope with the increase in data traffic. These modulation formats encode the information in the phase of the optical carrier making low phase noise a requirement for optical sources used in these systems.

In this thesis a novel type of single mode laser called a discrete mode laser was proposed for next generation fibre optic communications applications. This approach offers the potential for high-volume, low-cost fabrication of single-mode lasers.

Single-wavelength operation in DMLDs is achieved by introducing index perturbations in the form of etched features positioned at a small number of sites distributed along the surface of the ridge waveguide. The fabrication process does not involve epitaxial re-growth and only requires standard optical lithography. A significant element in the cost of producing a laser module is packaging: monolithic semiconductor lasers, such as the DMLD and DFBs, can use existing telecommunication laser packaging platforms to produce lasers in high volumes; this is not easily achieved with ECLs, which have more complex packaging requirements. Two types of laser were considered, a directly modulated transmitter and a narrow linewidth laser and the main results are summarised here:

Direct modulation

10 Gbit/s operation was demonstrated at 1310 nm and 1550 nm using a directly modulated DMLD. The transmission performance was also characterised, at 1310 nm after transmission through 22 km of SSMF a power penalty of only 0.3 dB was measured. At 1550 nm a power penalty of 0.8 dB was measured after 10 km but this increased to 5.3 dB after 20 km. A potential application area for 10 Gbit/s 1310 nm DMLDs is in access networks. However, limitations in this particular process run meant that the operating temperature was limited. In chapter 4 a 1310 nm DMLD demonstrated single mode operation over the range -40 ˚C ≤ T ≤ 97 ˚C, while there were differences in the design of this device compared to the 10 Gbit/s part, it does demonstrate that a wide operating temperature range can be achieved. The applications of 10 Gbit/s directly modulated lasers at 1550 nm may be limited in access networks due to dispersion effects. However, if dispersion compensation can be cost effectively deployed directly modulated lasers would be an attractive option for access networks because of their lower cost.

Narrow linewidth

In chapter 4 three variations of low linewidth DMLD designs were characterised and all demonstrated linewidths below 200 kHz. The first device results were presented on, displayed a minimum linewidth of 138 kHz. It also demonstrated that single mode operation could be maintained over a wide temperature range of -10 ˚C ≤ T ≤ 110 ˚C. The device also showed stable linewidth performance over the temperature range 0 ˚C ≤ T ≤ 85 ˚C, where at a constant power of 4 mW a maximum linewidth of 235 kHz was measured at 85 ˚C, and a minimum value of 212 kHz was measured at 25 ˚C, corresponding to a variation in the linewidth of only 23 kHz over the measured temperature range.

A second device was designed with a cavity length of 2 mm, and a minimum linewidth of 70 kHz was demonstrated when measured using the D-SH technique. The PSD of the laser was also measured to obtain more detailed information relating to the phase noise and to confirm the accuracy of the results obtained using the D-SH technique. From the PSD measurement a linewidth value of 67 kHz was extracted, and this agrees closely with the value measured using the D-SH technique.

A third device was designed for higher output powers and low linewidth. Using this device a linewidth below 200 kHz and an output power from the front facet in excess of 30 mW was demonstrated.

Chapter 6 characterised the performance of these low linewidth DMLDs in a coherent transmission test bed employing the advanced modulation formats QPSK and 16-QAM, and the performance levels achieved were compared with that obtained using an ECL. In the transmission setup a self-homodyne receiver was implemented, and EVM values within 1 % of those obtained using an ECL were

demonstrated using DMLDs. It was also demonstrated that DMLDs could be used as both TX and LO lasers in a heterodyne setup, and that tuning of the peak wavelength via the laser temperature could be used to match the wavelength of the TX and LO lasers. These were the first demonstrations where DMLDs were used as the TX or LO in a coherent transmission setup using these modulation formats.

7.2 Future work

The DMLDs presented in this thesis show potential for deployment in future optical systems. However, there are areas where further development will be necessary, and avenues for future research are outlined below:

1310 nm directly modulated lasers

Further work will be required to improve the temperature performance of the 1310 nm DMLD operating at 10 Gbit/s. Based on information gained from the previous development run, the epitaxial material appears to have the requisite bandwidth even at 85 ˚C. A first step is to use wafers from the same epitaxial growth and process a further DMLD development run. The steps in future development work include achieving single mode operation over a wide temperature range, and then assess the static and dynamic performance over the temperature range to determine its suitability, or otherwise, for 10 Gbit/s access applications.

1550 nm directly modulated lasers

Using existing 1550 nm devices there is potential to achieve improved dynamic performance. A first step is to package devices with a HR coated back facet and a cavity length of 300 μm, or less, in a high speed package in order to evaluate its performance. The applications of 10 Gbit/s, or higher speed, directly modulated

lasers operating at 1550 nm may be limited due to dispersion effects. However, the development of a high speed 1550 nm structure will also be required for on-going work in areas such as optical comb sources [2, 3] and monolithic integration of dual section devices, where improved performance can be achieved through optical injection [4].

Narrow linewidth lasers

The linewidth of DMLDs could be further reduced by increasing the cavity length beyond 2 mm. However, handling and packaging such a device becomes more difficult. Reducing the linewidth further is a focus for on-going research, and areas such as the material structure and using higher reflectivity on the front facet are being investigated. The development of a narrow linewidth device capable of full C or L-band tuneability could be implemented using an array of DMLDs. Each laser in the array is designed to cover a number of channels and course tuning of the wavelength is achieved by selecting a laser in the array and fine tuning is accomplished by adjusting the laser temperature. As demonstrated previously narrow linewidth DMLDs can achieve a wide temperature tuning range, and this would be a desirable characteristic in such a device. This approach has previously been used with DFBs, in [5] full C-band tuneability was demonstrated using an array of 12 DFBs and a micro-electro-mechanical system (MEMs) incorporated in an optical package. Light from the selected laser in the array is coupled to the output fibre by tilting a MEMs mirror. An alternative approach was used in [6] to produce an integrated chip, consisting of an array of 12 DFBs, an MMI and a semiconductor optical amplifier (SOA). Light from the laser array is coupled using the MMI and the SOA is used to control the output power.

References

[1] Cisco systems Inc., White paper, "Cisco Visual Networking Index: Forecast and Methodology, 2010–2015," 1 June 2011. [Online]. Available: http://www.cisco.com/en/US/solutions/collateral/ns341/ns525/ns537/ns705/ns827/white_paper_c11-481360.pdf.

[2] P. M. Anandarajah, R. Maher, Y. Q. Xu, S. Latkowski, J. O'Carroll, S. G. Murdoch, R. Phelan, J. O'Gorman and L. P. Barry, "Generation of Coherent Multicarrier Signals by Gain Switching of Discrete Mode Lasers," *IEEE Photonics Journal*, vol. 3, no. 1, pp. 112-122, Feb. 2011.

[3] R. Zhou, S. Latkowski, J. O'Carroll, R. Phelan, L. P. Barry and P. Anandarajah, "40nm wavelength tunable gain-switched optical comb source," in *European Conference and Exhibition on Optical Communication (ECOC)*, Geneva, Sept. 2011.

[4] C. Browning, K. Shi, S. Latkowski, P. Anandarajah, F. Smyth, B. Cardiff, R. Phelan and L. P. Barry, "Performance improvement of 10Gb/s direct modulation OFDM by optical injection using monolithically integrated discrete mode lasers," in *European Conference and Exhibition on Optical Communication (ECOC)*, Geneva, Sept. 2011.

[5] B. Pezeshki, E. Vail, J. Kubicky, G. Yoffe, S. Zou, J. Heanue, P. Epp, S. Rishton, D. Ton, B. Faraji, M. Emanuel, X. Hong, M. Sherback, V. Agrawal, C. Chipman and T. Razazan, "20-mW widely tunable laser module using DFB array and MEMS selection," *IEEE Photonics Technology Letters*, vol. 14, no. 10, pp. 1457-1459, Oct. 2002.

[6] H. Ishii, K. Kasaya and H. Oohashi, "Reduced spectral linewidth (≪ 0.6 MHz) in L-band wavelength tunable DFB laser array," in *IEEE International Semiconductor Laser Conference*, Sorrento, Sept. 2008.

Appendix A

List of Publications Arising From This Work

A.1 Referred Journals

1. **O'Carroll, J.**; Phelan, R.; Kelly, B; Huynh, T.N.; Cardiff, B.; Smyth, F; Anandarajah, P.M.; and Barry, L.P. "Narrow-Linewidth Discrete-Mode Laser Diodes for Coherent Communication Applications"; Journal of Optical Communications and Networking, Vol. 4, Issue 9, pp.: A90-A96 (2012)
2. Anandarajah, P.M.; Latkowski, S.; Browning, C.; Zhou, R.; **O'Carroll, J.**; Phelan, R.; Kelly, B.; O'Gorman, J.; Barry, L.P.; "Integrated Two-Section Discrete Mode Laser"; Photonics Journal, IEEE, Vol. 4, Issue 6, pp.: 2085-2094 (2012).
3. Phelan, R.; **O'Carroll, J.**; Byrne, D. ; Herbert, C. ; Somers, J. ; Kelly, B.; "In0.75Ga0.25As/InP Multiple Quantum Well Discrete Mode Laser Diode Emitting at 2 um"; Photonics Technology Letters, IEEE, Vol. 24, Issue 8, pp.: 652 – 654 (2012).
4. **O'Carroll, J.**; Phelan, R.; Kelly, B.; Byrne, D.; Barry, L.P.; O'Gorman, J.; "Wide temperature range $0 < T < 85$ °C narrow linewidth discrete mode laser diodes for coherent communications applications"; Optics Express, Vol. 19 Issue 26, pp.B90-B95 (2011).
5. Zhou, R.; Latkowski, S.; **O'Carroll, J.**; Phelan, R.; Barry, L.P.; Anandarajah, P.; "40nm wavelength tunable gain-switched optical comb source"; Optics Express, Vol. 19 Issue 26, pp.B415-B420 (2011).
6. Weerasuriya, R.; Sygletos, S.; Ibrahim, S.K.; Gunning, F.C.G.; Manning, R.J.; Phelan, R.; **O'Carroll, J.**; Kelly, B.; O'Gorman, J.; Ellis, A.D.; "Comparison of Frequency Symmetric Signal Generation From a BPSK Input

Using Fiber and Semiconductor-Based Nonlinear Elements"; Photonics Technology Letters, IEEE, Vol. 23 Issue:10, pp.: 651 – 653 (2011).

7. O'Brien, S.; Smyth, F.; Kai Shi ; **O'Carroll, J.**; Anandarajah, P.M.; Bitauld, D.; Osborne, S.; Phelan, R.; Kelly, B.; O'Gorman, J.; Peters, F.H.; Roycroft, B.; Corbett, B.; Barry, L.P.; "Design, Characterization, and Applications of Index-Patterned Fabry–Pérot Lasers"; IEEE Journal of Selected Topics in Quantum Electronics, Vol. 17, Issue 6, pp.: 1621–1631 (2011).
8. Anandarajah, P.M.; Maher, R.; Xu, Y.Q.; Latkowski, S.; **O'Carroll, J.**; Murdoch, S.G.; Phelan, R.; O'Gorman, J.; Barry, L.P.; "Generation of Coherent Multicarrier Signals by Gain Switching of Discrete Mode Lasers"; Photonics Journal, IEEE, Vol. 3, Issue 1, pp.: 112–122 (2011).
9. Phelan, R.; Slight, T.J.; Kelly, B.; **O'Carroll, J.**; McKee, A.; Revin, D.G.; Zhang, S.Y.; Krysa, A.B.; Kennedy, K.L.; Cockburn, J.W.; Ironside, C.N.; Meredith, W.; O'Gorman, J.; "Room-Temperature Operation of Discrete-Mode InGaAs–AlAsSb Quantum-Cascade Laser With Emission at λ =3.3 um"; Photonics Technology Letters, IEEE, Vol. 22 Issue 17, pp.: 1273–1275 (2010)
10. Maher, R.; Shi, K.; Barry, L.P.; **O'Carroll, J.**; Kelly, B; Phelan, R; O'Gorman, J; Anandarajah, P.M.; "Implementation of a cost-effective optical comb source in a WDM-PON with 10.7Gb/s data to each ONU and 50km reach"; Optics Express, Vol. 18 Issue 15, pp.15672-15681 (2010).
11. Herbert, C.; Jones, D.; Kaszubowska-Anandarajah, A.; Kelly, B.; Rensing, M.; **O'Carroll, J.**; Phelan, R.; Anandarajah, P.; Perry, P.; Barry, L.P.; O'Gorman, J.; "Discrete mode lasers for communication applications"; Optoelectronics, IET, Vol. 3 Issue 1, pp.: 1–17 (2009).
12. Phelan, R.; Kelly, B.; **O'Carroll, J.**; Herbert, C.; Duke, A.; O'Gorman, J.; "-40 °C < T < 95 °C mode-hop free operation of an uncooled AlGaInAs-MQW discrete-mode laser diode with emission at λ = 1.3 μm."; Electronics Letters, Vol.: 45 Issue 1, pp.: 43–45 (2009).
13. Anandarajah, P.M.; Shi, K.; **O'Carroll, J.**; Kaszubowska, A.; Phelan, R.; Barry, L.P.; Ellis, A.D.; Perry, P.; Reid, D.; Kelly, B.; O'Gorman, J.; "Phase

shift keyed systems based on a gain switched laser transmitter”; Optics Express, Vol. 17 Issue 15, pp.12668-12677 (2009).

A.2 Conference Papers

1. Phelan, R.; **O'Carroll, J.**; Byrne, D. ; Herbert, C. ; Somers, J. ; Kelly, B.; "In0.75Ga0.25As/InP Multiple Quantum Well Discrete Mode Laser Diode Emitting at 2 μm"; MIOMD-XI Infrared Optoelectronics: Materials and Devices Conference, 4 – 8 Sept. 2012
2. MacSuibhne, N.; Li, Z; Baeuerle, B.; Zhao, J.; Wooler, J.P.; Alam, S.U.; Poletti, F.; Petrovich, M.N.; Heidt, A.M.; Giles, I.P.; Giles, D.J.; Pálsdóttir, B.; Grüner-Nielsen, L.; Phelan, R.; **O'Carroll, J.**; Kelly, B.; Murphy, D.; Ellis, A.D.; Richardson, D.J.; Garcia Gunning, F.C.; "Wavelength Division Multiplexing at 2μm"; Postdeadline paper, European Conference and Exhibition on Optical Communication (ECOC), 16 – 20 Sept. 2012
3. Huynh, T.N.; **O'Carroll, J.**; Smyth, F.; Shi, K.; Nguyen, L.; Anandarajah, P.; Phelan, R.; Kelly, B.; Barry, L.P.; "Low linewidth lasers for enabling high capacity optical communication systems"; International Conference on Transparent Optical Networks (ICTON), 2 – 5 July 2012.
4. **O'Carroll, J.**; Phelan, R; Kelly, B; Byrne, D; Smyth, F; Cardiff, B; Anandarajah, P.M.; Barry L.P.; "Narrow linewidth discrete mode laser diodes at 1550 nm"; Paper 8432-25 of Conference 8432, Spie Photonics Europe 16 – 19 April 2012.
5. **O'Carroll, J**; Phelan, R; Kelly, B; Byrne, D; Anandarajah, P.M.; Latkowski, S.; Barry, L.P.; "Discrete mode laser diodes for FTTH/PON applications up to 10 Gbit/s"; Paper 8432-71 of Conference 8432, Spie Photonics Europe 16 – 19 April 2012.
6. **O'Carroll, J**; Phelan, R; Kelly, B; Byrne, D; Smyth, F; Cardiff, B; Anandarajah, P.M.; Barry L.P.; "Narrow Linewidth Discrete Mode Laser Diodes for Advanced Modulation Formats"; paper OTu1G.4, Optical Fiber Communication Conference and Exposition and The National Fiber Optic Engineers Conference (OFC/NFOEC), 4 – 8 March 2012.
7. **O'Carroll, J.**; Phelan, R.; Kelly, B.; Byrne, D.; Barry, L.P.; O'Gorman, J.; "Wide temperature range $0 < T < 85$ °C narrow linewidth discrete mode laser diodes for coherent communications applications"; European Conference and Exhibition on Optical Communication (ECOC), 18 – 22 Sept. 2011

8. **O'Carroll, J**; Phelan, R; Kelly, B; Byrne, D; Anandarajah, P.M.; Latkowski, S.; Barry, L.P.; O'Gorman, J.; "Uncooled Discrete Mode Laser Diodes for FTTH/PON Applications up to 10 Gbit/s"; Photonics Ireland conference, 7 – 9 September 2011.
9. Zhou R.; Latkowski, S.; **O'Carroll, J.**; Phelan, R.; Barry, L.P.; Anandarajah, P.; "40nm wavelength tunable gain-switched optical comb source"; European Conference and Exhibition on Optical Communication (ECOC), 18 – 22 Sept. 2011.
10. Fragkos, A.; Bogris, A.; Syvridis, D.; Phelan, R.; **O'Carroll, J.**; Kelly, B.; O'Gorman, J.; "Amplitude regeneration of phase encoded signals using injection locking in semiconductor lasers"; Optical Fiber Communication Conference and Exposition and The National Fiber Optic Engineers Conference (OFC/NFOEC), 6 – 10 March 2011.
11. Gruet, F.; Bandi, T.; Mileti, G.; Phelan, R.; **O'Carroll, J.**; Kelly, B.; O'Gorman, J.; "Development and spectral characterisation of discrete mode laser diodes (DMLDs) emitting at 780 nm for Rubidium atomic clocks"; European Conference on Lasers and Electro-Optics and the International Quantum Electronics Conference, 22 – 26 May 2011
12. Weerasuriya, R.; Sygletos, S.; Ibrahim, S.K.; Phelan, R.; **O'Carroll, J.**; Kelly, B.; O'Gorman, J.; Ellis, A.D.; "Generation of frequency symmetric signals from a BPSK input for phase sensitive amplification"; Optical Fiber Communication Conference and Exposition and The National Fiber Optic Engineers Conference (OFC/NFOEC), 21-25 March 2010.
13. Sygletos, S.; Weerasutiya, R.; Ibrahim, S.; Gunning, F.; Ellis, A.; Phelan, R.; O'Gorman, J.; **O'Carroll, J.**; Kelly, B.; "A novel method of pump and idler signal generation for non-degenerate FWM based phase sensitive amplification"; European Conference on Lasers and Electro-Optics and the International Quantum Electronics Conference, 16-21 May 2010.
14. Anandarajah, P.M.; Barry, L.P.; Kaszubowska, A.; O'Gorman, J.; **O'Carroll, J.**; Herbert, C.; Phelan, R.; Duke, A.S.; "Highly coherent picosecond pulse generation with sub-ps jitter and high SMSR by gain switching Discrete Mode laser diodes at 10 GHz line rate"; Optical Fiber Communication Conference and Exposition and The National Fiber Optic Engineers Conference (OFC/NFOEC), 22-26 March 2009.